On the Geometry of IFS Fractals and its Applications

by

József Vass

A thesis
presented to the University of Waterloo
in fulfillment of the
thesis requirement for the degree of
Doctor of Philosophy
in
Applied Mathematics

Waterloo, Ontario, Canada, 2013

I hereby declare that I am the sole author of this thesis. This is a true copy of the thesis, including any required final revisions, as accepted by my examiners.

I understand that my thesis may be made electronically available to the public.

Abstract

Visually complex objects with infinitesimally fine features, naturally call for mathematical representations. The geometrical property of self-similarity - the whole similar to its parts - when iterated to infinity generates such features.

Finite sets of affine contractions called Iterated Function Systems (IFS), with their compact attractors IFS fractals, can be applied to represent detailed self-similar shapes, such as trees or mountains. The fine local features of such attractors prevent their straightforward geometrical handling, and often imply a non-integer Hausdorff dimension.

The main goal of the thesis is to develop an alternative approach to the geometry of IFS fractals in the classical sense via bounding sets. The results are obtained with the objective of practical applicability.

The thesis thus revolves around the central problem of determining bounding sets to IFS fractals - and the convex hull in particular - emphasizing the fundamental role of such sets in their geometry. This emphasis is supported throughout the thesis, from real-life and theoretical applications to numerical algorithms crucially dependent on bounding.

Acknowledgements

First and foremost, I would like to thank my dear wife Angela for supporting me over the years that led to this thesis. Her curiosity induced many chit-chats about my developing work, and I shared many results with her in a nutshell, to which she sometimes replied: "Oh that's trivial!" I feel lucky to call such a bright woman my wife!

I would also like to thank the thesis committee Profs. Sue Ann Campbell, Ruxandra Moraru, Xinzhi Liu, and the external examiner Prof. Christopher Essex for their careful review and consideration of this thesis. I am especially grateful to Prof. Campbell for her constant support.

The detailed reviews provided by Profs. Julio M. Ottino, Tamás Tél, and Stephen Wiggins on my turbulence work have been particularly helpful, as well as the discussion with Prof. Morten Brøns on the related conjectures.

I am grateful to Prof. Edward R. Vrscay for the various ways he has supported the manifestation of this thesis. Due to his broad awareness of the literature, it seemed as if he knew every fractal paper ever published. In particular, he introduced me to the magnificent invariant measure and the inverse problem. His unbiased criticism also kept motivating me to polish my work further, while balanced with occasional praise. Certainly few would have been willing to entrust me with the freedom he has.

Dedication

The thesis is dedicated to Prof. László Czách, a former student of L.V. Kantorovich, who instilled in me a special affinity for mathematical rigour and integrity, and whose Analysis lectures remain unforgettable.

Contents

List of Figures

Chapter 1

Introduction

1.1 Overview

We begin by reworking the standard definition of IFS fractals and the associated address set in Section 1.3 - the gained virtues becoming clear as the thesis progresses. Two fundamental lemmas are introduced, the Containment Lemma and the Slope Lemma, the former underpinning our geometrical approach, while the latter comes to our aid in the most unexpected situations, and hints at the relevance of periodic points to our discussion.

Next some real-life applications are reviewed in Section 1.4, to provide motivation for the rest of our discussion. Some relevant applications are detailed in biology, fractal antennas, computer graphics, and fluid dynamics.

We proceed to stating the "Thesis Problem" in Section 1.5, elevating the determination of bounding sets as the central problem of IFS Fractal Geometry, versus other currently upheld approaches, such as dimension analysis or other ad hoc methods.

An entire section is dedicated to two theoretical applications, intended to be further motivation for the subsequently presented geometry via bounding sets. Section 2.1 and Theorem 2.1.2 in particular, solidifies the role of the convex hull in deciding the perhaps most elementary question about an IFS fractal, its intersection with traversing lines. The model of Fractal Potential Flows - hereby presented in the context of Fractal Analysis in Section 2.2 - through its formerly reasoned connection to turbulence [73], calls for the geometrical investigation of its set of singularities, being an IFS fractal itself.

On the basis of the real-life and theoretical applications presented, we undertake the determination of bounding sets, upon the elaboration of "Geometry via Containment" in Section 3.1, with supporting algorithms in Section 3.1.2. We proceed to determining explicit bounding circles for IFS fractals in Section 3.2 - their novelty lying in that the currently known bounding circles have been the product of algorithms, not explicit formulas.

In Section 3.3, the main results of the thesis are presented on the convex hull of IFS fractals. The objective is to derive theorems for the "exact" convex hull, not merely a numerically approximative one as often is the case in the literature. Novel concepts are introduced, such as the "rationality" of IFS fractals, and the cardinality of extrema. A practical method is detailed for finding the convex hull of "regular" fractals via linear optimization in a special target direction in Section 3.3.3. Then some examples are solved to show the applicability of the method in practice. The implicit intention throughout the section, is to lay down the foundations for future generalizations.

The thesis contains mostly original ideas and results, with surveys of the literature, spanned by the overarching philosophy of IFS fractal geometry via iterative containment. The contributions of this thesis to the field can be found in Sections 1.3.2-1.3.3, and Chapters 2-3, with literature reviews in the "Introduction" to each subsection. All results are original unless cited. The thesis contains additional material to the three articles written during the course of the PhD program [71, 72, 73], specifically in Sections 1.3.3, 2.2.11, 2.2.12, 3.1.2, and 3.3.

1.2 History of Fractals

The discovery of fractalline features dates back to prehistoric times in Africa, where the various visual and auditory implications of self-similarity have intrigued artists for millenia [28]. In modern times, the idea of self-similarity first appears in the writings of Leibniz [51]. Towards the end of the 19th century, upon deeper investigations into the peculiarities of continuity and differentiability, Weierstrass discovered an everywhere continuous but nowhere differentiable function, inspiring further research by Cantor, Klein, Poincaré, Peano and others.

The greatest impetus to fractal research came from Gaston M. Julia and Pierre Fatou in the early 20th Century. Julia investigated the invariant sets of complex rational maps in a 199 page article, awarded with the Grand Prix de l'Académie des Sciences [42]. Even though highly popular in its day, his work lay forgotten until Mandelbrot emphasized its importance later.

Visual investigation into fractals did not widely begin until the advent of computers, when chaos in dynamical systems first came to surface with bifurcations visualized by Edward N. Lorenz. Indeed, fractals and dynamical systems are related concepts, since the recursive generation rule of most fractals may be thought of as a discrete dynamical system itself. A variety of attractors in the phase space of dynamical systems possess fractional Hausdorff dimension, hence the word "fractal". Widespread popularity of fractals came thanks to Benoît B. Mandelbrot [55] who gave their name, and linked the numerous quasi-self-similar features of Nature to mathematical fractals. The large variety of his examples include: seacoasts, plants, mountain ranges, turbulence, as well as financial data.

The attractors of Iterated Function Systems - IFS Fractals - are likely the most elementary kinds of fractals possible. We restrict ourselves to their study, in attempting to uncover their geometric nature. They are the attractors of a finite set of linear contractive maps - the "function system" - combined and iterated to infinity, converging to an attracting limit set, the IFS Fractal itself. There is a fundamental motivation in studying linear contractive maps in the plane, as they are the simplest contractions possible, and give rise to many logarithmic spiral structures in Nature, such as snail shells, galaxies, or eddies. Their iterative interactions reveal models for analogous interactions in Nature. The study of IFS fractals was first systematically undertaken by John E. Hutchinson in his highly influential paper [41]. Kenneth Falconer [31] and Michael F. Barnsley [4] have also contributed notable results and surveys of fractal geometry research, along with many other researchers from various fields.

1.3 IFS Fractals

1.3.1 Definition and Existence

The attractors of Iterated Function Systems - IFS Fractals - were pioneered by Hutchinson [41], further discussed by Barnsley and Demko [5], and may be the most elementary fractals possible. They are the attractors of a finite set of affine linear contraction mappings on the plane - the Iterated Function System (IFS) - which when combined and iterated to infinity, converges to an attracting limit set, the IFS fractal itself. IFS fractals as introduced here, can be considered the linearized version of Julia fractals, for which the IFS maps are nonlinear.

Definition 1.3.1 *Let a planar similarity affine contractive mapping (briefly similarity **contraction**, contraction map, or similitude)* $T : \mathbb{C} \to \mathbb{C}$ *be defined for all* $z \in \mathbb{C}$ *as* $T(z) := p + \varphi(z - p)$ *where* $p \in \mathbb{C}$ *is the **fixed point** of* T*, and* $\varphi = \lambda e^{\vartheta i} \in \mathbb{C}$ *is the **factor** of* T*, with* $\lambda \in (0, 1)$ *the **contraction factor** of* T*, and* $\vartheta \in (-\pi, \pi]$ *the **rotation angle** of* T*.*

Note that an equivalent definition may be given using unitary rotation matrices $R \in \mathbb{R}^{d\times d}, R^T R = I, d \in \mathbb{N}$ corresponding to $e^{\vartheta i}$ when $d = 2$. Then contraction maps take the following form

$$T(z) = p + \lambda R(z - p) \quad (z \in \mathbb{R}^d,\ p \in \mathbb{R}^d,\ \lambda \in (0, 1)).$$

This version shall be useful for certain proofs in later sections. At times we will consider the more general case when instead of λR we have a contractive matrix M in some matrix norm induced by a vector norm.

Definition 1.3.2 *Let a planar similarity affine contractive* n*-map iterated function system (briefly **IFS** or* n*-map IFS,* $n \in \mathbb{N}$*) be defined as a finite set of contractions, and denoted as* $\mathcal{T} := \{T_1, \ldots, T_n\}$*. We will denote the set of **indices** as* $\mathcal{N} := \{1, \ldots, n\}$*, the respective fixed points as* $\mathcal{P} := \{p_1, \ldots, p_n\}$*, and the factors as* $\varphi_1, \ldots, \varphi_n$*.*

Definition 1.3.3 *Let* $\mathcal{T} = \{T_1, \ldots, T_n\}, n \in \mathbb{N}$ *be an IFS. We define the **Hutchinson operator*** H *belonging to the IFS* $\mathcal{T}$ *as*

$$\mathrm{H}(S) = \mathrm{H}_{\mathcal{T}}(S) := \bigcup_{k=1}^{n} T_k(S) \quad \text{where} \quad T_k(S) := \{T_k(z) : z \in S\} \quad \text{for any} \quad S \subset \mathbb{C}$$

and call $\mathrm{H}(S)$ *the Hutchinson of the set* S*.*

Theorem 1.3.1 (Hutchinson [41]) *For any IFS $\mathcal{T}$ with Hutchinson operator $\mathrm{H}_{\mathcal{T}}$, there exists a unique compact set $F_{\mathcal{T}} \subset \mathbb{C}$ such that $\mathrm{H}_{\mathcal{T}}(F_{\mathcal{T}}) = F_{\mathcal{T}}$. Furthermore, for any nonempty compact $S_0 \subset \mathbb{C}$, the recursive iteration $S_{n+1} := \mathrm{H}_{\mathcal{T}}(S_n)$ converges to $F_{\mathcal{T}}$ in the Hausdorff metric.*

Proof The proof follows from the Banach Fixed Point Theorem, since it can be shown that $\mathrm{H}_{\mathcal{T}}$ is contractive over the complete metric space of nonempty compact subsets with the Hausdorff metric. □

Definition 1.3.4 *Let the set $F_{\mathcal{T}}$ in the above theorem be called a fractal generated by an IFS $\mathcal{T}$ (briefly **IFS fractal**). Denote $\langle \mathcal{T} \rangle = \langle T_1, \ldots, T_n \rangle := F_{\mathcal{T}}$.*

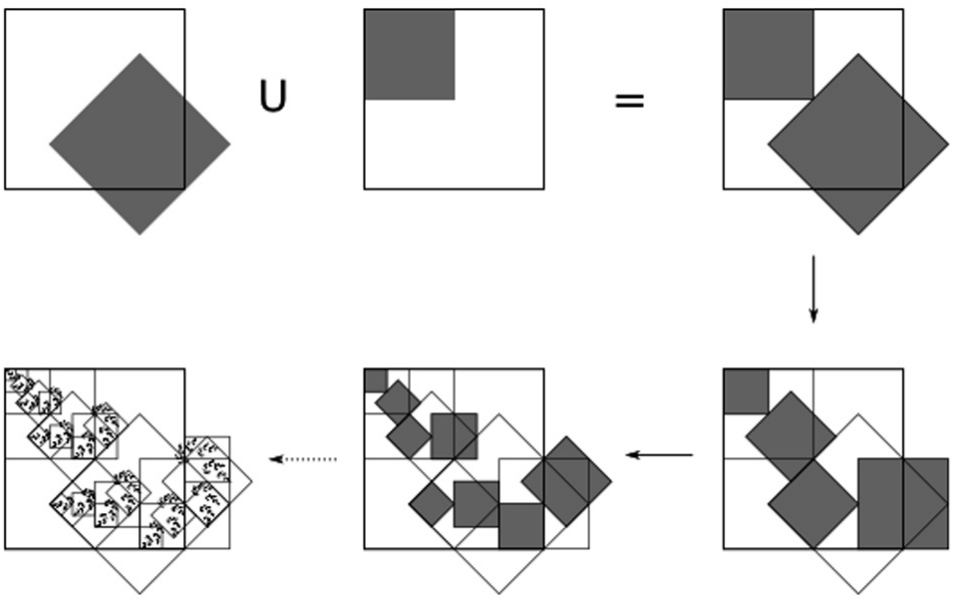

Figure 1.1: Generation of a fractal by iterating a square, with the following parameters $p_1 = 1 + \frac{1}{2}\mathrm{i},\ p_2 = \mathrm{i},\ \varphi_1 = \frac{1}{\sqrt{2}}\mathrm{e}^{\frac{\pi}{4}\mathrm{i}},\ \varphi_2 = \frac{1}{2}\mathrm{e}^{0\mathrm{i}}$ (figure by S. Draves).

1.3.2 The Address Set

Definition 1.3.5 *Let $\mathcal{N}^L := \mathcal{N} \times \ldots \times \mathcal{N}$ be the index set to the L-th Cartesian power, and call this $L \in \mathbb{N}$ the* ***iteration level****. Then define the* ***address set*** *as*

$$\mathcal{A} := \{0\} \cup \bigcup_{L=1}^{\infty} \mathcal{N}^L \cup \mathcal{N}^{\mathbb{N}}.$$

For any $a \in \mathcal{A}$ denote its k-th ***coordinate*** *as $a(k)$, $k \in \mathbb{N}$. Let its dimension or* ***length*** *be denoted as $|a| \in \mathbb{N}$ so that $a \in \mathcal{N}^{|a|}$ and let $|0| := 0$. Define the* ***map with address*** *$a \in \mathcal{A}$ acting on any $z \in \mathbb{C}$ as the function composition $T_a(z) := T_{a(1)} \circ \ldots \circ T_{a(|a|)}(z)$. Let the* ***identity map*** *be $T_0 := \mathrm{Id}$. Further denote*

$$\mathcal{A}_{fin} := \{a \in \mathcal{A} : |a| < \infty\},\ \mathcal{A}_{\infty} := \{a \in \mathcal{A} : |a| = \infty\} = \mathcal{N}^{\mathbb{N}}.$$

For the weights $w_1, \ldots, w_n \in (0,1)$ let $w_a := w_{a(1)} \cdot \ldots \cdot w_{a(|a|)}$, for the factors $\varphi_1, \ldots, \varphi_n$ let $\varphi_a := \varphi_{a(1)} \cdot \ldots \cdot \varphi_{a(|a|)}$, and for the angles $\vartheta_1, \ldots, \vartheta_n$ let $\vartheta_a := \vartheta_{a(1)} + \ldots + \vartheta_{a(|a|)}$.

The above definition of the address set revises the two standard definitions currently in use - numerical and symbolic - both only accounting for elements of $\mathcal{A}_{\infty}$. One relates addresses to decimal number representations of a certain basis (first introduced by Barnsley et al. [5, 4]), and the other to strings of letters usually for a small number of maps (Mandelbrot et al. [56]). The above formal language representation also accounts for finite addresses by defining vectors of numbers preferable to the string formalism when $|\mathcal{N}| > 24$. We proceed to ideas particularly useful for Sections 3.1.2 and 3.3.

Definition 1.3.6 *Let ab denote (a,b) for any $a, b \in \mathcal{A}_{fin}$ so that $T_{ab} = T_a T_b := T_a \circ T_b$. We say that the address $a \in \mathcal{A}$ is a* ***truncation*** *of $b \in \mathcal{A}$ if $|a| < \infty$ and there is a $c \in \mathcal{A}$ such that $b = ac$, denoted as $a < b$ (note that this includes $a = 0$). Let the* ***L-long truncation*** *of $a \in \mathcal{A}$ be denoted as $\mathrm{trn}_L(a)$ where $|a| \geq L \in \mathbb{N}$. Let $a \wedge b$ denote the* ***longest common truncation*** *of $a, b \in \mathcal{A}$. Finally, let $\bigwedge \mathcal{A}_0$ denote the longest common truncation of all elements of $\mathcal{A}_0 \subset \mathcal{A}_{fin}, |\mathcal{A}_0| < \infty$.*

Definition 1.3.7 *Since we can start the iteration towards F with any compact set, we shall normally choose the* ***primary fixed point*** *p for simplicity, which is any fixed point in $\mathcal{P}$ of our preference. We also call this p the* ***seed*** *or the* ***base****.*

This idea of appointing one of the fixed points to be "primary" and addressing the rest of the fractal points relative to it, is novel in the literature (to the author's best knowledge),

yet much of the discussion to follow seems impossible without it. It is formalized in the next theorem and the subsequent definition.

Theorem 1.3.2 *For any primary fixed point $p \in \mathcal{P}$ we have*

$$\langle T_1, \ldots, \mathrm{T}_n \rangle = \lim_{L\to\infty} \mathrm{H}^L(\{p\}) = \mathrm{Cl}\{T_a(p) : a \in \mathcal{A}_{fin}\} = \mathrm{Cl}\{T_a(p_k) : a \in \mathcal{A}_{fin},\ p_k \in \mathcal{P}\}.$$

We call this the ***address generation*** *of the IFS fractal $F = \langle T_1, \ldots, \mathrm{T}_n \rangle$.*

Proof The proof follows from Theorem 1.3.1 with the compact sets $\{p\}$ or $\mathcal{P}$. □

Definition 1.3.8 *Let the* ***address of a fractal point*** *$f \in F$ with respect to some primary fixed point $p \in \mathcal{P}$ be the shortest address $a \in \mathcal{A}$ such that $f = T_a(p)$ (if two such addresses exist equal in length, then take the lexicographically lower one). Denote it as* $\mathrm{adr}(f) = \mathrm{adr}_p(f) := a$.

Note that this address is potentially infinite, in which case the choice of p becomes irrelevant. In a sense, the primary fixed point can be considered the "base" of this representation. The following definitions of (eventual) periodicity are by Barnsley [4].

Definition 1.3.9 *We say that a fractal point $f \in F$ is a* ***periodic point*** *if its address $a \in \mathcal{A}$ is periodic, meaning it is infinite with a finite repeating part $a = \bar{x} := xx\ldots$ where $x \in \mathcal{A}_{fin}$, denoted as $p_x := f$ (for which $T_x(f) = f$). Let the set of all periodic points be denoted as* $\mathrm{Per}(F) := \{p_x : x \in \mathcal{A}_{fin}\}$. *Let the* ***cycle*** *of a finite address x be the set* $\mathrm{Cyc}(x) := \{p_{ba} : x = ab, a < x\}$.

Note that the periodic point p_x above is the fixed point of T_x. This abuse of notation is consistent with the fixed points of the IFS for which $p_k = T_k(p_k), k \in \mathcal{N}$. Also note that $p_x \in \mathrm{Cyc}(x)$ since $a = 0 < x$, and that $|\mathrm{Cyc}(x)| = |x|$.

Definition 1.3.10 *A fractal point $f \in F$ with address $a \in \mathcal{A}_\infty$ is* ***eventually periodic*** *(briefly: eventual) if $T_b^{-1}(f) \in \mathrm{Per}(F)$ is periodic for some $b < a$. Let the set of all eventual points be denoted as* $\mathrm{Eve}(F)$. *(Clearly* $\mathrm{Per}(F) \subset \mathrm{Eve}(F)$ *with $b = 0$.)*

Theorem 1.3.3 *A fractal point $f \in F$ is eventually periodic iff it is the fixed point of the conjugate of an address, meaning $f = T_a T_b T_a^{-1}(f)$ for some $a, b \in \mathcal{A}_{fin}$.*

Proof $f = T_a T_b T_a^{-1}(f) \Leftrightarrow f = \lim_{L\to\infty}(T_a T_b T_a^{-1})^L(f) = \lim_{L\to\infty} T_a T_b^L T_a^{-1}(f) = T_a(p_b)$ so $T_a^{-1}(f) = p_b \in \mathrm{Per}(F), |a| < \infty$. Therefore by definition $f \in \mathrm{Eve}(F)$. □

1.3.3 Lemmas

The following lemma will serve as the basis for the philosophy of the thesis. It is a rather well-known fact that occurs in various places in the literature. It has been applied to the Connectedness Problem of IFS fractals by Hardin, Barnsley, and Harrington [37, 8, 7], and in various computer graphics publications about IFS. The lemmas hold for n-map IFS $\mathcal{T}$ and its corresponding attractor $F = \langle \mathcal{T} \rangle$ and Hutchinson operator H.

Lemma 1.3.1 (Containment Lemma)
If for a nonempty compact set $S \subset \mathbb{C}$: $\mathrm{H}(S) \subset S$ then $F \subset S$. On the other hand, if $F \subset S$ then $F \subset \mathrm{H}^L(S)$ for any $L \in \mathbb{N}$.

Proof The first part of the lemma follows directly from Theorem 1.3.1 by observing that $S \supset \mathrm{H}^L(S) \to F$ as $L \to \infty$. The second part by observing that $F = \mathrm{H}(F)$ implies $F = \mathrm{H}^L(F)$ for any $L \in \mathbb{N}$, and that $F \subset S$ implies $F = \mathrm{H}^L(F) \subset \mathrm{H}^L(S)$. $\square$

The lemma essentially states that the containment of the self-similar IFS fractal $F = \langle T_1, \ldots, T_n \rangle$ by a compact set S, implies self-similar containment by the iterates of S according to the Hutchinson operator belonging to the IFS.

We proceed to showing another important lemma, which will prove useful in some unexpected situations - the noted corollaries already highlighting its relevance.

Lemma 1.3.2 (Slope Lemma)
The slope of the map T_a, $a \in \mathcal{A}_{fin}$ is the constant $\varphi_a \in \mathbb{C}$, meaning

$$\frac{T_a(z_1) - T_a(z_2)}{z_1 - z_2} = \varphi_a \quad \textit{for any distinct} \quad z_{1,2} \in \mathbb{C}.$$

Proof We show the property by induction with respect to $|a|$. For any $|a| = 1$ address, i.e. $k \in \mathcal{N}$ we have

$$T_k(z_1) - T_k(z_2) = p_k + \varphi_k(z_1 - p_k) - p_k - \varphi_k(z_2 - p_k) = \varphi_k(z_1 - z_2).$$

Now let us suppose the property holds for $|a| \leq L$ and we show it for length $L + 1$. Taking any $k \in \mathcal{N}$ we need the property for (k, a).

$$T_{(k,a)}(z_1) - T_{(k,a)}(z_2) = T_k(T_a(z_1)) - T_k(T_a(z_2)) = \varphi_k(T_a(z_1) - T_a(z_2)) =$$

$$= \varphi_k \varphi_a(z_1 - z_2) = \varphi_{(k,a)}(z_1 - z_2). \square$$

Corollary 1.3.1 *Any periodic point* $p_a \in \mathrm{Per}(F), a \in \mathcal{A}_{fin}$ *takes the form* $p_a = \frac{T_a(0)}{1-\varphi_a}$.

Proof Follows from the lemma with $z_1 = p_a$ and $z_2 = 0$. Note that the identity still holds if $p_a = 0$ since then $T_a(0) = 0$. □

Corollary 1.3.2 *The action of a map composition is centered at a periodic point as* $T_a(z) = p_a + \varphi_a(z - p_a) = T_a(0) + \varphi_a z \ (z \in \mathbb{C},\ a \in \mathcal{A}_{fin})$.

Proof The first equality follows from the lemma with $z_1 = z$ and $z_2 = p_a$, and note that it still holds if $z = p_a$. The second equality follows by applying the previous corollary. □

Many beautiful algebraic properties can be shown for periodic points using the Slope Lemma, which we omit for their lack of utility in this thesis. We also note that in the first corollary, 0 is just part of the identity, and not necessarily a (primary) fixed point of the IFS.

Lemma 1.3.3 (Affine Lemma)
For any affine map $M(z) = cz+d,\ c, d, z \in \mathbb{C}$ *we have* $M\langle\mathcal{T}\rangle = \langle M\mathcal{T}M^{-1}\rangle$. *Furthermore*

$$MT_kM^{-1}(z) = M(p_k) + \varphi_k(z - M(p_k)) \quad (k \in \mathcal{N}).$$

Proof According to Theorem 1.3.2, any point $f \in F$ can be represented by an infinite address $a \in \mathcal{A}_\infty$ and seed $p \in \mathcal{P}$ as $f = \lim_{L\to\infty} T_{\mathrm{trn}_L(a)}(p)$ implying

$$M(f) = \lim_{L\to\infty} M \circ T_{a(1)} \circ \ldots \circ T_{a(L)}(p) = \lim_{L\to\infty} MT_{a(1)}M^{-1} \circ \ldots \circ MT_{a(L)}M^{-1}(M(p))$$

which are clearly all the possible infinite address representations in $\langle M\mathcal{T}M^{-1}\rangle$. (The new seed $M(p)$ is irrelevant to convergence.) The second identity follows by observing that both M and M^{-1} preserve complex combinations. □

1.4 Real-Life Applications

The birth of this thesis was motivated by a number of seemingly disparate fields of science and engineering utilizing IFS fractals. Their common factor is the set of underlying geometrical questions which we hereby seek to identify and resolve. A significant emphasis is placed on the inherent mathematical beauty of IFS fractals and these questions about them. Our quest indeed will be two-fold - applied and pure - while revolving around the focal question of bounding.

This section will detail some applications under ongoing discussion in the literature. Here only the problems are described - their translation to the language of mathematics to follow.

1.4.1 Computer Graphics

Research on fractals only gained popularity with the advent of computers in the second half of the 20th century, as their visualization by hand seems next to impossible. Various expository books have appeared for both the mathematician and the lay reader, visually affirming the utility of fractals in generating self-similar features of Nature, such as mountains, seacoasts, or even trees [55].

The idea of generating a complex shape agreeing with Nature, just from a few functions iterated to near-infinity, is an appealing concept. So it was for the developing field of computer graphics, where computational efficiency is key to real-time display. The early ideas of Mandelbrot and Barnsley that fractals are all around us, shaped computer graphics to the extent that fractal-based image compression techniques were developed. The power of these ideas being "iteration of a few functions" (the IFS) to produce a "complex lifelike object" or an image close to the original.

As we will also see in the upcoming Botany section, trees and most plants in general may be represented by a type of formal grammar called L-systems, a recursive notation for describing the growth of plants, and their branching in particular. L-systems and IFS fractals are directly related mathematically - one can typically convert between the two representations. Indeed trees as well as other 3D objects, are often generated in an iterative way, essentially producing "embellished" IFS fractals with added leaves, texture, etc. [53].

Although this thesis discusses the first step - answering questions in the 2D plane - the

presented methods and results should translate to 3D space. In the spatial visualization of IFS generated sets, or really for any object in virtual space, there are two primary questions implied by the problem of lighting the object or "ray tracing": its spatial extent, and its intersection with various rays of light [38]. Naturally we would like to know in advance as much as we can about the object. With classical Euclidean objects these questions are easier than with sets generated via self-similar iteration.

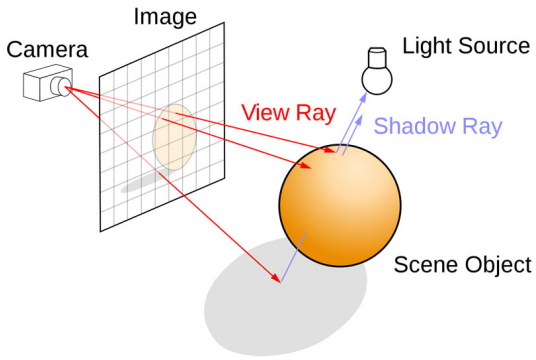

Figure 1.2: Ray tracing.

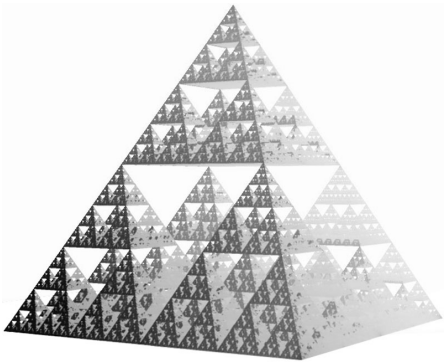

Figure 1.3: The Sierpinski Pyramid.

As illustrated by the above figure, ray tracing is composed of a series of steps for shading an object and its environment. Testing for whether a camera ray intersects the object to be visualized or shaded involves:
(1) Sending out a test ray in a particular direction from the camera;
(2) testing for intersection with the convex hull of the object (or can also be projected to the image plane a priori);
(3) if the ray intersects the convex hull, testing for intersection with the object itself.
Shading by rays from a light source, instead of camera rays, involves similar steps.

Other than ray tracing, the fundamental question of handling a 3D IFS fractal in virtual space remains. One must be able to calculate its interaction with other virtual objects. We must know the object's extent for collision detection with other objects, such as holding it in an avatar's hands in virtual space. If we do not know the extent of something, we are simply incapable of "handling" it. The idea of "extent" here clearly corresponds to finding the fractal's convex hull, and the iteration of the hull to some level. Thus we may conclude, that the intersection of an IFS fractal and any line, as well as the determination of the convex hull, are fundamental geometrical questions in computer graphics applications.

1.4.2 Fractal Antennas

Antennas exploiting the virtues of self-similarity, have recently found widespread applications in the commercial and military sphere. Because of their self-similar structure, they are inherently more powerful than classical antennas, and thus can be made much smaller and more compact. Indeed they tend to be 50-75% smaller than their analogous traditional counterparts, with near-identical characteristics.

Fractal antennas also have the additional property that they are multiband and wideband, in terms of receiving electromagnetic signals. For this reason, they require less parts, and are thus lighter and less likely to break than traditional antenna designs. The keywords multiband and wideband, refer to the variety and breadth of the scale of frequencies an antenna is able to process.

Indeed compact antenna design is a challenge concerning mobile devices, where small size and light weight are relevant targets. Generally fractal antennas are flat, but the Menger Sponge is also being used for increased power. Variability in the shape of the fractal antenna is key, so that it can be designed to fit within the particular mobile device, and done so as compactly as possible.

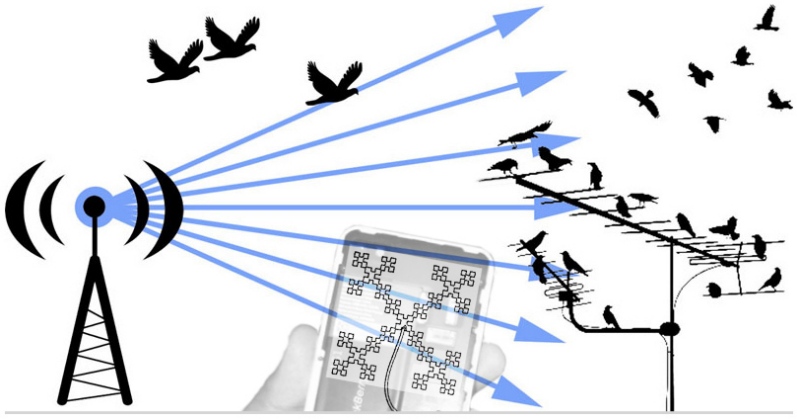

Figure 1.4: Signals received by antennas.

Geometrically the problem revolves again around the question of the convex hull and line intersection. Since electromagnetic wavefronts are locally close to a spatial hyperplane, their intersection with the plane of the fractal antenna (which is typically flat in mobile devices), reduces to the problem of line intersection with the fractal.

As shown in Theorem 2.1.2, the question of line intersection and finding the convex hull are interdependent. This serves as motivation for finding the precise extremal points - and thus the exact convex hull - also aiding compact engineering. Having a certain shaped space to fit the antenna within, we must be able to predetermine the necessary IFS parameters, in order to arrive at a fractal with a convex hull shape that fits the given space within the design. This procedure is typically done by perturbing the IFS parameters, and seeing what convex hull they result in. For this it would help, if the attractor - and thus its convex hull - depended continuously on the IFS parameters (to be discussed).

For an overview of fractal antennas see [79, 80, 16, 36, 67], for the foundational work of Cohen et al. see [17, 39, 1, 21] and initial patents [20, 19, 18]. For an introduction to antennas, see Frenzel [35].

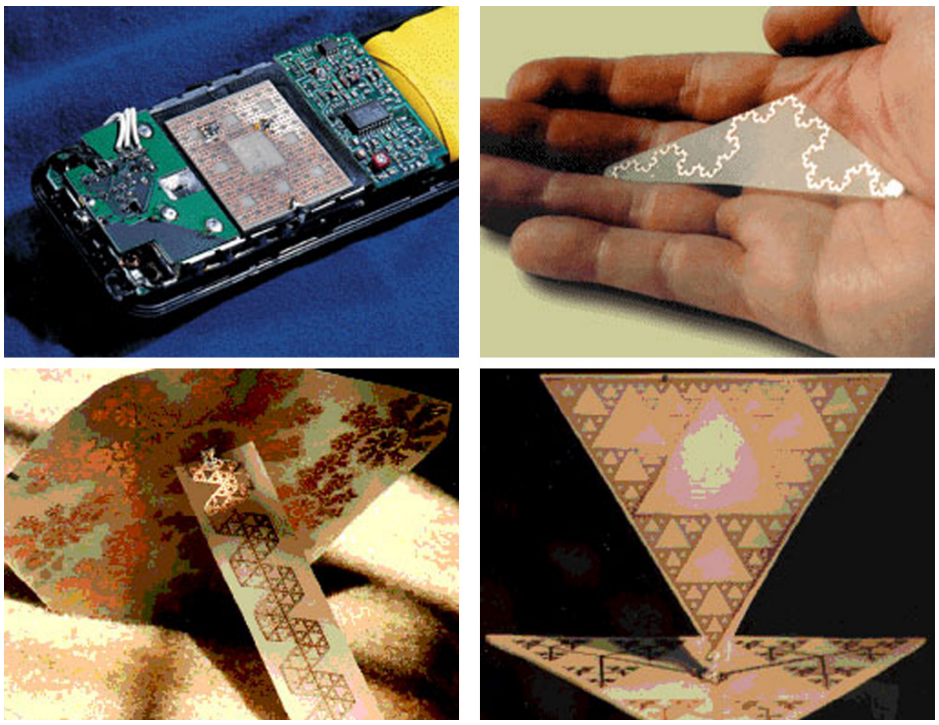

Figure 1.5: Microstrip patch fractal antennas [19] (photos provided by Nathan Cohen, Fractal Antenna Systems, Inc.).

1.4.3 Botany

As mentioned earlier, L-systems (abbreviation for Lindenmayer Systems) can be used to describe the spatial growth of a wide variety of plants in Nature. They were originally introduced in 1968 by the Hungarian theoretical biologist and botanist Aristid Lindenmayer [53], and can often be generated as IFS fractals.

Figure 1.6: A Barnsley fern, a Pythagoras tree, and a raytraced L-system tree (figures by J.L.D. Rubio, A.V.D. Ploeg, and Solkoll).

An L-system is a type of formal grammar, which has a recursive rule for describing growth. L-systems and IFS fractals are mostly convertible representations of the same self-similar object - in fact 3D plants are often generated in this manner. Lindemayer devised L-systems to describe plant growth in Nature.

Viewing the crowns of trees for instance as a collection of leaves on a self-similar system of branches, we may deduce that the question of optimizing the design of the tree crown for maximal light reception, is indeed a purely 3D IFS fractal question. Thus it has relevance for theoretical botany (as well as 3D fractal antenna design). Such tree crowns are likely to be hyperdense, as discussed in Section 2.1 [82].

1.4.4 Medicine

The relevance of this to tumor treatment is only briefly discussed here, as it is intended to be an inspiration for future research. Radiation therapy is about bombarding tumors with rays of energy. Tumors are essentially the system of veins which feed them, thus their vasculature define their structure. The fractalline structure (possibly L-system) of vasculature in organs as well as tumors, has been discussed in a number of publications to date, including [3, 81, 65].

Understanding deformed L-system or IFS fractal formation, however must precede any such investigation. For even if the governing rule of tumor growth is recursive and ultimately fractalline in a non-restraining growth environment, internally in the body, such growth is hindered. Thus the surrounding forces due to the density and weight of various organs must be considered, as the growing tumor experiences their hindrance. Essentially this calls for a theory of deformational IFS fractal formation - currently non-existent, as far as the author is aware. It is beyond the scope of this thesis to resolve this question.

Such a theory would also bear relevance to the design of fractal antennas within an allocated space - the antenna being essentially analogous to the tumor, and other parts of the phone to the surrounding organs. Due to ray bombardment, clearly the mathematical questions involved once again are the convex hull, fractal-line intersection, and their relationship.

1.4.5 Turbulence

In paper [73] it was argued that Fractal Potential Flows - with an IFS fractal set of singularities - pose as an exact model for fully developed turbulence. These flows are the attractors of certain transfer operators over stream functions in an appropriately defined function space.

Fully Developed Turbulence (FDT) occurs at the infinite extreme of the Reynolds spectrum. It is a theoretical phenomenon which can only be approximated experimentally or computationally, and thus its precise properties are only hypothetical, though widely accepted. It is considered to be a chaotic yet stationary flow field, with self-similar fractalline features. A number of approximate models exist, often exploiting this self-similarity. The precise ideal conditions for FDT to occur are currently unknown, and its exact causes, evolution, and characteristics are hypothetical. With some contemplation, one may realize that a mathematical theory is the only possible resolution.

On the basis of temporal intermittency, the paper argues that the evolution towards FDT cannot be described under the Continuum Hypothesis of Fluid Dynamics, due to the lack of temporal differentiability. Instead we draw inspiration from, and thereby reformulate, the alternative approach to Navier-Stokes modelling of turbulence, called Chaotic Advection / Mixing.

The reformulation translates the IFS Markov operator iteratively converging to the invariant measure [41], to a corresponding transfer operator over potential stream functions, converging to the invariant flow (or fractal potential flow). The translation is carried out via an isometric isomorphism between probability measures and stream functions, based on Poisson's Equation. The mathematics of the model is presented in Section 2.2 in the context of Fractal Analysis, with a new section on the inverse problem, relative to the mentioned paper.

1.5 The Thesis Problem

In the previous sections, three interconnected problems have been identified for IFS fractals:
(1) Find bounding sets to the fractal (preferably invariant under H).
(2) Describe the exact convex hull, i.e. find the extremal points.
(3) Determine the conditions for a line to intersect the fractal.
Thus we formulate the following problem to guide us throughout the thesis.

Problem 1.5.1 (Thesis Problem)
Find bounding sets to IFS fractals - preferably the convex hull itself - and discuss their relevance to answering geometrical questions about a fractal in the plane. Specifically, resolve the fractal and line intersection question, central to the described real-life applications. Discuss the generalization of any results to higher dimensions where possible.

The central problem of the thesis has been stated in a flexible yet definitive manner, so as to leave sufficient freedom for its resolution, while still acting as a guide. We will approach it both numerically and theoretically. The numerical approach will find bounding sets to the fractal, often circles, while the theoretical approach is to find the exact convex hull. Here "theoretical" does not refer to "impractical" - in fact the presented methods have been designed with practical implementability in mind.

One reason that bounding sets are emphasized in the problem statement, has to do with the iteration of such sets by the Hutchinson operator H, as detailed in Section 3.1.1 building upon the Containment Lemma 1.3.1. The initial bounding set, can be a circle, the convex hull, or any other, which may then be iterated for increasingly closer bounding sets to the fractal. It is clear however, that an iterated bounding circle is sufficient to resolve any geometrical question to some $\varepsilon > 0$ accuracy. Essentially, bounding circles constitute a numerical panacea.

As for finding the convex hull, one may certainly employ numerical methods - such as bounding circles - to estimate the extremal points, as is often done in the literature. In Section 3.3 however, we set our sail to finding explicit formulas for the extremal points, giving a definitive practical solution for the first time in the context of a general method.

In the next chapter we discuss two theoretical problems, as further motivation for the subsequent investigation of the geometry of IFS fractals.

Chapter 2

Theoretical Applications

2.1 The Fractal-Line Intersection Problem

2.1.1 Introduction

As discussed earlier, IFS Fractals have motivated plenty of theoretical investigations to date, due to their simplicity and applicability in various fields, such as the modeling of plants in computer graphics, and the design of fractal antennas. The statement and resolution of the Fractal-Line Intersection Problem is imperative for a more efficient treatment of these real-life applications. This section intends to take further steps towards this resolution, building on the literature.

A verifiable condition guaranteeing intersection with any line passing through the convex hull of an IFS fractal is derived, shown in general $\mathbb{R}^d$ for hyperplanes. The condition also implies a constructive algorithm for finding the points of intersection. We give various other conditions that guarantee an infinite number of approximate intersections if there is at least one. This work was first presented in [72].

Falconer [31] provides an extensive overview of Fractal Geometry, summarizing the work of several researchers. In particular, he examines the behaviour of Euclidean attractors under projections to hyperplanes. When the projection is carried out in $\mathbb{R}^2$ or $\mathbb{R}^3$ onto a line or plane respectively, we can think of the resulting set as the "shadow" of the fractal, which may be analyzed for its own dimension. Furthermore, we may ask how many fractal points are projected to a certain point on the line, or if there are any at all, in essence trying to uncover the distribution of such a projection.

What are the actual fundamental underlying questions here? Upon further thought, we may realize that the projection problem breaks down to two partial questions, since the directional ray of projection can be thought of as an intersecting line.

Problem 2.1.1 (Fractal-Line Intersection Problem)
Given a line and an IFS fractal in the plane, do they intersect? If they intersect, how many points of intersection are there? Or alternatively, within some $\varepsilon > 0$ neighbourhood of the line?

Resolutions to these questions are hereby provided, while their relevance demonstrated from the viewpoint of applications. It is shown that for certain broad classes of IFS fractals - hyperdense, or specifically chain fractals - the shadow is always filled in, no matter where the light shines from, proven in general in $\mathbb{R}^d$. Furthermore, the segment shadow in $\mathbb{R}^2$ is shown to receive an infinite number of projected points, in any $\varepsilon > 0$

subinterval of the segment. These properties make some of these potentially disconnected fractals ideal for 2D fractal antenna design or as light-absorbing tree crowns - suggesting that tree crowns could be considered 3D fractal antennas.

Recently Mendivil and Taylor [63] have also approached these questions from a projectional point of view. Defining a certain parametrized class of planar IFS fractals, they guarantee that the shadow in all directions is a segment. It is proven that this holds for some domain of parameters. In other words, for this specific class of planar fractals, any line or ray of light that intersects the convex hull, also intersects the fractal, thereby contributing to its shadow. We shall hereby examine the problem further for the broadest possible class of attractors in $\mathbb{R}^d$ called hyperdense fractals, and in particular for the verifiable subclass of chain fractals.

The Fractal-Line Intersection Problem is relevant to a number of real-life applications, among which we have mentioned ray tracing in computer science, the design of fractal antennas in engineering, and the study of tree crown density for light absorption in botany and forestry. In computer science, ray tracing involves the shading of an object in virtual space, which is detailed in Hart and DeFanti [38] in regards to 3D IFS fractals. The study of tree crowns for light absorption is a vast field, and we recommend the work of Lindenmeyer et al. [53] and Zeide [82], and note the pioneering inspirational work of Mandelbrot [55]. Fractal antennas are flat metal antennas with an IFS fractal layout that must be optimized for the amount of material used vs. the efficiency of signal reception. These antennas were introduced by Cohen et al. [17, 39].

Further research into the projection of fractals has been carried out by Besicovitch [10] and Federer [33] examining s-sets; Marstrand [58], Kaufman [44], and Mattila [60, 61] showing projection theorems for arbirary sets in $\mathbb{R}^d$; as well as Davies [22], Falconer et al. [30, 32], and Howroyd [40] giving results for box and packing dimensions. This research is summarized in the expository book by Falconer [31], also providing an introduction to IFS fractals.

2.1.2 Preliminary Concepts

We hereby consider affine contraction mappings in a more general setting. Let $T : \mathbb{R}^d \to \mathbb{R}^d$ be defined for all $z \in \mathbb{R}^d$ as $T(z) := p + M(z - p)$ where $p \in \mathbb{R}^d$, with the induced matrix norm $\|M\|_2 < 1$. We keep the notations $\mathcal{T}, \mathrm{H}, \mathcal{N}, \mathcal{P}$ introduced for $n \in \mathbb{N}$ number of contractions in Section 1.3.1. We examine the attractor $F = \langle T_1, \ldots, T_n \rangle$ and denote $C_F := \mathrm{Conv}(F)$. Theorem 1.3.1 still holds in this setting [41], as well as the definitions related to the address set $\mathcal{A}$ in Section 1.3.2. We proceed by introducing the particular subclass of fractals to be studied further.

Definition 2.1.1 *Let an IFS fractal in $\mathbb{R}^d$ be **hyperdense** if any hyperplane that intersects its convex hull, also intersects the Hutchinson of its convex hull. We will call an IFS fractal a **chain fractal**, if the Hutchinson of its convex hull is connected.*

Theorem 2.1.1 *Chain fractals are hyperdense.*

Proof First we see that for any $T \in \mathcal{T}$ we have $T(\mathrm{Conv}(S)) = \mathrm{Conv}(T(S))$ since T is affine. We also note that for any $S_1, \ldots, S_N \subset \mathbb{R}^d$

$$\mathrm{Conv}\left(\bigcup_{k=1}^{N} S_k\right) = \mathrm{Conv}\left(\bigcup_{k=1}^{N} \mathrm{Conv}(S_k)\right)$$

since the convex combination of convex combinations, is a convex combination. Considering the fact that $\mathrm{H}(F) = F$ as well as the above ideas, we have that

$$\mathrm{Conv}(F) = \mathrm{Conv}\left(\bigcup_{k=1}^{n} \mathrm{Conv}(T_k(F))\right) = \mathrm{Conv}\left(\bigcup_{k=1}^{n} T_k(\mathrm{Conv}(F))\right)$$

meaning that $C_F = \mathrm{Conv}(\mathrm{H}(C_F))$. Since F is compact so is C_F and thus $\mathrm{H}(C_F)$, since H is continuous. We now turn to showing that F is hyperdense. Let us take any hyperplane $L \subset \mathbb{R}^d$ that intersects $C_F = \mathrm{Conv}(\mathrm{H}(C_F))$ in some point $q = \mu h_1 + (1 - \mu)h_2,\ h_{1,2} \in \mathrm{H}(C_F),\ \mu \in [0, 1]$. If $\mu \in \{0, 1\}$ then $q \in \mathrm{H}(C_F)$ so we are done. Otherwise L separates the space into two half spaces, with h_1 in one and h_2 in the other. Since F is a chain fractal, we know that $\mathrm{H}(C_F)$ is connected, thus it is path-connected, so there is a path $\gamma \subset \mathrm{H}(C_F)$ connecting h_1 and h_2. Since $h_{1,2}$ are on separate sides of L, we must have that $L \cap \gamma \neq \varnothing$. This can be shown by parametrizing $\gamma : [0, 1] \to \mathbb{R}^d$ and writing the plane as $L = \{z \in \mathbb{R}^d : \langle a, z \rangle = b\}$ for some $a \in \mathbb{R}^d,\ b \in \mathbb{R}$. Denoting $f(t) = \langle a, \gamma(t) \rangle - b$ we have that $f(0)f(1) < 0$, so by Bolzano's Theorem f must have a root $t_0 \in (0, 1)$, implying that $\gamma(t_0) \in L \cap \gamma \subset L \cap \mathrm{H}(C_F)$.
Therefore by $L \cap \gamma \neq \varnothing$ and $\gamma \subset \mathrm{H}(C_F)$ we have that $L \cap \mathrm{H}(C_F) \neq \varnothing$. □

Lemma 2.1.1 *For a hyperdense fractal $F = \langle T_1, \ldots, T_n \rangle$ and any address $a \in \mathcal{A}$, if a hyperplane L intersects $T_a(C_F)$ then it also intersects $T_a(\mathrm{H}(C_F))$.*

Proof It is clear that since the $M_k \in \mathbb{R}^{d \times d}$ factors in T_k are invertible, the inverses of the maps are $T_k^{-1}(z) = p_k + M_k^{-1}(z - p_k)$. Thus T_a^{-1} also exists, and it is also an affine mapping, so it takes the hyperplane L into another hyperplane L'. Thus $L \cap T_a(C_F) \neq \varnothing$ is equivalent to $T_a^{-1}(L) \cap C_F \neq \varnothing$, which by the hyperdensity of F implies that $T_a^{-1}(L) \cap \mathrm{H}(C_F) \neq \varnothing$, and so $L \cap T_a(\mathrm{H}(C_F)) \neq \varnothing$. $\square$

2.1.3 Exact Intersection

Theorem 2.1.2 *A hyperplane intersects a hyperdense fractal if and only if it intersects its convex hull. This equivalence holds only if the fractal is hyperdense.*

Proof The proof is based on Cantor's Intersection Theorem and the address generation of $F = \langle T_1, \ldots, T_n \rangle \subset \mathbb{R}^d$ in Theorem 1.3.2. We will show that the hyperdensity of F implies a decreasing sequence of compact sets, which tend to a point by Cantor's Intersection Theorem. The index sequence itself will correspond to an address, which in the limit locates a fractal point, since the fractal is the closure of all possible mapped addresses, with respect to some primary fixed point. Let us now begin the proof.
If a hyperplane L intersects F, it must clearly intersect $C_F := \text{Conv}(F)$. On the other hand, if L intersects C_F, by the fractal's hyperdensity, it also intersects $\text{H}(C_F)$. So L must intersect $T_{k_1}(C_F)$ for some $k_1 \in \mathcal{N}$. Let this intersection be denoted as $I_1 := L \cap T_{k_1}(C_F) \subset \mathbb{R}^d$. Then I_1 is compact, because C_F is compact.
Since $T_{k_1}(\text{H}(C_F)) = \bigcup_{k=1}^{n} T_{k_1} \circ T_k(C_F)$, according to Lemma 2.1.1 with $a = (k_1)$, the fact that L intersects $T_{k_1}(C_F)$ implies that it also intersects $T_{k_1}(\text{H}(C_F))$ and thus $T_{k_1} \circ T_{k_2}(C_F)$ for some $k_2 \in \mathcal{N}$. Once again denoting $I_2 := L \cap T_{k_1} \circ T_{k_2}(C_F)$ we have that this set is compact, and $I_2 \subset L \cap T_{k_1}(C_F) = I_1$.
Continuing to apply Lemma 2.1.1 in the above recursive procedure, by induction we get a strictly monotonically decreasing sequence (since $T_k,\ k \in \mathcal{N}$ are contractive) of compact sets in $\mathbb{R}^d$: $I_1 \supset I_2 \supset \ldots \supset I_j \supset \ldots$ each with a corresponding address composition: $T_{k_1} \circ \ldots \circ T_{k_j}$. According to Cantor's Intersection Theorem $\bigcap_{j=1}^{\infty} I_j \neq \varnothing$ and it contains a single point $f \in \mathbb{R}^d$, since the address composition contracts to a point in the limit.
Starting with any seed $p \in \mathcal{P} \cap C_F$ we have that $f = \lim_{j \to \infty} T_{k_1} \circ \ldots \circ T_{k_j}(p) \in F$ by the address generation of F, so L intersects F in f. Note that such an intersection may not be unique, since in this recursive proof, we have only chosen one indexed set in the Hutchinson union at each step, though L may intersect multiple.
The above is under the condition that F is hyperdense. If it is not, then by definition there is a hyperplane which intersects C_F but not $\text{H}(C_F)$. Since $F \subset \text{H}(C_F)$ this hyperplane will not intersect F either, countering the equivalence. □

Corollary 2.1.1 *A line intersects a chain fractal in $\mathbb{R}^2$ if and only if it intersects its convex hull.*

The following algorithm in pseudocode is based on the above proof, which by its nature is constructive. The function diam determines the diameter of a set. Comments are noted at each ▷ and variable assignments are denoted with := as usual.

Algorithm 1 Determines the intersection of a hyperdense fractal $F \subset \mathbb{R}^2$ and the line $L \subset \mathbb{R}^2$ up to some $\varepsilon > 0$ accuracy along the line, using the convex hull C_F. To be called with $a = (0), I = \varnothing$. Returns the intersection in I.

```
1: function IntFractalLine(I, a, 𝒯, C_F, ε)
2:     if L ∩ T_a(C_F) ≠ ∅ then          ▷ Assuming a subroutine that decides this.
3:         if diam(L ∩ T_a(C_F)) ≤ ε then
4:             return I ∪ (L ∩ T_a(C_F))                    ▷ Update of I occurs.
5:         else
6:             for k ∈ 𝒩 do                                 ▷ Recursive and cumulative loop.
7:                 I := IntFractalLine(I, (a, k), 𝒯, C_F, ε)
8:             end for
9:             return I
10:        end if
11:    else
12:        return I                                         ▷ Nothing added to I.
13:    end if
14: end function
```

2.1.4 Approximate Intersection

We now turn to examining the second question posed earlier, namely the number of intersections within some $\varepsilon > 0$ accuracy. These results are also relevant for applied reasons, such as the signal-reception efficiency of fractal antennas. If an antenna is designed so that it is hyperdense - possibly a chain fractal - then not only will it intercept all signal planes crossing its convex hull - making it space-efficient - but it will do so an infinite number of times, in an approximate sense.

Theorem 2.1.3 *If an open set has a common point with an IFS fractal, then it has an uncountably infinite number.*

Proof Let $S \subset \mathbb{C}$ the open set and $f \in F \cap S$. We may suppose that f has a finite address $a \in \mathcal{A},\ |a| < \infty$, since in the address generation of F, the fractal points with a finite address are dense in F, which is their closure according to Theorem 1.3.2. So we may replace f with another fractal point f' that has a finite address, and which is close enough to f to be still be an element of S. Thus we may suppose that f has a finite address, with a corresponding map T_a and primary fixed point p, meaning $f = T_a(p),\ p \in \mathcal{P}$. Denote the contraction belonging to p as $T \in \mathcal{T}$.
Let $\varepsilon' > 0$ be the radius of some ball centered at f - denoted by $B' := B(f, \varepsilon')$ - that is still contained in S. If we show that there are an uncountably infinite number of fractal points in B', then that implies the theorem.
Let us map back $f = T_a(p)$ and B' by T_a^{-1} to $p = T_a^{-1}(f)$ and $B'' := T_a^{-1}(B') = B(p, \varepsilon'')$ respectively. Here $\varepsilon'' = \frac{\varepsilon'}{|\varphi_a|}$ where φ_a is the product of the factors of the contractions in $\mathcal{T}$ making up T_a. Then since F is compact, we may map it iteratively by T until it is contained in B'', that is $\exists k \in \mathbb{N} : T^k(F) \subset B''$, and clearly $T^k(F)$ has an uncountably infinite number of points.
Mapping it all back by T_a, we have that $T_a \circ T^k(F) \subset F \cap B' \subset F \cap S$. Thus we have shown an uncountably infinite number of common points of F and S. $\square$

Corollary 2.1.2 *If for some $\varepsilon > 0$ the translational neighborhood of a line L*

$$L_\varepsilon^t := \{z \in \mathbb{C} : d_2(L, z) < \varepsilon\}$$

has a common point with an IFS fractal F, then it has an infinite number.

Corollary 2.1.3 *If for some $\varepsilon > 0$ the angular neighborhood of a line L*

$$L_\varepsilon^a := \{z \in \mathbb{C} : \angle(L, z - q) < \varepsilon\}$$

has a common point with an IFS fractal F, then it has an infinite number.

Theorem 2.1.4 *Let $\mathcal{T}$ be a planar similarity IFS with at least one map $T \in \mathcal{T}$ that has a rotation angle ϑ for which $\frac{\vartheta}{2\pi}$ is irrational. Then any line L that intersects $F = \langle \mathcal{T} \rangle$ in some point f with a finite address, intersects it in at least a countably infinite number of points, with any $\varepsilon > 0$ angular accuracy around f, meaning*

$$\forall \varepsilon > 0 \ \exists (f_k)_{k=1}^{\infty} \subset F : \angle(L, f_k - f) < \varepsilon, \ k \in \mathbb{N}.$$

Proof The address of f is finite, meaning that $f = T_a(p), \ p \in \mathcal{P}, \ a \in \mathcal{A}, \ |a| < \infty$. Let us transform back f and L to $p \in \mathcal{P}$ by T_a^{-1}. Then we have that $p = T_a^{-1}(f)$, and denote $L' := T_a^{-1}(L)$ which is also a line. The ε angular neighborhood of L around f is transformed by T_a^{-1} to an ε angular neighborhood of L' around p. Clearly $p \in L'$ since $f = T_a(p) \in L = T_a(L')$. For the theorem to hold, it is sufficient to find an infinite number of fractal points within the angular neighborhood of L', since we can map these points with T_a to the angular neighborhood of L.
Let us choose any $q \in F, \ r \in L'$, with $\alpha := \mathrm{Arg}(q - p), \ \beta := \mathrm{Arg}(r - p)$. Then $\mathrm{Arg}(T^k(q) - p) = (k\vartheta + \alpha) \bmod 2\pi$ and the iterations of q by T will be along a logarithmic spiral around p. We will show that the iterations visit the ε angular neighborhood of L' infinitely often.

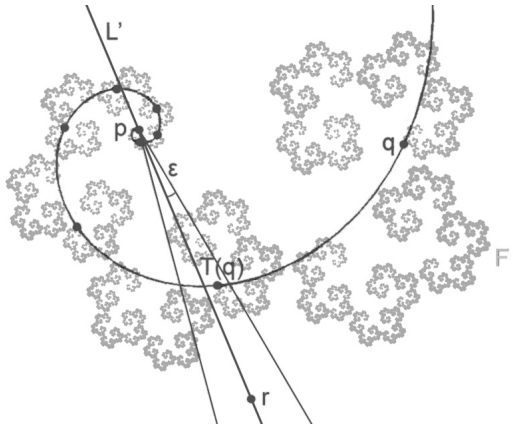

Figure 2.1: Illustration of the ε angular neighborhood of L' around p.

We have supposed that $\frac{\vartheta}{2\pi}$ is irrational, so by the Equidistribution Theorem, the sequence $(k\vartheta \bmod 2\pi)_{k \in \mathbb{N}}$ is uniformly distributed in $[0, 2\pi)$, and thus it is also dense in this interval. So approximating the angle between q and r with respect to p, ie. $\beta - \alpha$, we have the following:

$$\forall j \in \mathbb{N} \ \exists k_j \in \mathbb{N} : ((k_j\vartheta + \alpha) - \beta) \bmod 2\pi < \frac{\varepsilon}{j} < \varepsilon.$$

Therefore the sequence $(T^{k_j}(q))_{j\in\mathbb{N}}$ will be within the ε angular neighborhood of L' with respect to p. Thus mapping the sequence back by T_a, it will be in the required ε angular neighborhood of L with respect to f, and clearly $(T_a \circ T^{k_j}(q))_{j\in\mathbb{N}} \subset F$. So with $f_j := T_a \circ T^{k_j}(q),\ j \in \mathbb{N}$ we have shown a countably infinite number of fractal points in the ε angular neighborhood of the intersecting line. □

Corollary 2.1.4 *Suppose a line intersects a planar IFS fractal in a point with a finite address, and has some $\varepsilon > 0$ angular neighborhood around the point that contains only a finite number of fractal points. Then all contractions in the IFS have a rotation angle ϑ for which $\frac{\vartheta}{2\pi} \in \mathbb{Q}$.*

The above corollary hints at the relevance of a certain class of planar IFS fractals, having roots of unity as rotation factors. They may hold a special place in a theory of the distribution / connectivity of fractal sets. Examining such "rational fractals" further may prove to be a fruitful venture in general, and the case of primitive roots of unity may be even more worthwhile. Indeed these results seem to call for an investigation into the translational and angular distribution of IFS fractals.

The recursive formula for the invariant measure in Section 2.2.2 applied to a Borel set S, assigns weights w_a to each fractal point $T_a(p)$ with an address of length L, and checks which points fall into S, then sums the weight of those points. One may thus find the "density of intersections" with the fractal in between parallel rays of light, reasonably spaced at $\varepsilon := \lambda_{\min}^{L}\mathrm{diam}(\mathcal{P})$, to see the intensity of the shadow in a particular direction, as illustrated on the figure below.

This kind of analysis has clear applications to the design of fractal antennas for instance, and the tomography of fractalline structures.

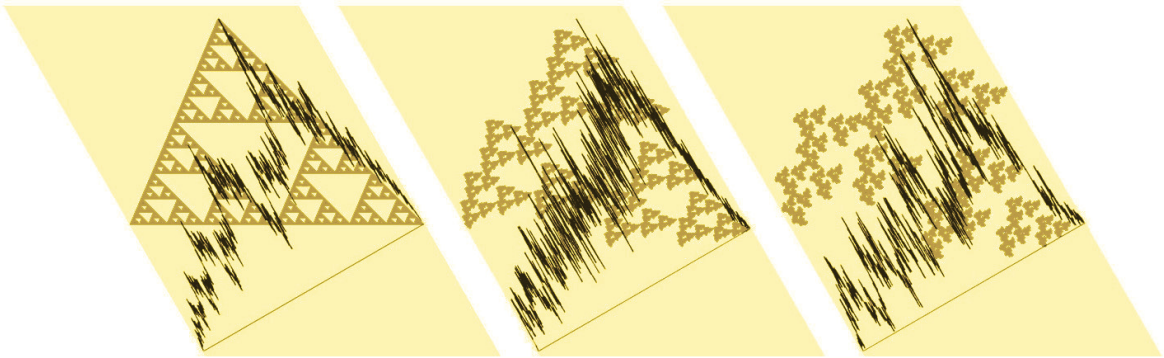

Figure 2.2: Ray absorption density plots under rotational perturbation of the IFS factors.

2.1.5 Concluding Remarks

We have discussed the connection between the projection of IFS fractals and the Fractal-Line Intersection Problem, relevant to applications in computer graphics and antenna design. Classes of fractals have been introduced for which the projection from any direction is a segment in the plane. This was done in a general setting, examining the intersection of hyperplanes and IFS fractals in $\mathbb{R}^d$, $d \in \mathbb{N}$. The method implies an algorithm for finding the points of intersection. Finally the cardinality of the intersection has been determined in the translation and angular neighborhoods of a line.

2.2 Fractal Potential Flows

2.2.1 Introduction

The theory of Fractal Potential Flows is hereby presented in the context of Fractal Analysis. It was formerly introduced in [73] and reasoned to be an idealized exact model for Fully Developed Turbulence (FDT). The model hinges on the recursive iteration of a fluid dynamical transfer operator, often called the Markov operator in the theory of IFS, modelling the interaction of a finite system of eddies. We show the existence of its unique attractor in an appropriate function space - called the invariant flow - which served as a model for the FDT flow field. Its sink singularities are shown to form an IFS fractal.

The contractive action of each eddy sink on the flow field, is modelled with a corresponding pushforward transfer map acting over the stream function, induced by a contraction map of an IFS. Since the collective action of the eddies is probabilistically weighted, it can be interpreted as an "expected value" expression, while physically speaking as the weighted effect each eddy has on the flow field. The iteration of the transfer operator, is reasoned to correspond to the non-smooth discrete energy bursts of intermittency.

Our goal consequently becomes to show that the transfer operator converges to a unique attractor flow - the invariant flow - in some appropriate function space. In finding the correct space, eddies remain our guiding inspiration, considering that a system of eddies becomes a superposed eddy when zoomed out, possessing a complex "character" (Neumann boundary condition) at complex infinity. In their local universe, the eddies interact to produce an increasingly fractalline flow field, approaching the desired invariant flow. The required iteration number to reach the attractor is infinite, while the total time can be potentially finite, if the time-spacing is for instance in geometric regression.

Lastly, the sinks of the invariant flow field are shown to form an IFS fractal, implying the ultimate conclusion that the geometrical study of such sets, is of fundamental relevance to analyzing the invariant flow field.

The key to building this model is the "measure map" which is a bijective isometry linking stream functions to probability measures, for which the unique existence of an invariant measure is known. This is done via Poisson's Equation, which is shown to have a unique solution up to a gradient with the aforementioned boundary condition at infinity (the fundamental solution being an eddy).

The model works for any IFS fractal with zero Lebesgue measure, as a corollary modelling the planar electric field of an IFS fractal antenna.

The current standard model for examining Poisson's Equation over IFS fractals is Kigami's formulation [46, 47, 48], reviewed and further developed by Strichartz [68] and various other researchers. The obvious shortcoming of this rather cumbersome model is that it is limited to a subclass called post-critically finite fractals, while our formulation is not. Though it is true that Kigami's formulation has been generalized to broader classes, the broadest class of all planar IFS fractals is still an open problem. It is hereby resolved for IFS fractals of vanishing Lebesgue measure, which only has a few exceptions like the dragon curves, resolvable via the continuity of the attractor in the IFS parameters.

2.2.2 The Invariant Measure

Theorem 2.2.1 (Kantorovich and Rubinstein [43]) *Let $X \subset \mathbb{R}^2$ be a nonempty compact set, and let $\mathcal{M}_X$ be the set of Borel probability measures over X. Denote with $\mathcal{L}_1(X)$ the Lipschitz-1 functions over X. Then taking any $\nu_{1,2} \in \mathcal{M}_X$ the function*

$$d(\nu_1, \nu_2) = d_X(\nu_1, \nu_2) := \sup \left\{ \int_X f \ \mathrm{d}(\nu_1 - \nu_2) : f \in \mathcal{L}_1(X) \right\}$$

is a metric over $\mathcal{M}_X$, and $(\mathcal{M}_X, d_X)$ is a complete metric space.

The above metric is variously called the Monge-Kantorovich-Rubinstein-Wasserstein-Hutchinson metric after its originators, though in IFS Theory it is usually referred to by the latter name. The theorem is stated in $\mathbb{R}^2$ though it also holds in a more general setting, in particular $\mathbb{R}^d, d \in \mathbb{N}$ as do the following.

A pushforward map (transfer operator) is of the form $T^*\nu = \nu \circ T^{-1}$ ($\nu \in \mathcal{M}_X$). If T^* is contractive in d, then by the Banach Fixed Point Theorem it has a unique invariant measure $\bar{\nu} = T^*\bar{\nu}$. Taking a finite weighted average of such pushforward operators, the resulting weighted transfer operator (sometimes called the Markov operator)

$$\mathrm{T} = w_1 T_1^* + \ldots + w_n T_n^* \quad \text{where} \quad w_k \in (0,1),\ w_1 + \ldots + w_n = 1$$

will also be contractive in d over $\mathcal{M}_X$, and possesses a fixed point. Thus the following theorem holds for an IFS $\{T_1, \ldots, \mathrm{T}_n\}$ in the form $T_k(z) = p_k + \lambda_k R_k(z - p_k),\ z \in \mathbb{R}^2$ supposing that $F \subset X \subset \mathbb{R}^2$.

Theorem 2.2.2 (Hutchinson [41]) *For any IFS $\{T_1, \ldots, T_n\}$ and weights $\{w_1, \ldots, w_n\}$, the transfer operator $\mathrm{T} = w_1 T_1^* + \ldots + w_n T_n^*$ is contractive on $(\mathcal{M}_X, d)$ and attains a unique invariant probability measure $\bar{\nu} = \mathrm{T}\bar{\nu}$ over the compact set $X \subset \mathbb{R}^2$, with support $\langle T_1, \ldots, T_n \rangle$. We call this the invariant measure with respect to the IFS $\{T_1, \ldots, T_n\}$. For any $\nu_0 \in \mathcal{M}_X$ the recursion $\nu_{L+1} = w_1 T_1^* \nu_L + \ldots + w_n T_n^* \nu_L \in \mathcal{M}_X,\ L \in \mathbb{N}$ converges to the invariant measure.*

We remark that with the primary fixed point p and the notations of Section 1.3.2, the measures

$$\nu_0 = \delta_p, \quad \nu_L = \sum_{|a|=L} w_a T_a^* \delta_p \in \mathcal{M}_X,\ L \in \mathbb{N}$$

satisfy the above recursion, and so $\bar{\nu}(S) = \lim(\nu_L)$ as discussed in [72]. We also observe that the support of ν_L is concentrated on the L-th iterate

$$F_L := \mathrm{H}^L(\{p\}) = \{T_a(p) : a \in \mathcal{A}, |a| = L\}$$

approaching the compact IFS fractal $F = \langle T_1, \ldots, T_n \rangle$ by Theorem 1.3.2.

We further remark that defining

$$\mathcal{D}_X := \left\{ \varrho \in C_{ae}(\mathbb{R}^2, \mathbb{R}) : \varrho \geq 0,\ \text{Supp}\ \varrho \subset X,\ \int_X \varrho = 1 \right\}$$

$$\mathcal{P}_X := \left\{ \nu \in \mathcal{M}_X :\ \exists \varrho \in \mathcal{D}_X\ \forall S \subset X \text{ Borel set} : \nu(S) = \int_S \varrho \right\}$$

and keeping the above metric d, then $\mathrm{Conv}\{\delta_p : p \in \mathbb{R}^2\} \subset \mathcal{P}_X \subset \mathcal{M}_X$ and $\bar{\nu} \in \mathcal{P}_X$, so it remains true that there exists a unique invariant measure in $(\mathcal{P}_X, d)$ with respect to T, and it is the same as the earlier one. Furthermore $\mathrm{T} : \mathcal{P}_X \to \mathcal{P}_X$ since $\mathrm{Supp}(\mathrm{T}\nu) = \mathrm{H}(\mathrm{Supp}\ \nu) \subset X$ if $\nu \in \mathcal{P}_X$.

The study of transfer operators - also called Ruelle(-Perron-Frobenius-Markov) operators - is a rich field, and their largest eigenvalue is typically one, while their eigenfunctions are usually fractalline or self-similar in some sense. This has profound implications for classical mechanics, such as the increase of entropy or the irreversibility of time. An eigenvalue of one, corresponds to a state of equilibrium.

For a more complete overview of IFS, the reader is referred to [41, 5, 75, 49].

2.2.3 Potential Flows

Our aim is to link probability measures to potential flows bijectively via Poisson's Equation in the upcoming sections, in order to show the unique existence of an invariant flow. Speaking in terms of Fluid Dynamics, potential flows are assumed to be steady (time-independent), ideal (zero viscosity / inviscid, uniform density, and incompressible), and irrotational (almost everywhere with respect to the Lebesgue measure leb, denoted as a.e.). We derive the stream and potential functions of the superposition of a sink and a vortex, resulting in an eddy.

By the conditions, conservation of mass for a velocity field $v = (v_1, v_2) : \mathbb{R}^2 \to \mathbb{R}^2$ is

$$0 = \text{div } v = \partial_1 v_1 + \partial_2 v_2 \quad \text{a.e.}$$

and the equations of motion become

$$\frac{1}{2}\nabla|v|^2 - v \times \text{curl } v = -\frac{1}{\varrho}\nabla p$$

where ϱ is the density and p is pressure, further reducing to

$$p(z) = \left(p(z_0) + \frac{\varrho}{2}|v(z_0)|^2\right) - \frac{\varrho}{2}|v(z)|^2$$

under the irrotationality requirement

$$0 = \text{curl } v = \partial_2 v_1 - \partial_1 v_2 \quad \text{a.e.}$$

Supposing that $\psi, \phi \in C^2_{ae}(\mathbb{R}^2, \mathbb{R})$ are harmonic conjugates, meaning they satisfy the Cauchy-Riemann Equations

$$\Delta\psi = \Delta\phi = 0 \text{ a.e.} \quad \text{and} \quad \partial_1\phi = \partial_2\psi,\ \partial_2\phi = -\partial_1\psi \text{ a.e.}$$

then $v := -\nabla\phi = \mathrm{i}\nabla\psi$ satisfies mass conservation and irrotationality a.e. The pressure field can be calculated from v as above. We call such a.e. harmonic ψ for which a conjugate exists, the stream function of a potential flow, and ϕ the potential function. We note that the potential function corresponding to a stream function is only unique up to a gradient. Nevertheless we denote it as $\tilde{\psi} := \phi$, and denote equivalence in the gradient as

$$\phi_1 \equiv \phi_2 \ \Leftrightarrow\ \nabla\phi_1 = \nabla\phi_2 \text{ a.e.}$$

A harmonic function is known to admit a conjugate if its domain is simply connected. Furthermore $\tilde{\tilde{\psi}} = -\psi$. By their relation to the velocity field, the curves of constant ψ represent the streamlines of the flow, and the curves of constant ϕ the equipotential lines. Having two pairs of harmonic conjugates ψ_1, ϕ_1 and ψ_2, ϕ_2 their linear combinations $a\psi_1 + b\psi_2$ and $a\phi_1 + b\phi_2$ for any $a, b \in \mathbb{R}$ are also harmonic conjugates. So the principle of superposition holds, as long as the boundary conditions are also correspondingly combined. Since the equations of motion have a unique solution for a set of boundary conditions, and they translate to Laplace's equation (the solution of which for appropriate boundary conditions also exists and is unique up to a gradient), we may conclude that potential flows fully characterize the set of all flows which are steady, ideal, and irrotational a.e.

Elementary potential flows, which are often superposed to create more complex ones, include sinks, sources and the (circular) vortex. The stream and potential functions of a source ($q > 0$) or a sink ($q < 0$) with strength $q \in \mathbb{R}$ are defined at $z \in \mathbb{C}$ as

$$\psi(z) = -\frac{q}{2\pi}\text{Arg } z \bmod |q| \quad \text{and} \quad \phi(z) = -\frac{q}{2\pi}\ln|z|$$

while for the orthogonal circular vortex

$$\psi(z) = \frac{\Gamma}{2\pi}\ln|z| \quad \text{and} \quad \phi(z) = -\frac{\Gamma}{2\pi}\text{Arg } z \bmod |\Gamma|$$

where Γ is the circulation around any closed path containing the vortex (strength of the vortex). Superposing a sink and a circular vortex with a general center $p \in \mathbb{C}$ results in a logarithmic vortex (eddy) as follows

$$\psi(z) = -\frac{q}{2\pi}\text{Arg}(z-p) + \frac{\Gamma}{2\pi}\ln|z-p| \mod |q|$$

$$\phi(z) = -\frac{q}{2\pi}\ln|z-p| - \frac{\Gamma}{2\pi}\text{Arg}(z-p) \mod |\Gamma|.$$

Since ψ is differentiable in the $\mathbb{R}^2$ sense almost everywhere (except at p and along the branch $\psi(z) = q$) we have that the corresponding velocity field (extended continuously to the entire plane) is the following

$$v(z) = \frac{q + \Gamma\mathrm{i}}{2\pi}\frac{1}{|z-p|}\frac{z-p}{|z-p|} \quad (z \in \mathbb{C}).$$

Here we consider the gradient vectors to be on the complex plane and differentiation in the bivariate sense, meaning $\nabla\psi = \partial_1\psi + \mathrm{i}\partial_2\psi$. In general, we will sloppily identify $z \mapsto \psi(z),\ z \in \mathbb{C}$ with $(x, y) \mapsto \psi(x + y\mathrm{i}),\ (x, y) \in \mathbb{R}^2$ when it is more convenient.

2.2.4 Eddy Invariance

The stream function of an eddy with sink strength $q = C \ln \lambda$ and vortex strength or circulation $\Gamma = C\vartheta$ becomes

$$\psi(z) = -\frac{C \ln \lambda}{2\pi} \mathrm{Arg}(z-p) + \frac{C\vartheta}{2\pi} \ln|z-p| \mod -C \ln \lambda$$

where $\varphi \in \mathbb{C},\ \lambda = |\varphi| < 1,\ \vartheta = \mathrm{Arg}\ \varphi$ and $C > 0$ is an arbitrary parameter. The associated velocity field (continuously extended to the entire plane) becomes

$$v[\psi](z) := \frac{C\mathrm{Log}\ \varphi}{2\pi} \frac{1}{|z-p|} \frac{z-p}{|z-p|}.$$

We observe that the eddy stream function is invariant under the contraction $T(z) = p + \varphi(z-p)$, meaning $T^*\psi = \psi$. This is expected geometrically, since the orbit $T^t(z_0) = p + \varphi^t(z_0 - p),\ t \in \mathbb{R}$ traces out a logarithmic spiral centered at $p \in \mathbb{C}$, and the streamlines of constant ψ are spirals of the same pitch. So in other words, ψ is the fixed point of the pushforward transfer operator T^*. This raises the question whether ψ is unique, and if not, then what space would guarantee its uniqueness. Defining $\psi_0(z) := \mathrm{Arg}(z-p) \bmod \vartheta$ we see that $T^*\psi_0 = \psi_0$ also holds, therefore ψ cannot be unique in such a general setting. So our ultimate goal becomes finding the proper function space where uniqueness can be guaranteed, with a reasonable physical interpretation. We begin our search by deriving some fundamental properties of transfer, which will have profound implications.

Theorem 2.2.3 *For a similarity contraction of the form $T(z) = p + \varphi(z-p),\ |\varphi| < 1$ the following properties hold (with differentiation in the $\mathbb{R}^2$ sense, and $v[\psi]$ being the continuous extension of $\mathrm{i}\nabla\psi$ to the plane).*

$$\Delta T^* = \frac{1}{\lambda^2}\, T^*\Delta \quad \textit{and} \quad \widetilde{T^*\psi} \equiv T^*\tilde{\psi} \quad \textit{and} \quad v[T^*\psi] = \frac{\varphi}{|\varphi|^2}\, T^* v[\psi].$$

Proof We show the above in the $\mathbb{R}^2$ sense first, which translates to the complex sense, using $T(z) = p + \lambda R(z-p),\ p, z \in \mathbb{R}^2$ where R is the rotation matrix corresponding to $\mathrm{e}^{\vartheta \mathrm{i}}$. We first show the third property, keeping in mind that $v[\psi](z) = i\nabla\psi(z)$ a.e. Gradient is a column vector in $\mathbb{R}^2$, which corresponds to the complex vector $\partial_1 + \mathrm{i}\partial_2$. Differentiation D results in a row vector however, so we must take a transpose, meaning $\nabla = \mathrm{D}^T$. Applying the generalized chain rule, we get

$$\nabla(\psi \circ T^{-1}) = \mathrm{D}(\psi \circ T^{-1})^T = \left((\mathrm{D}\psi \circ T^{-1}) \cdot \frac{1}{\lambda} R^{-1} \right)^T = \frac{1}{\lambda} R \cdot \nabla\psi \circ T^{-1}.$$

Multiplying by i (90° rotation), we get the third property. To get the first property, we observe that $\Delta = \text{tr } \mathrm{D}\nabla$, so by the Chain Rule, the properties of trace, and the above equation, we may derive

$$\Delta T^*\psi = \text{tr } \mathrm{D}\nabla T^*\psi = \text{tr } \mathrm{D}\left(\frac{1}{\lambda}R \cdot T^*\nabla\psi\right) = \text{tr}\left(\frac{1}{\lambda}R \cdot T^*\mathrm{D}\nabla\psi \cdot \frac{1}{\lambda}R^{-1}\right) = \frac{1}{\lambda^2}T^*\Delta\psi.$$

The second property also follows from the third, observing that in the above complex sense ψ and $\tilde{\psi}$ are conjugates iff $\nabla\psi = \mathrm{i}\nabla\tilde{\psi}$ by Section 2.2.3. So taking T^* of both sides, multiplying by i and dividing by λ, we get that $\nabla(T^*\psi) = \mathrm{i}\nabla(T^*\tilde{\psi})$ implying that $\nabla(T^*\tilde{\psi}) = \nabla(\widetilde{T^*\psi})$ and thus $\widetilde{T^*\psi} \equiv T^*\tilde{\psi}$. □

Among many things, the first property also implies that if ψ is a.e. harmonic then so is $T^*\psi$. Together with the second property, this implies that the space of potential flows is closed under pushforward transfer by a similarity contraction.

One application of T^* to a flow field represented by the stream function, corresponds to a transformation of the field along the logarithmic spiral orbits of T. If T^* can be shown to be contractive over stream functions in some complete space, then the final equilibrium fixed point stream can also be shown.

2.2.5 The Transfer Operator

Considering that potential flows form a vector space as discussed in Section 2.2.3 and by Theorem 2.2.3, the weighted transfer operator

$$\mathrm{T}\psi = w_1 T_1^*\psi + \ldots + w_n T_n^*\psi$$

for any IFS $\{T_1, \ldots, \mathrm{T}_n\}$, $T_k(z) = p_k + \varphi_k(z - p_k)$ and weights $w_k \in (0,1), \sum_k w_k = 1$, maps the stream function of a potential flow to another such flow. One application of T to a flow field corresponds to the weighted application of $T_k^* \in \{T_1^*, \ldots, T_n^*\}$ with probability $\Pr(\mathrm{T}\psi(z_0) = T_k^*\psi(z_0)) = w_k$ at some point $z_0 \in \mathbb{C}$ in the plane. Indeed, the iteration of the transfer operator T corresponds to the intermittent randomly alternating contractive action of a system of n eddies along the orbits of T_k. The partitioning intermittent moments in time t_L can be spaced in any way over the timeline.

We see that after the L-th iteration we have

$$\psi_L = \mathrm{T}^L\psi_0 = \sum_{|a|=L} w_a T_a^*\psi_0$$

where T_a and w_a were defined in Definition 1.3.5. Probabilistically speaking, this implies that ψ_L is the stochastic superposition of n^L eddies with transfers T_a^*, transforming the flow field at the L-th intermittent moment t_L with probabilities

$$\Pr(\psi_L(z_0) = T_a^*\psi_0(z_0)) = w_a \quad (z_0 \in \mathbb{C}).$$

We also note that by Theorem 2.2.3 the corresponding velocity transfer operator is

$$v[\mathrm{T}\psi] = w_1 \frac{\varphi_1}{|\varphi_1|^2}\, T_1^* v[\psi] + \ldots + w_n \frac{\varphi_n}{|\varphi_n|^2}\, T_n^* v[\psi]$$

There are two possible interpretations of the weighted transfer iteration - probabilistic and physical. Probabilistically it means that considering the next iterate $\psi_{L+1}(z_0)$ to be a random variable located at each $z_0 \in \mathbb{C}$, its expected value is $\mathrm{T}\psi_L(z_0)$. Physically, weighted transfer can be interpreted as weighting the effect each eddy - represented by T_k^* - has on the fluid at an intermittent moment at a particular point in space. This is essentially a random walk over logarithmic spirals.

It is conjectured that the iteration of T ad infinitum converges to an invariant flow $\mathrm{T}\bar{\psi} = \bar{\psi}$. Showing the unique existence of this $\bar{\psi}$ becomes our primary goal, along with finding an appropriate function space where this is possible.

Theorem 2.2.4 *For the weighted transfer operator* T *the following properties hold*

$$\Delta \mathrm{T} = \sum_{k=1}^{n} \frac{w_k}{\lambda_k^2}\, T_k^* \Delta \quad \textit{and} \quad \widetilde{\mathrm{T}\psi} \equiv \mathrm{T}\tilde{\psi} \quad \textit{and} \quad v[\mathrm{T}\psi] = \sum_{k=1}^{n} w_k \frac{\varphi_k}{|\varphi_k|^2}\, T_k^* v[\psi].$$

Proof The proof follows from Theorem 2.2.3. Note that the first property implies the preservation of harmonicity a.e. or physicality upon transfer, as discussed in Section 2.2.3. □

2.2.6 Flow Character

In constructing the proper flow space, our inspiring objective is to ensure the unique existence of an eddy as the attractor of its generating pushforward transfer map. In resolving this question, we show a correspondence between eddies and the Dirac delta function, which hints at a possible general correspondence between stream functions and the density functions of probability measures, via Poisson's Equation. Finding the ideal kind of boundary condition will prove crucial to our quest, and meanwhile the proper space of flows shall slowly reveal itself.

First of all, we observe that the velocity field of the eddy discussed in Section 2.2.4 is characterized by the complex parameter $c = \frac{C}{2\pi}\text{Log } \varphi$ which can be extracted from the stream function ψ by the operation

$$v[\psi](z)\ \overline{z-p} = c\ \frac{z-p}{|z-p|^2}\ \overline{z-p} = c.$$

We will denote the stream function of an eddy with character $c \in \mathbb{C},\ \text{Re } c < 0$ and centered at $p \in \mathbb{C}$, with $q_c := -2\pi\text{Re } c,\ \Gamma_c := 2\pi\text{Im } c$ as

$$\psi_{c,p}(z) := \frac{q_c}{2\pi}\text{Arg}(z-p) + \frac{\Gamma_c}{2\pi}\ln|z-p| \mod q_c \quad \text{and} \quad \psi_c := \psi_{c,0}.$$

Certain flows may have a similar "eddy character" when their flow field is zoomed out, even if they exhibit varying streamline behaviour locally around the origin, as defined below.

Definition 2.2.1 *We say that a stream function $\psi : \mathbb{C} \to \mathbb{R}$ satisfies the boundary condition at infinity with* ***character*** *$c \in \mathbb{C}$, if for any $p \in \mathbb{C}$ and any sequence $(z_j) \subset \mathbb{C}, |z_j - p| \to \infty$ we have $\exists \lim_{j\to\infty} v[\psi](z_j)\ \overline{z_j - p} = c$ where the limit is taken in the complex sense. We denote this property as $\psi \in BC_c^\infty$ or $\text{char}(\psi) = c$.*

We remark that character is independent of the choice of $p \in \mathbb{C}$. To see this, take

$$\lim_{j\to\infty}|v[\psi](z_j)| = \lim_{j\to\infty}\left|\frac{v[\psi](z_j)\ \overline{z_j-p}}{\overline{z_j-p}}\right| = \lim_{j\to\infty}\frac{|c|}{|z_j-p|} = 0$$

so $\lim(v[\psi](z_j)) = 0$. Taking some other $p' \in \mathbb{C}$ we have for the above (z_j) that $|z_j - p'| \to \infty$ since $|z_j - p| \le |z_j - p'| + |p' - p|$ and that

$$v[\psi](z_j)\ \overline{z_j - p'} = v[\psi](z_j)\ \overline{z_j - p} + v[\psi](z_j)\ \overline{p - p'}\ \to\ c + 0 = c \ \text{ as } \ j \to \infty.$$

Theorem 2.2.5 *Character is a linear map that is invariant under weighted transfer, or convolution with a density function over the plane.*

Proof The linearity of char is trivial by definition. Let us suppose that $\mathrm{char}(\psi) = c$. Since for some p and (z_j), $|z_j - p| \to \infty$ sequence $z_j - p = \varphi_k(T_k^{-1}(z_j) - p_k) + (p_k - p)$ and applying Theorem 2.2.3 we have that

$$v[\mathrm{T}\psi](z_j)\ \overline{z_j - p} = \sum_{k=1}^{n} w_k \frac{\varphi_k}{|\varphi_k|^2}\ v[\psi](T_k^{-1}(z_j))\ \overline{\varphi_k(T_k^{-1}(z_j) - p_k) + (p_k - p)} =$$

$$= \sum_{k=1}^{n} w_k \frac{\varphi_k \bar{\varphi}_k}{|\varphi_k|^2}\ v[\psi](T_k^{-1}(z_j))\ \overline{T_k^{-1}(z_j) - p_k} + \sum_{k=1}^{n} w_k \frac{\varphi_k}{|\varphi_k|^2}\ v[\psi](T_k^{-1}(z_j))\ \overline{p_k - p}$$

which approaches $\sum_k w_k c + \sum_k 0 = c$ as $j \to \infty$ meaning $\mathrm{char}(\mathrm{T}\psi) = c$.
Now let ϱ be a density function over $\mathbb{R}^2$ and (z_j) be the above sequence. We employ scalar and complex vector Riemann integrals as follows

$$\nabla(\psi * \varrho)(z) = \int_{\mathbb{R}^2} \nabla\psi(z - w)\varrho(w)\ \mathrm{d}w \quad \Rightarrow \quad v[\psi * \varrho](z_j)\ \overline{z_j - p} =$$

$$= \int_{\mathbb{R}^2} \mathrm{i}\nabla\psi(z_j - w)\ \overline{(z_j - w) - (p - w)}\ \varrho(w)\ \mathrm{d}w \quad \to \quad \int_{\mathbb{R}^2} c\varrho(w)\ \mathrm{d}w = c \ \text{ as } \ j \to \infty. \ \square$$

In what follows, we will denote with $L^\infty(\mathbb{R}^2)$ the set of bounded functions over the plane, and with $C^2_{ae}(\mathbb{R}^2)$ the a.e. defined and twice a.e. continuously differentiable functions ψ, for which $\mathrm{i}\nabla\psi$ can be continuously extended to the entire plane, denoted as $v[\psi]$, furthermore the set of singularities S_ψ of $v[\psi]$ is compact and nonempty.

Theorem 2.2.6 *For any density function ϱ over the plane and any $c \in \mathbb{C}$, $\mathrm{Im}\ c \neq 0$, there exists a $\psi \in L^\infty(\mathbb{R}^2) \cap C^2_{ae}(\mathbb{R}^2) \cap BC^\infty_c$ for which $\Delta\psi = \Gamma_c\varrho$* a.e. *Furthermore, this ψ is unique up to a gradient* (a.e.) *and $\psi = \psi_c * \varrho$.*

Proof The existence of such a ψ is guaranteed using the Green function method of convolving the fundamental solution ψ_c ($\Delta\psi_c = \Gamma_c\delta_0$ a.e.) with ϱ which will also have a character of c by the previous theorem, and will also be bounded by trivial calculation. Furthermore, convolution is known to preserve differentiability as many times as its terms are differentiable in total.
Let us proceed to the question of uniqueness (up to a gradient), and suppose indirectly that $\exists\psi_{1,2} \in BC^\infty_c, \psi_1 \not\equiv \psi_2$ such that $\Delta\psi_1 = \Gamma_c\varrho = \Delta\psi_2$ a.e. Then $\Delta\psi = 0$ a.e. with

$\psi := \psi_1 - \psi_2$. By the Divergence Theorem, for some compact $S \subset \mathbb{R}^2$ with piecewise smooth boundary

$$\int_S |\nabla\psi|^2 = \int_S |\nabla\psi|^2 + \psi\Delta\psi = \int_S \operatorname{div}(\psi\nabla\psi) = \int_{\partial S} \psi\langle\nabla\psi, u\rangle.$$

Since $\psi_{1,2}$ are bounded, then so is ψ with say $|\psi| \leq M$.
So for any sequence of disks $S_j := B(p, r_j),\ 0 < r_j < r_{j+1},\ j \in \mathbb{N},\ \lim(r_j) = \infty$ for which $S_\psi \subset S_1,\ \partial S_\psi \cap \partial S_1 = \varnothing$

$$\int_{S_j} |\nabla\psi|^2 = \left| \int_{\partial S_j} \psi\langle\nabla\psi, u\rangle \right| \leq M \int_{\partial S_j} \left| \left\langle \nabla\psi(z), \frac{z-p}{|z-p|} \right\rangle \right| \mathrm{d}z \leq M \int_{\partial S_j} |v[\psi](z)|\ \mathrm{d}z$$

where the integrals are in the usual $\mathbb{R}^2$ sense. If we can show that this last integral vanishes as $j \to \infty$, then $\int_{\mathbb{R}^2} |\nabla\psi|^2 = 0$ and so $\nabla\psi = 0$ a.e. which would contradict $\psi_1 \not\equiv \psi_2$.
Let us define $z_j := \operatorname{argmax}_{z\in\partial S_j} |v[\psi](z)|,\ j \in \mathbb{N}$ which exist by the Extreme Value Theorem, considering the compactness of ∂S_j and the continuity of $v[\psi]$ on $\partial S_j \subset \mathbb{R}^2 \backslash S_\psi$. Since $z_j \in \partial S_j,\ j \in \mathbb{N}$ we have $|z_j - p| = r_j \to \infty,\ j \to \infty$ which by $\operatorname{char}(\psi_{1,2}) = c$ implies that $v[\psi](z_j)\ \overline{z_j - p} \to 0$ so

$$\int_{\partial S_j} |v[\psi](z)|\ \mathrm{d}z \leq \int_{\partial S_j} |v[\psi](z_j)|\ \mathrm{d}z = |v[\psi](z_j)\ \overline{z_j - p}|\ \frac{1}{|z_j - p|}\ 2\pi r_j\ \to\ 0\ \text{ as }\ j \to \infty. \square$$

By the above results, we may conclude among many things that the eddy $\psi_{c,p}$ uniquely corresponds via Poisson's Equation to the Dirac delta function δ_p among all bounded functions of character c, where the uniqueness is guaranteed up to a gradient.

2.2.7 The Flow Space

Definition 2.2.2 *Let $X \subset \mathbb{R}^2$ be a compact set that contains the IFS fractal $F = \langle T_1, \ldots, T_n \rangle \subset X$, $\text{leb}(F) = 0$ and $c \in \mathbb{C}$ some number for which $\text{Re } c < 0$, $\text{Im } c \neq 0$. For a function $\psi \in C^2_{ae}(\mathbb{R}^2)$ define*

$$\mu[\psi](S) = \mu_c[\psi](S) := \frac{1}{\Gamma_c} \int_S \Delta\psi \quad (S \subset \mathbb{R}^2).$$

*Let the set of **flows** with character c be defined as*

$$\Psi_{X,c} := \{\psi \in C^2_{ae}(\mathbb{R}^2) \cap BC^\infty_c : \ \text{Ran}(\psi) \subset [0, q_c), \ \mu[\psi] \in \mathcal{P}_X\}.$$

*We will call $\mu : \Psi_{X,c} \to \mathcal{P}_X$ the **measure map**, and $\mu[\psi]$ the **induced measure** by ψ. Recalling the metric d from Section 2.2.2, for any $\psi_{1,2} \in \Psi_{X,c}$ denote*

$$D(\psi_1, \psi_2) = D_{X,c}(\psi_1, \psi_2) := d(\mu[\psi_1], \mu[\psi_2]) = \sup \left\{ \frac{1}{\Gamma_c} \int_X f \ \Delta(\psi_1 - \psi_2) : f \in \mathcal{L}_1(X) \right\}.$$

*As in Section 2.2.3, we will consider two flows $\psi_{1,2} \in \Psi_{X,c}$ to be **congruent** $\psi_1 \equiv \psi_2$ iff $\nabla\psi_1 = \nabla\psi_2$ a.e. over X. Let the equivalence classes be denoted as*

$$[\psi] := \{\psi_0 \in \Psi_{X,c} : \psi \equiv \psi_0\}, \quad [\Psi_{X,c}] := \{[\psi] : \psi \in \Psi_{X,c}\} = \Psi_{X,c}/\text{Ker}(\mu_c).$$

Further denote $D([\psi_1], [\psi_2]) = D_{X,c}([\psi_1], [\psi_2]) := D_{X,c}(\psi_1, \psi_2)$.
*Then we call $([\Psi_{X,c}], D)$ the **flow space** over X with character c.*

Theorem 2.2.7 *$([\Psi_{X,c}], D)$ is a well-defined metric space. The above measure map $\mu : [\Psi_{X,c}] \to \mathcal{P}_X$ is an isometric isomorphism, and the weighted transfer operator preserves flows $\mathrm{T} : \Psi_{X,c} \to \Psi_{X,c}$. Furthermore, the two maps commute.*

Proof First of all, we observe that $\mu : [\Psi_{X,c}] \to \mathcal{P}_X$ is clearly an isometry, since by definition $d(\mu[\psi_1], \mu[\psi_2]) = D([\psi_1], [\psi_2])$. μ is bijective iff $\forall \nu \in \mathcal{P}_X \ \exists! [\psi] \in [\Psi_{X,c}] : \mu[\psi] = \nu$. The equality $\mu[\psi] = \nu$ here means that with the density function ϱ belonging to $\nu \in \mathcal{P}_X$ we need

$$\mu[\psi](S) = \frac{1}{\Gamma_c} \int_S \Delta\psi = \nu(S) = \int_S \varrho \quad \forall S \subset X$$

which is equivalent to $\Delta\psi = \Gamma_c \varrho$ a.e. on X by the du Bois-Reymond Lemma. The unique existence of such a $\psi \in \Psi_{X,c}$ for any ϱ was shown in Theorem 2.2.6 up to a

gradient, meaning up to a congruence or equivalence class. So we have that μ is a bijective isometry, also called an isometric isomorphism.
For the well-definition of the space, we must show that D is a metric over the set $[\Psi_{X,c}]$. D is positive, symmetric, and inherits the triangle inequality from d. The only question that remains is whether $D([\psi_1],[\psi_2]) = 0$ implies $[\psi_1] = [\psi_2]$. Since $0 = D([\psi_1],[\psi_2]) = d(\mu[\psi_1],\mu[\psi_2])$ we have that $\mu[\psi_1] = \mu[\psi_2]$, and since μ has been shown to be bijective, this implies that $[\psi_1] = [\psi_2]$ or $\psi_1 \equiv \psi_2$.
We go on to showing that T and μ commute, meaning $\mathrm{T}\mu = \mu\mathrm{T}$. We recall from Theorem 2.2.4 that

$$\Delta(\mathrm{T}\psi)(z) = \sum_{k=1}^{n} \frac{w_k}{\lambda_k^2}\ (\Delta\psi) \circ T_k^{-1}(z)$$

and also see that for any $S \subset X \subset \mathbb{R}^2$ and $k \in \{1,\dots,n\}$, by taking Riemann integrals over $\mathbb{R}^2$ we have that

$$\mu[T_k^*\psi](S) = \frac{1}{\Gamma_c}\int_S \Delta(\psi \circ T_k^{-1}) = \frac{1}{\Gamma_c}\int_S \frac{1}{\lambda_k^2}(\Delta\psi)(T_k^{-1}(z))\ \mathrm{d}z =$$

$$= \frac{1}{\Gamma_c}\int_{T_k^{-1}(S)} \Delta\psi(w)\ \mathrm{d}w = \mu[\psi](T_k^{-1}(S)) = (T_k^*\mu[\psi])(S)$$

so taking a convex combination and using the linearity of μ we have the desired property $\mu[\mathrm{T}\psi] = \mathrm{T}\mu[\psi],\ \psi \in \Psi_{X,c}$ or succinctly $\mu\mathrm{T} = \mathrm{T}\mu$.
Lastly, we show that T maps from $\Psi_{X,c}$ to itself. T preserves $C^2_{ae}(\mathbb{R}^2)$ since $S_{\mathrm{T}\psi} = H(S_\psi)$, and it also preserves character according to Theorem 2.2.5. Since T is a convex combination, it preserves that $\mathrm{Ran}(\mathrm{T}\psi) \subset [0, q_c)$. Furthermore, we have that $\mu[\mathrm{T}\psi] = \mathrm{T}\mu[\psi] \in \mathcal{P}_X$ since $\mu[\psi] \in \mathcal{P}_X$ and the measure transfer is known to map $\mathrm{T} : \mathcal{P}_X \to \mathcal{P}_X$ by Section 2.2.2. □

The above space $([\Psi_{X,c}], D)$ represents the fact that the intermittent interaction of a system of n eddies, can be considered in a locally isolated manner over a compact $X \subset \mathbb{R}^2$ of reasonable scale. $[\Psi_{X,c}]$ versus $\Psi_{X,c}$ signifies that it is only the velocity field induced by a stream function that matters. Prior to the start of their interaction, the eddies ψ_{c_k,p_k} (notation of Section 2.2.6) superpose initially in a flow with a certain character c as follows. Letting $\psi_0 := \sum_k w_k T_k^* \psi_{c_k,p_k}$ then by Theorem 2.2.3

$$v[\psi_0] = \sum_{k=1}^{n} w_k \frac{\varphi_k}{|\varphi_k|^2}\ T_k^* v[\psi_{c_k,p_k}] = \sum_{k=1}^{n} w_k\ v[\psi_{c_k,p_k}]$$

so clearly $c = \mathrm{char}(\psi_0) = \sum_k w_k c_k$. As the intermittent interaction of the eddies progresses according to the transfer operator T, their overall character will be preserved to be this c by Theorem 2.2.5.

2.2.8 The Invariant Flow

Theorem 2.2.8 *The transfer operator* T *is contractive over* $([\Psi_{X,c}], D)$. *For any* $\psi_0 \in \Psi_{X,c}$ *the iteration* $\psi_{L+1} = \mathrm{T}\psi_L \in \Psi_{X,c}$ *converges to*

$$\bar{\psi} = \psi_c * \bar{\nu} = \lim_{L\to\infty} \sum_{|a|=L} w_a \psi_c(\cdot - T_a(p)) \in \Psi_{X,c}$$

for which $\mathrm{T}\bar{\psi} \equiv \bar{\psi}$, *and here* $\bar{\nu}$ *is the invariant measure of Theorem 2.2.2 and* p *is the primary fixed point. We will call this* $\bar{\psi}$ *the invariant flow (or fractal potential flow) with respect to the IFS* $\{T_1, \ldots, T_n\}$, *the weights* $\{w_1, \ldots, w_n\}$, *the compact set* X, *and character* $c \in \mathbb{C}$.

Proof The contractivity of transfer over stream functions, follows directly from that of the measure transfer in Theorem 2.2.2, considering that the measure map is isometric by definition.
At this point one would expect to show the completeness of $([\Psi_{X,c}], D)$ in order to conclude the unique existence of a fixed flow of T by the Banach Fixed Point Theorem. This however becomes unnecessary, considering that we have an isometric isomorphism $\mu : [\Psi_{X,c}] \to \mathcal{P}_X$ between flows and measures, which commutes with T by Theorem 2.2.7. By Theorem 2.2.2 and the remarks we have made on it, there exists a unique $\bar{\nu} \in \mathcal{P}_X$: $\mathrm{T}\bar{\nu} = \bar{\nu}$. By Theorem 2.2.7 there exists a unique $[\bar{\psi}] \in [\Psi_{X,c}] : \mu[\bar{\psi}] = \bar{\nu}$ and

$$\mu[\mathrm{T}\bar{\psi}] = \mathrm{T}\mu[\bar{\psi}] = \mathrm{T}\bar{\nu} = \bar{\nu} = \mu[\bar{\psi}] \;\Rightarrow\; \mathrm{T}\bar{\psi} \equiv \bar{\psi}$$

since μ is bijective. Now let us suppose indirectly that $[\bar{\psi}]$ is not a unique fixed point, meaning there is another $\psi \not\equiv \bar{\psi}$ for which $\mathrm{T}\psi \equiv \psi$. Then

$$\mu[\psi] = \mu[\mathrm{T}\psi] = \mathrm{T}\mu[\psi] \;\Rightarrow\; \mu[\psi] = \bar{\nu} = \mu[\bar{\psi}] \;\Rightarrow\; \psi \equiv \bar{\psi}$$

which is a contradiction.
Now let $\psi_0 \in \Psi_{X,c}$ be any flow, and consider the recursion $\psi_{L+1} = \mathrm{T}\psi_L \in \Psi_{X,c}$ and define $\nu_L := \mu[\psi_L]$. Then $\nu_{L+1} = \mu[\mathrm{T}\psi_L] = \mathrm{T}\nu_L$ so by Theorem 2.2.2 we have that $\exists \lim(\nu_L) = \bar{\nu}$ in $(\mathcal{P}_X, d)$. Since $D([\,\cdot\,], [\,\cdot\,]) = d(\mu[\,\cdot\,], \mu[\,\cdot\,])$ and μ is injective, we have that $\exists \lim([\psi_L]) = [\bar{\psi}]$.
We proceed to characterizing the exact form of $\bar{\psi}$. From Section 2.2.2 we recall that

$$\bar{\nu} = \lim_{L\to\infty} \sum_{|a|=L} w_a T_a^* \delta_p.$$

From the proof of Theorem 2.2.6 we see that $\psi_c \in \Psi_{X,c} : \Delta\psi_c = \Gamma_c\delta_0$ so

$$\bar{\psi} = \psi_c * \bar{\nu} = \lim_{L\to\infty} \sum_{|a|=L} w_a \psi_c * (\delta_p \circ T_a^{-1}) = \lim_{L\to\infty} \sum_{|a|=L} w_a \psi_c(\cdot - T_a(p)). \ \square$$

We remark that $\Delta\bar{\psi} = 0$ a.e. and if $\Delta\psi_0 = 0$ a.e. then $\Delta\psi_L = 0$ a.e. $(L \in \mathbb{N})$. Furthermore, taking $\psi_0 := \psi_{c,p}$

$$\mathrm{T}^L\psi_{c,p} = \sum_{|a|=L} w_a T_a^*\psi_{c,p} \equiv \sum_{|a|=L} w_a \psi_c(\cdot - T_a(p)) \pmod{q_c}.$$

The first equality is clear, while the second equivalence requires some consideration. By the Slope Lemma $z - T_a(p) = \varphi_a(T_a^{-1}(z) - p)$, and since $\psi_{c,p} = \psi_c(\cdot - p)$ we have

$$\psi_{c,p}(T_a^{-1}(z)) = \psi_c(T_a^{-1}(z) - p) \equiv \psi_c(z - T_a(p)) - \psi_c(\varphi_a) \pmod{q_c}.$$

Summing over all addresses $|a| = L$ with factors w_a we get the earlier congruence.

Examining the intriguing quantities $\psi_c(\varphi_a)$ further, using the notations of Definition 1.3.5, we see that

$$\sum_{|a|=L} w_a \psi_c(\varphi_a) \equiv \frac{q_c}{2\pi} \sum_{|a|=L} w_a \vartheta_a + \frac{\Gamma_c}{2\pi} \sum_{|a|=L} w_a \ln \lambda_a \pmod{q_c}.$$

Choosing the weights $w_k = \lambda_k^s$ (where $s > 0$, $\sum_k \lambda_k^s = 1$ is the so-called pseudodimension of the IFS fractal $\langle T_1, \ldots, T_n\rangle$ which corresponds to its Hausdorff dimension if the open set condition holds) we have as the factor of $\frac{\Gamma_c}{2\pi}$ above the following quantity

$$-\frac{1}{s} \sum_{|a|=L} \lambda_a^s \ln \lambda_a^s = -\frac{1}{s} \sum_{|a|=L} w_a \ln w_a.$$

Considering the weights $w_k = \lambda_k^s$ to be probabilities, this is the Gibbs Entropy Formula for a collection of classical particles. This can be interpreted as the entropy of the set of points $F_L = \{T_a(p) : a \in \mathcal{A}, |a| = L\}$ at each level $L \in \mathbb{N}$ during the Chaos Game evolution towards the IFS fractal attractor $F = \langle T_1, \ldots, T_n\rangle = \mathrm{Cl}\{T_a(p) : a \in \mathcal{A}\}$. Remarkably $\frac{1}{s}$ plays the role of Boltzmann's constant, hinting at some potentially deeper interpretations.

2.2.9 The Evolution towards Invariance

An interesting question is whether invariance can be achieved in finite time. The answer is, it certainly can due to the observation that the iterative steps need not occur at equal time intervals, and in fact the spacing in time can be arbitrary. If the time spacing of each iteration decreases say geometrically, then the total time to reach the $L = \infty$ level iteration (corresponding to $\bar{\psi}$) will be finite. This is clearly true for any convergent sequence of time spacing.

Another question which may arise when considering the previous sections, is how the global superposition of n pushforwarded stream functions according to the transfer operator T relates to the local picture of the splitting of eddies. Upon some contemplation, we may realize that the global and local viewpoints are the direct consequence of the associativity of transfer $\mathrm{T}(\mathrm{T}^L\psi_{c,p}) = \mathrm{T}^L(\mathrm{T}\psi_{c,p})$. Executing an iteration of T over the entire flow field $\mathrm{T}^L\psi_{c,p}$ corresponds to the local intermittent splitting of the initial eddy $\psi_{c,p}$ into n eddies $\mathrm{T}\psi_{c,p}$ and therefore the splitting of all of its level L iterates.

2.2.10 Equilibrium Points of the Invariant Flow

From the representation shown for the invariant flow

$$\bar{\psi}(z) = \lim_{L\to\infty} \sum_{|a|=L} w_a \psi_c(z - T_a(p))$$

where the limit is taken in the sense of $([\Psi_{X,c}], D)$, we see that $\bar{\psi}$ is an infinite shifted superposition of the eddy ψ_c of character c, preserved by $\bar{\psi}$. Since ψ_c is centered at the origin, each weighted eddy $w_a\psi_c(z - T_a(p))$ is centered at $T_a(p)$. Therefore the set of sink singularities of $\bar{\psi}$ is the IFS fractal $F = \langle T_1, \ldots, T_n\rangle = \mathrm{Cl}\{T_a(p) : a \in \mathcal{A}\}$ where p is the primary fixed point. Note that it was assumed in Definition 2.2.2 that $\mathrm{leb}(F) = 0$, since IFS fractals mostly have a non-integer Hausdorff dimension and thus zero Lebesgue measure, but in certain special cases, such as Dragon Curves, the dimension can equal two (resolved in Section 2.2.12).

Since the flow concentrates on an IFS fractal, we must focus our efforts on the geometrical study of such sets, in order to uncover the characteristics of fractal potential flows. We also emphasize that by Theorems 2.2.3 and 2.2.4, having similarity contractions is necessary for preserving the harmonicity of flows under transfer.

When visualizing $\mathrm{T}^L\psi_{c,p}$ for large enough $L \in \mathbb{N}$, one observes a thinning of the basins of attraction of each eddy center $F_L = \{T_a(p) : a \in \mathcal{A}, |a| = L\}$ which raises the question whether the thinning continues on to a width of zero. The basins are partitioned by directrices (manifolds) of the saddle points (hyperbolic equilibria) of the flow field. In the neighbourhood of each partitioning infinite separatrix (stable manifold) belonging to these saddles (the unstable one ending in sinks), the flow behaviour becomes chaotic - meaning a tracer particle starting down the streamline near one side of the separatrix, may end up at a distant sink singularity, relative to if it had started near the other side. When the flow field is considered as the phase portrait of a Hamiltonian system, then this signifies sensitivity to initial conditions near the particular separatrix. For the entire flow field to be considered chaotic, we must show that such partitioning separatrices "cover" the flow field, in some sense. We also intuit that this covering would be implied if the saddle points could be shown to be dense in the IFS fractal F.

Conjecture 2.2.1 *The infinite separatrices of the saddle points of $\bar{\psi}$ are dense in $\mathbb{R}^2$.*

Conjecture 2.2.2 *The saddle points of $\bar{\psi}$ are dense in $F = \langle T_1, \ldots, \mathrm{T}_n\rangle$.*

It is further conjectured that the second conjecture implies the first.

2.2.11 The Inverse Problem

We now turn to translating the well-known inverse problem of IFS to fractal potential flows. We will discuss the corresponding necessary Collage Theorem, as well as the continuity of the invariant flow in the IFS parameters. Lastly, we mention some solution approaches from the literature.

Problem 2.2.1 (Inverse Problem - Applications) *Given a finite number of intermittently stirred eddies, model their resulting interaction region as closely as possible.*

In terms of the introduced model, this vaguely stated problem becomes the following more precise formulation, based on articles [6, 73] and further detailed in [75, 49].

Problem 2.2.2 (Inverse Problem - Theoretical) *Given a target flow $\psi \in \Psi_{X,c}$ and an $\varepsilon > 0$ accuracy, find an IFS of similarity contractions $\{T_1, \dots, T_n\}$ and weights $\{w_1, \dots, w_n\}$ for some given $n \in \mathbb{N}$, such that for the induced invariant flow $\bar{\psi}$ we have*

$$D(\psi, \bar{\psi}) = \sup_{f \in \mathcal{L}_1(X)} \frac{1}{\Gamma_c} \int_X f \ \Delta(\psi - \bar{\psi}) \ < \varepsilon.$$

The computation of D can be carried out according to existing efficient methods for the Hutchinson metric [11, 25], considering that $D(\psi_1, \psi_2) = d(\mu[\psi_1], \mu[\psi_2])$. As we have seen in Theorem 2.2.7, the measure map μ is an isometric isomorphism between measures $\mathcal{P}_X$ and flows $\Psi_{X,c}$ (for some fixed c character). Viewing each element of $\mathcal{P}_X$ as a (potentially infinite) convex combination of Dirac deltas, the metric D measures the difference between flows according to the power of their constituent sink singularities. So the inverse problem is about matching singularities. The rest of the flow field is only consequential, due to Poisson's Equation and the boundary condition called character (Theorem 2.2.6). We interpret another crucial result from article [6].

Theorem 2.2.9 (Collage Theorem) *Let $\psi \in \Psi_{X,c}$ be a target flow, and suppose that there exists an IFS $\{T_1, \dots, T_n\}$ and weights $w_1, \dots, w_n$ for some $n \in \mathbb{N}$ such that*

$$D(\psi, \mathrm{T}\psi) < (1 - \lambda_*)\varepsilon \quad \text{with} \quad \lambda_* := \max_{k \in \mathcal{N}} \lambda_k$$

where $\mathrm{T} = w_1 T_1^* + \ldots + w_n T_n^*$. Then for its attractor $\bar{\psi} \equiv \mathrm{T}\bar{\psi}$ we have $D(\psi, \bar{\psi}) < \varepsilon$.

Proof It follows from the triangle inequality for D. □

The above theorem allows us to design algorithms for resolving the inverse problem, which focus on improving / minimizing the distance $\mathrm{T} \mapsto D(\psi, \mathrm{T}\psi)$ over all transfer operators (i.e. varying IFS parameters and weights), for the given fixed ψ. Then the attractor $\bar{\psi}$ of this approximate minimizer T will be "close" to ψ, i.e. resolve the inverse problem up to the required ε accuracy. The Collage Theorem thus greatly simplifies this resolution, as originally discussed in [6]. The following is a straightforward translation of the result by Centore and Vrscay [14].

Theorem 2.2.10 (Continuity of the Invariant Flow in Transfer Parameters)
Let $\mathcal{T}_{X,c}$ be the set of all transfer operators $\mathrm{T} : \Psi_{X,c} \to \Psi_{X,c}$ with respect to any IFS and weights. Taking any two transfer operators $\mathrm{T}_{1,2} \in \mathcal{T}_{X,c}$ with contraction factors $c_{1,2} \in (0,1)$ and corresponding invariant flows $\bar{\psi}_{1,2} \in \Psi_{X,c}$ then

$$D(\bar{\psi}_1, \bar{\psi}_2) \;\leq\; \frac{1}{1 - \min(c_1, c_2)} \sup_{\psi \in \Psi_{X,c}} D(\mathrm{T}_1(\psi), \mathrm{T}_2(\psi)).$$

This theorem tells us that if the transfer operators T_1 and T_2 are close in the above supremum metric, then so will their attracting invariant flows $\bar{\psi}_{1,2}$ be. This ensures the stability of the aforementioned process of minimization.

The solution approaches to the Inverse Problem come in many forms. They often rely on the fact that convergence in moments implies convergence in the Hutchinson metric, based on the idea of "moment matching" [5, 76, 12, 34], oft-performed via gradient methods [76], simulated annealing with memory [57], and genetic algorithms [75]. Other methods include "exact methods" for solving the IFS inverse problem [24], as well as the methods of Barnsley and Iterated Systems Inc., reported by Lu [54].

For a recent survey of the aforementioned techniques, see [49].

2.2.12 Degenerate Cases

There are two possible ways the above model may degenerate. The first is when $\Gamma_c = 0$ in the measure map, seemingly preventing the rest of the discussion, from Definition 2.2.2 onwards. This case can be resolved rather easily however, and it is important because it models the planar electric field of an IFS fractal.

We split the initial stream function ψ_0 of character $c = \operatorname{Re} c < 0$ into the average of two $\psi_{1,2}$ with characters $c_{1,2} := \operatorname{char}(\psi_{1,2}) = c \pm d\mathrm{i}$ for some arbitrary $d \in \mathbb{R} \setminus \{0\}$. (Note that such a representation of ψ_0 exists, since a ψ_1 of character $c + d\mathrm{i}$ clearly exists, such as an eddy $\psi_{c+d\mathrm{i}}$, and then $\psi_2 := 2\psi_0 - \psi_1$ will have a character of $c - d\mathrm{i}$ and $\psi_0 = \frac{\psi_1+\psi_2}{2}$.

Keeping the IFS, the weights, and X, by Theorem 2.2.8 the invariant flows $\bar{\psi}_{1,2} \equiv \mathrm{T}\bar{\psi}_{1,2} \in \Psi_{X,c_{1,2}}$ exist for both $c_{1,2}$ since $\operatorname{Im} c_{1,2} = \pm d \neq 0$. Since $\equiv$ means equality in gradient, we have for $\bar{\psi} := \frac{\bar{\psi}_1+\bar{\psi}_2}{2}$ that $\bar{\psi} \equiv \mathrm{T}\bar{\psi}$ and

$$\operatorname{char}(\bar{\psi}) = \frac{1}{2}\left(\operatorname{char}(\bar{\psi}_1) + \operatorname{char}(\bar{\psi}_2)\right) = \frac{c_1 + c_2}{2} = c$$

as required.

The other degenerate case is when the $\operatorname{leb}(F) = 0$ condition is not satisfied by the IFS in Definition 2.2.2. Again, the discussion cannot proceed. However, by the continuity of the invariant flow in the IFS parameters (Theorem 2.2.10), we can approximate the invariant flow field of such a degenerate case, by the invariant flows induced by approximating IFS parameters.

2.2.13 Visualization

When considering the transfer operator over stream functions, one encounters a proliferation of branch cuts, as the transfer iteration progresses. This can make the visualization of streamlines - the level curves of the stream function - quite difficult. Note that stream functions in $[\Psi_{X,c}]$ are only required to be almost everywhere smooth, and the transfer iteration results in a countably infinite Hutchinson union of branch cuts in $\bar{\psi}$, which pose no issue theoretically, despite the visual and algorithmic mess they create in practice. This is illustrated by Figure 2.3 with transfer parameters

$$p_1 = 0,\ p_2 = 1,\ \varphi_1 = 0.65\mathrm{e}^{-\frac{2\pi}{6}\mathrm{i}},\ \varphi_2 = 0.65\mathrm{e}^{\frac{2\pi}{4}\mathrm{i}},\ w_{1,2} = 0.5.$$

Therefore in order to iteratively visualize the flow field, one seems to have no option but to resort to an iteration over the velocity field. ψ_0 can be chosen arbitrarily, as apparent from Theorem 2.2.8, so we choose $\psi_0 := \sum_k w_k T_k^* \psi_{c_k,p_k}$ as discussed at the end of Section 2.2.7, where $c_k = \mathrm{Log}\ \varphi_k$ (choosing $C = 2\pi$ in Section 2.2.4) for an IFS of Section 1.3. The evolution in the velocity field progresses according to Theorem 2.2.4. So we have the following recursive iteration for the velocity field, over the flow space $([\Psi_{X,c}], D)$ with preserved character $c = \sum_k w_k \mathrm{Log}\ \varphi_k$ and $X \supset \langle T_1, \ldots, T_n \rangle$.

$$v_0(z) = v[\psi_0] = \sum_{k=1}^{n} w_k (\mathrm{Log}\ \varphi_k) \frac{z - p_k}{|z - p_k|^2}$$

$$v_{L+1}(z) = v[\mathrm{T}\psi_L](z) = \sum_{k=1}^{n} w_k \frac{\varphi_k}{|\varphi_k|^2}\ v_L(T_k^{-1}(z)).$$

Once at a large enough iteration level $L \in \mathbb{N}$, one may execute a streamline solver algorithm, resulting in a preferable image as in Figure 2.4. The transfer iteration is visualized in Figure 2.5. Note the apparent convergence to an attractor flow field, as predicted by Theorem 2.2.8.

In order to visualize the level curves of the corresponding potential function - the equipotential lines - we first note the correspondence in character $\mathrm{char}(\tilde{\psi}) = -\mathrm{i}\ \mathrm{char}(\psi)$ by Definition 2.2.1. If one does not wish to deal with the arising sources in the conjugate to the above ψ_0 (as we did in Figure 2.6), we may choose simply instead $\psi_0 := \psi_{c,p}$ and thus $\tilde{\psi}_0 = \psi_{-\mathrm{i}c,p}$ with the primary fixed point p and the above c, as discussed in Section 2.2.8. Then in order to arrive at the potential field at level L, we execute the same velocity recursion on $\tilde{v}_0(z) := v[\tilde{\psi}_0]$ as above on $v_0(z) = v[\psi_0]$. The iterative formula remains the same because of Theorems 2.2.3 and 2.2.4.

This implies the following recursion, with $\tilde{v}_L := v[\tilde{\psi}_L],\ L \in \{0\} \cup \mathbb{N}$

$$\tilde{v}_0(z) = v[\tilde{\psi}_0](z) = -\mathrm{i}c\ \frac{z-p}{|z-p|^2}$$

$$\tilde{v}_{L+1} = v[\tilde{\psi}_{L+1}] = v[\widetilde{\mathrm{T}\psi_L}] = v[\mathrm{T}\tilde{\psi}_L] = \sum_{k=1}^{n} w_k \frac{\varphi_k}{|\varphi_k|^2}\ T_k^* v[\tilde{\psi}_L] = \sum_{k=1}^{n} w_k \frac{\varphi_k}{|\varphi_k|^2}\ T_k^* \tilde{v}_L.$$

Depending on the sign of Im c, it may be more convenient from the viewpoint of a streamline solver, to take the negative of $\tilde{v}_0$ so that Re char$(\tilde{v}_0) < 0$.

The depicted region in Figures 2.3 and 2.4 is $\pm 20\%$ of the horizontal and vertical span of the above IFS iterated from the initial set $\{p_1, p_2\}$ to the iteration level $L = 4$. For $p_1 = 0,\ p_2 = 1$ the approximate region is $[-0.86, 2.00] \times [-1.34, 0.61] \subset \mathbb{R}^2$. For other $p_{1,2}$ the figures scale according to their distance.

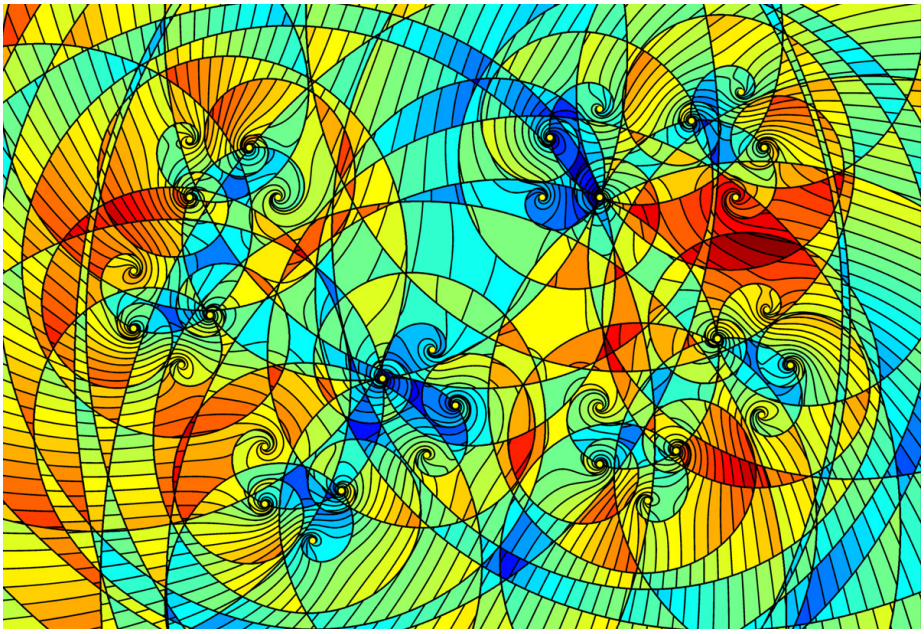

Figure 2.3: Level curves of the stream function $T^4\psi_0$ with logarithmic spiral branch cuts.

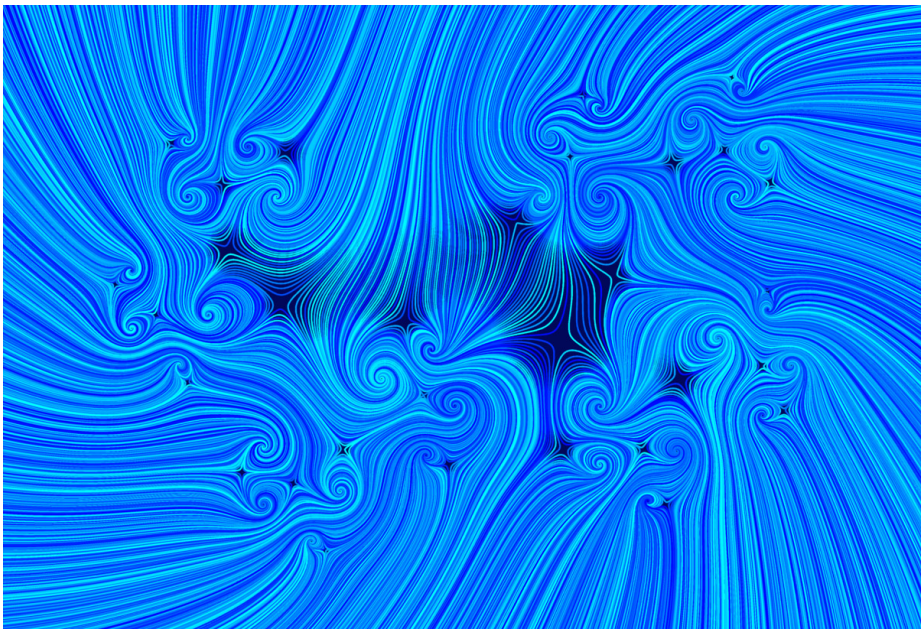

Figure 2.4: The same streamlines solved from the velocity field.

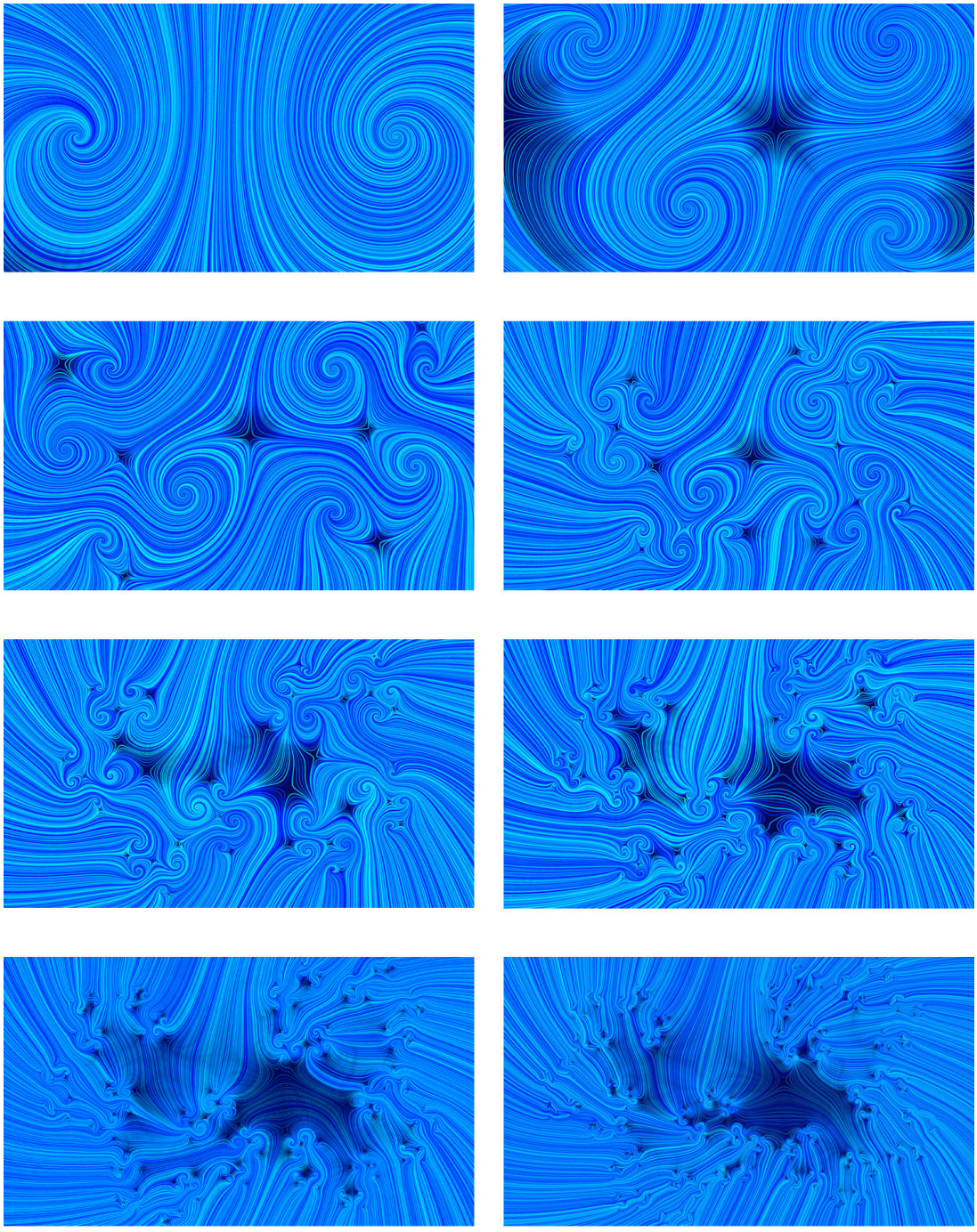

Figure 2.5: Converging transfer iteration from ψ_0 to $\mathrm{T}^7\psi_0$.

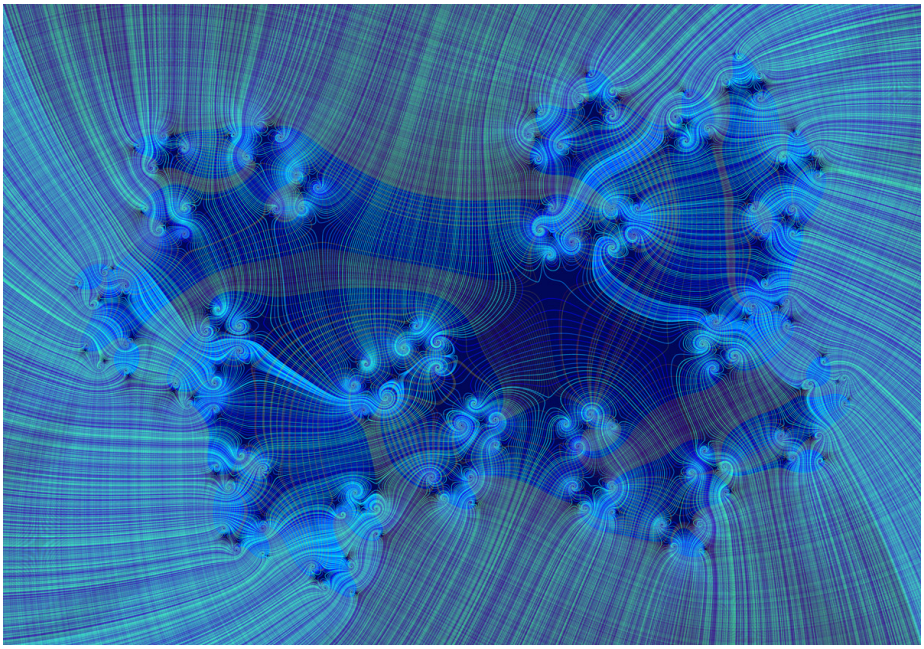

Figure 2.6: The equipotential lines at iteration level $L = 6$.

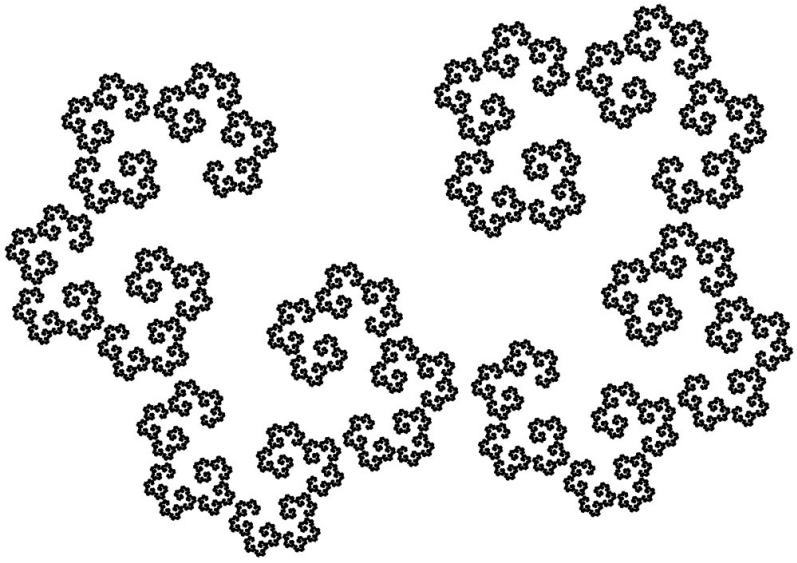

Figure 2.7: The IFS fractal of sink singularities in the invariant flow.

2.2.14 Concluding Remarks

To make some suggestions for future research, we note the conjectures stated in Section 2.2.10, as well as the inspirational remarks on entropy in Section 2.2.8. Furthermore, the isometric isomorphism introduced in Section 2.2.7 between flows and probability measures, may be exploited to translate former results on measures to the language of flows, while examining the physical implications.

Considering Section 2.2.10, the study of Fractal Potential Flows reduces essentially to studying the geometry of IFS Fractals with similarity contractions, which is the quest we shall now undertake.

Chapter 3

The Geometry of IFS Fractals

3.1 Geometry via Containment

3.1.1 Iterative Containment

The relevance of bounding sets to an IFS fractal, lies in their property of "iterative containment" by which they provide improving approximations to the fractal. According to the Containment Lemma 1.3.1, for any compact set B for which $\mathrm{H}(B) \subset B$ we have $B \supset \mathrm{H}^L(B) \to F$ as $L \to \infty$. Since H is contractive in the Hausdorff metric over compact sets, this means that $\mathrm{H}^L(B)$ will get progressively closer to F in the metric. In practice, this implies that taking such a bounding set - often a circle or the convex hull - we can improve it by the iteration of H to new tighter bounding sets formed as a Hutchinson union.

Definition 3.1.1 *We say that a bounding set $B \subset \mathbb{C}: \ F \subset B$ is **invariant** under the IFS $\mathcal{T} = \{T_1, \ldots, T_n\}$ if B is compact and $\mathrm{H}_{\mathcal{T}}(B) \subset B$.*

The idea of "invariant bounding" is also important to ensure that no points of the fractal are excluded in a "divide and conquer" iterative Hutchinson cascade, and thus we may devise numerical algorithms for virtually any geometrical question about an IFS fractal, such as its intersection with Euclidean sets, or even other fractals. The initial bounding set can be a circle, the convex hull (see Theorem 3.3.1), or any other set, which may then be iterated for better approximations to the fractal. This is illustrated below.

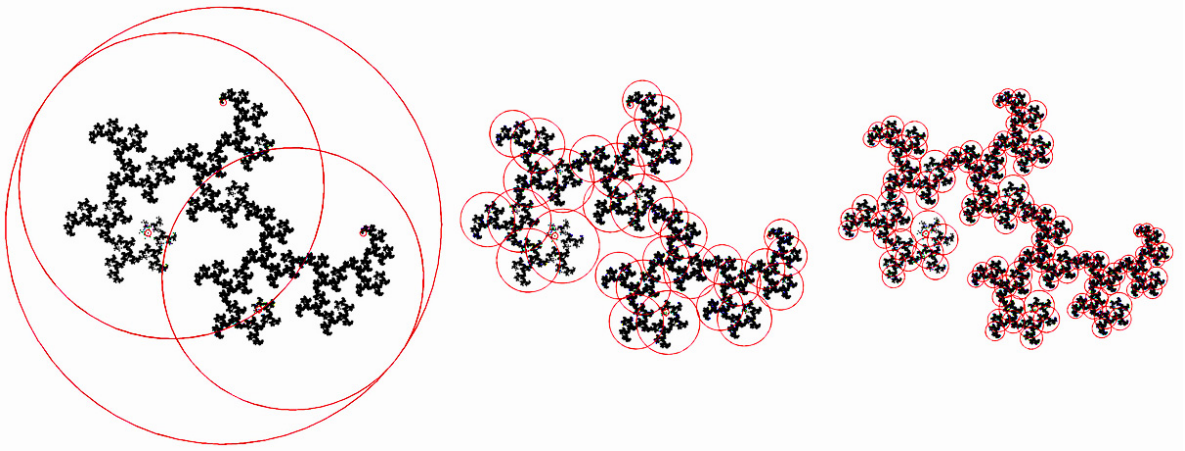

Figure 3.1: An invariant bounding circle iteratively approximating the fractal.
(IFS factors: $\varphi_1 = 0.7 \exp\left(\frac{5\pi}{15}\mathrm{i}\right)$, $\varphi_2 = 0.6 \exp\left(\frac{3\pi}{15}\mathrm{i}\right)$.)

An invariant bounding set can thus be utilized for answering geometrical questions numerically to any $\varepsilon > 0$ accuracy. The efficiency of the algorithms can be expected to depend on the "closeness" of the bounding set to the fractal. A common challenge is therefore to find regular bounding sets which are as tight as possible. Other times, the ease of computation may also become relevant (possibly even more than tightness), such as in the case of morphing IFS fractals where the IFS parameters vary in real-time.

The virtue of bounding circles, is clearly the simplicity of their representation with just two parameters, which carry beneficial implications for the efficiency of numerical algorithms for IFS fractals, as we shall see. On the other hand, certain algorithms may not be devised in any other way, than via employing a bounding circle. The tightest convex bounding set, the convex hull, is likely to be ideal for the theoretical efficiency of many algorithms. As we will see however in Section 3.3, finding the precise loci of the extrema is by far not trivial. Though the trade-off in computational complexity between algorithmically handling the (potentially large number of) extremal points versus the two parameters of a bounding circle may still be worthwhile, depending on the nature of the algorithm and how its complexity depends on the type of bounding set. This requires further investigation, which the author found to be beyond the scope of the thesis, with only a few illustrative algorithms presented in Section 3.1.2. In light of the nature of these algorithms, the virtue of tighter bounding potentially with other kinds of invariant bounding sets besides a circle, is explained in Section 3.1.3. Some explicit bounding circles shall be derived in Section 3.2.

3.1.2 Numerical Algorithms for IFS Fractals

We hereby detail some algorithms which utilize invariant bounding sets. Some of them specifically require an invariant bounding circle, while others run more optimally using a tighter set, preferably the convex hull. The list of algorithms given is meant by no means to be exhaustive. The presented algorithms run over the complex plane, but they are generalizable to in any dimension in a straightforward manner. We will be dealing with general n-map IFS fractals $F = \langle \mathcal{T} \rangle = \langle T_1, \ldots, T_n \rangle \subset \mathbb{C}$, $\mathcal{P} = \{1, \ldots, n\}$. The desired accuracy for these numerical procedures will be some $\varepsilon > 0$. We employ some invariant set $B \subset \mathbb{C}$ with respect to the IFS. We will also use the notation $f \in_{\varepsilon,B} F$ to denote that $f \in \mathrm{H}^{L_*}(B) \subset \mathrm{Nei}_\varepsilon(F)$, implying $f \notin_{\varepsilon,B} F \Rightarrow f \notin F$. Reasonably let

$$L_* := \left\lceil \frac{\ln \varepsilon - \ln \operatorname{diam}(B)}{\ln \lambda_*} \right\rceil \quad \text{by} \quad \lambda_*^{L_*} \operatorname{diam}(B) \leq \varepsilon \quad \text{where} \quad \lambda_* := \max_{k \in \mathcal{N}} \lambda_k.$$

Algorithm 2 Decides if a point f is in the fractal F up to some ε accuracy, meaning $f \in_{\varepsilon,B} F$, using an invariant bounding set B. Returns a Boolean true or false.

```
1:  function IsFractalPt(f, T, B, ε)
2:      if f ∈ B then                          ▷ Assuming a subroutine that decides this.
3:          if diam(B) ≤ ε then
4:              return true                                          ▷ Then f ∈_{ε,B} F.
5:          else
6:              i := false                          ▷ Keeps track of whether f ∈_{ε,B} F.
7:              for k ∈ N do
8:                  i_k := IsFractalPt(f, T_k T T_k^{-1}, T_k(B), ε)   ▷ Recursively over T_k(F).
9:                  i := i ∨ i_k
10:             end for
11:             return i
12:         end if
13:     else
14:         return false
15:     end if
16: end function
```

In the above algorithm, we have assumed the availability of a subroutine that decides if a point is in B - a reasonable assumption, if B has a "simple" definition, for instance a bounding circle. Note that $T_k(F) = \langle T_k \mathcal{T} T_k^{-1} \rangle$ by the Affine Lemma 1.3.3.

In the following algorithm, we assume that the set $S \subset \mathbb{C}$ also has a simple enough definition - for instance a line, or a region enclosed by a polygon - so that the non-emptiness of $T_a(B) \cap S$ can be "easily" verified for any $a \in \mathcal{A}_{fin}$.

Algorithm 3 Determines the set $F \cap S$ up to some ε accuracy (meaning a subset of $S \cap \mathrm{Nei}_\varepsilon(F)$), using an invariant bounding set B. To be called with $I = \varnothing$; returns a bounding set of the intersection.

```
1: function IntFractalSet(I, 𝒯, B, S, ε)
2:     if B ∩ S ≠ ∅ then                          ▷ Assuming a subroutine.
3:         if diam(B) ≤ ε then
4:             return I ∪ B
5:         else
6:             for k ∈ 𝒩 do
7:                 I := IntFractalSet(I, T_k 𝒯 T_k^{-1}, T_k(B), S, ε)   ▷ Recursively.
8:             end for
9:             return I
10:        end if
11:    else
12:        return I                               ▷ No update.
13:    end if
14: end function
```

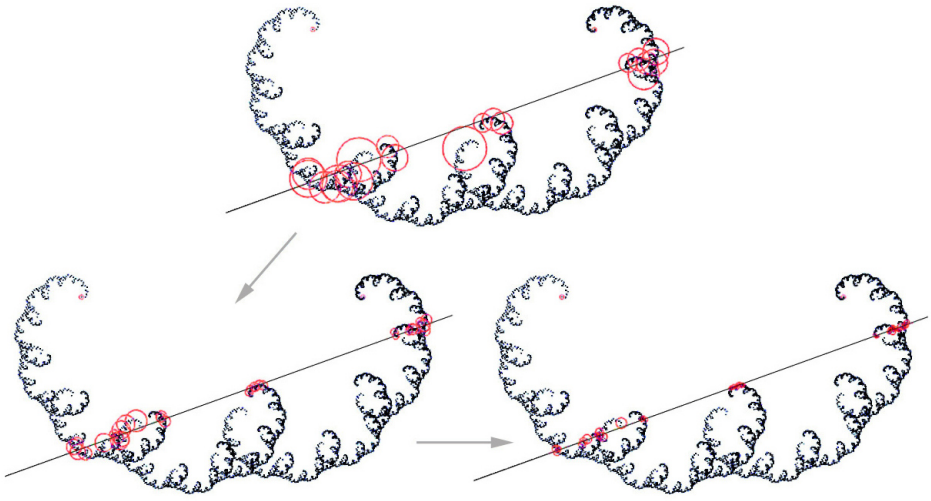

Figure 3.2: Intersecting a fractal with a line numerically.

While the above algorithm resolves the question of numerical line intersection, we are left to ponder the problem of maximizing a linear target function over the fractal. This is resolved in the algorithm to follow. We begin with an important definition.

Definition 3.1.2 *We say that a circle (closed ball) $C = B(c, r) \subset \mathbb{C}, (c, r) \in \mathbb{C} \times \mathbb{R}_+$ is a* ***bounding circle*** *if it contains F. It is an* ***ideal bounding circle*** *if it is invariant with respect to the IFS $\mathcal{T}$ and $c \in$ int Conv(F), where $F = \langle \mathcal{T} \rangle$.*

As before, we shall search recursively over the iterates $T_a(C), a \in \mathcal{A}$ for the desired maximizing address(es) (the first few coordinates). To make the search efficient, we must be able to compare and discard iterates which are "dominated" by others, with respect to a target vector $\tau \in \mathbb{C} \setminus \{0\}$ and the corresponding target function $z \mapsto \langle \tau, z \rangle, z \in \mathbb{C}$, where $\langle \cdot, \cdot \rangle$ is the dot product. We introduce an ordering relation between circles to formalize this idea.

Definition 3.1.3 *We say that a finite address $a \in \mathcal{A}_{fin}$* ***dominates*** *another $b \in \mathcal{A}_{fin}$ of the same length, with respect to the target vector $\tau \in \mathbb{C}$, the IFS $\mathcal{T} = \{T_1, \ldots, T_n\}$, and the ideal bounding circle $C = B(c, r) \subset \mathbb{C}$ (denoted as $a \succ_{\tau,\mathcal{T},C} b$ or simply $a \succ b$), if $\langle \tau,\ T_a(c) - T_b(c) \rangle \geq \lambda_b r |\tau|$.*

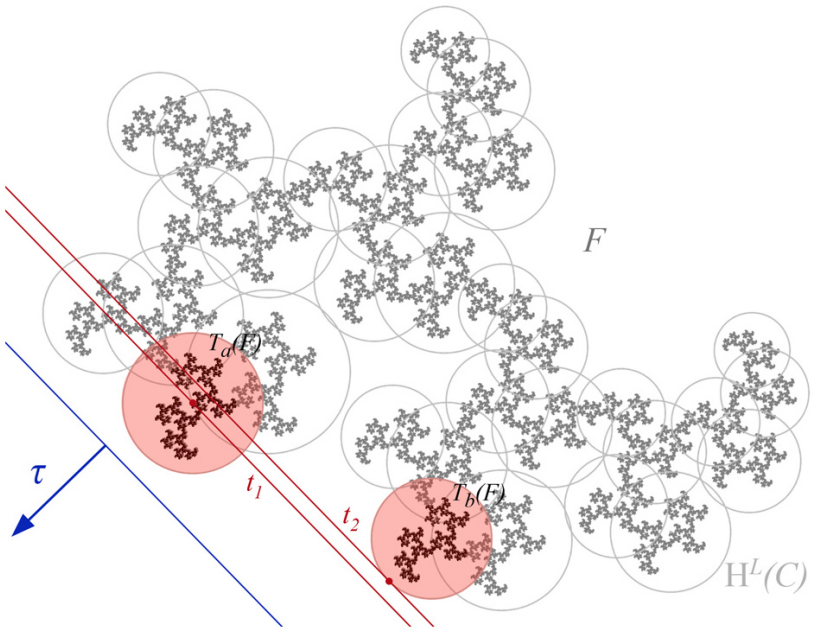

Figure 3.3: Illustration of a finite address dominating another.

Note that the inequality of the definition is equivalent to the following

$$t_1 := \langle \tau, T_a(c) \rangle \geq t_2 := \left\langle \tau,\ T_b(c) + \lambda_b r \frac{\tau}{|\tau|} \right\rangle .$$

This is illustrated in the above figure. Since the centre of the iterated circle $T_a(C) \subset \mathrm{H}^L(C), L \in \mathbb{N}$ has a larger target value t_1 than any point (including the maximizing value t_2) over $T_b(C) \subset \mathrm{H}^L(C)$, and by $c \in \text{int Conv}(F)$, we can infer that there must be a point in the subfractal $T_a(F) \subset \mathrm{H}^L(F) = F$ which has a strictly larger target value than any of the points in the subfractal $T_b(F) \subset \mathrm{H}^L(F) = F$, and therefore the maximizing algorithm can discard $T_b(F)$.

Theorem 3.1.1 *The relation $\succ$ is a strict partial order over finite addresses - i.e. it is an ordering relation that is irreflexive, transitive, and asymmetric.*

Proof We see that the relation is irreflexive, since $a \succ a$ would imply that $0 = \langle \tau, T_a(c) - T_a(c) \rangle \geq \lambda_b r|\tau| \neq 0$ which is a contradiction. To show transitivity, let us assume that $a_1 \succ a_2 \succ a_3,\ a_{1,2,3} \in \mathcal{A}_{fin}$ and we need that $a_1 \succ a_3$.

$$\langle \tau,\ T_{a_1}(c) - T_{a_3}(c) \rangle = \langle \tau,\ T_{a_1}(c) - T_{a_2}(c) \rangle + \langle \tau,\ T_{a_2}(c) - T_{a_3}(c) \rangle \geq$$

$$\geq \lambda_{a_2} r|\tau| + \lambda_{a_3} r|\tau| \geq \lambda_{a_3} r|\tau| \quad \Rightarrow \quad a_1 \succ a_3.$$

Lastly for asymmetry, we need that if $a \succ b$ then $b \succ a$ cannot hold. Clearly $a \succ b$ implies that $\langle \tau, T_a(c) - T_b(c) \rangle$ is strictly positive, but if $b \succ a$ also held then $\langle \tau, T_b(c) - T_a(c) \rangle = -\langle \tau, T_a(c) - T_b(c) \rangle$ would also be, which is a contradiction. □

Naturally, our next inquiry is to devise a definition for the "maximal element(s)" in a subset of finite addresses. We do this in the customary manner for partial ordering relations in the following definition, illustrated below.

Definition 3.1.4 *We say that an element is **maximal** in a subset of finite addresses $\mathcal{A}_0 \subset \mathcal{A}_{fin}$ if no other element dominates it. Furthermore, denote the subset of maximal addresses as* $\text{Argmax}(\mathcal{A}_0) = \text{Argmax}_{\tau,\mathcal{T},C}(\mathcal{A}_0) := \{a \in \mathcal{A}_0 :\ \nexists b : b \succ a\}$.

The figure below depicts in the highlighted circle iterates the four maximal addresses with respect to the target τ and a bounding circle C, at some iteration level $L \in \mathbb{N}$ by the Hutchinson operator H. These addresses are considered to be maximal, since no other address dominates them at that iteration level.

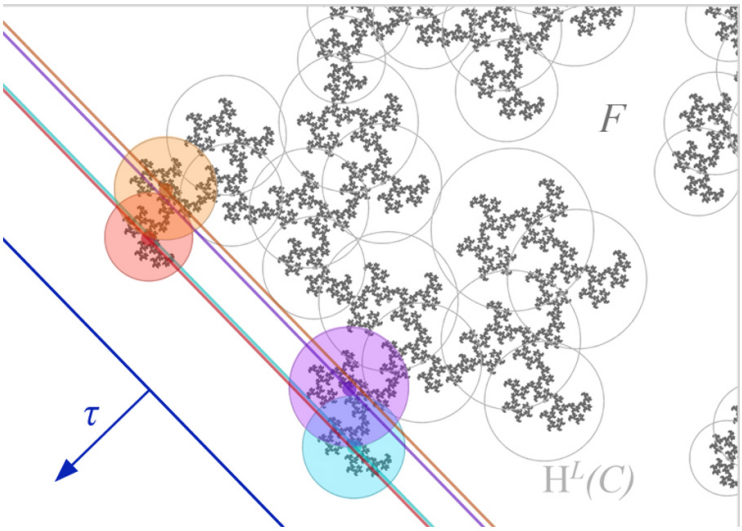

Figure 3.4: Illustration of Argmax at some iteration level.

Finally, we arrive at the algorithm employing the above concepts, as well as those of Definition 1.3.6. The algorithm uses the invariance of $C \supset \mathrm{H}(C)$ to eliminate the redundant non-maximal iterated circles of the form $T_a(C)$. The recursiveness lies in the step from $\mathcal{A}_0$ to $\mathcal{A}_0 \times \mathcal{N}$, corresponding to the iteration of each circle $T_a(C), a \in \mathcal{A}_0$ by the local Hutchinson $\mathrm{H}_{T_a(\mathcal{T})}$ resulting in $n = |\mathcal{P}|$ new sub-circles to be tested for maximality. Only the maximal ones survive the fifth line below, which can again be subdivided by their respective local Hutchinsons.

Algorithm 4 Determines the L-long truncation(s) of the potential maximizing address(es), meaning $\mathrm{trn}_L\left(\mathrm{Argmax}_{\tau,\mathcal{T},C}(\mathcal{N}^M)\right)$, with respect to the target τ using an ideal bounding circle $C = B(c, r)$ iterated up to a maximum iteration number $M \geq L$. To be called with $\mathcal{A}_0 = \{0\}$.

1: **function** FractalLinOpt($\mathcal{A}_0, \tau, \mathcal{T}, C, L, M$)
2: **if** $|\bigwedge \mathcal{A}_0| \geq L$ **or** $M = 0$ **then**
3: **return** $\mathrm{trn}_L\ \mathcal{A}_0$
4: **else**
5: $\mathcal{A}_0 := \mathrm{Argmax}_{\tau,\mathcal{T},C}(\mathcal{A}_0 \times \mathcal{N})$ ▷ Subdivision of $\mathrm{H}^L(C)$ into $\mathrm{H}^L(\mathrm{H}(C))$.
6: **return** FractalLinOpt($\mathcal{A}_0, \tau, \mathcal{T}, C, L, M - 1$)
7: **end if**
8: **end function**

The algorithm is conclusive iff it terminates due to $|\bigwedge \mathcal{A}_0| \geq L$ (not $M = 0$), since then the maximizing L-long truncation is unique. Otherwise if non-uniqueness is expected (such as when checking if two extrema are neighbors; Section 3.3.3) then M should be chosen large enough, so as to distill the likely maximizing truncations sufficiently.

To ensure that the pseudocode can be implemented in a practical way, we must relate the elements of $\mathcal{A}_0$ to the calculation of $\text{Argmax}_{\tau,\mathcal{T},C}(\mathcal{A}_0 \times \mathcal{N})$. This corresponds to the subdivision of circles into their local iterates, and finding the maximal among them. The calculation of Argmax is simplified via the following equivalences.

$$a \in \text{Argmax}_{\tau,\mathcal{T},C}(\mathcal{A}_0 \times \mathcal{N}) \;\Leftrightarrow\; \nexists b \in \mathcal{A}_0 \times \mathcal{N} : b \succ a \;\Leftrightarrow$$

$$\Leftrightarrow\; \forall b \in \mathcal{A}_0 \times \mathcal{N} : \left\langle \tau,\; T_a(c) + \lambda_a r \frac{\tau}{|\tau|} \right\rangle > \langle \tau, T_b(c) \rangle \;\Leftrightarrow$$

$$\left\langle \tau,\; T_a(c) + \lambda_a r \frac{\tau}{|\tau|} \right\rangle > \max_{b \in \mathcal{A}_0 \times \mathcal{N}} \langle \tau, T_b(c) \rangle \quad \text{for} \quad a \in \mathcal{A}_0 \times \mathcal{N}.$$

Therefore we get that the next-level iterates of C can be tested for maximality amongst one another, by first calculating the max in the last inequality, and then comparing it to each new target value on the left, for $a \in \mathcal{A}_0 \times \mathcal{N}$.

In order to make the above calculations even more efficient, we must keep track of the iterated centers $T_a(c)$ and the iterated fixed points $T_a(\mathcal{P})$, since they imply the next-level iterated centers and fixed points as follows.

$$T_a T_k(c) = T_a(p_k) + \varphi_k(T_a(c) - T_a(p_k)) \quad (a \in \mathcal{A}_0,\; k \in \mathcal{N})$$

$$T_a T_j(p_k) = T_a(p_j) + \varphi_j(T_a(p_k) - T_a(p_j)) \quad (a \in \mathcal{A}_0,\; j \in \mathcal{N}).$$

These equations follow from the fact that T_a is an affine map (Corollary 1.3.2).

3.1.3 The Virtue of Tighter Bounding

This section is dedicated to emphasizing the effect of running the above algorithms with tighter invariant bounding sets, which will further underline the relevance of our upcoming effort in Section 3.3 to determine the tightest convex bounding set - the convex hull - which happens to be invariant itself.

The virtue of tighter bounding is the increase of algorithmic efficiency. Redundant iterates of the bounding set are eliminated with a greater likelihood, and thus entire algorithmic branches can be spared on the recursive tree.

Let us consider Algorithm 2 for instance. The invoked subroutine that decides if $f \in B$ returns false with greater likelihood if B is a tighter set, thereby potentially eliminating a recursive branch. The case $\operatorname{diam}(B) \leq \varepsilon$ is also likely to occur quicker, resulting in an even earlier termination of the algorithm. This argument can clearly be made more precise by analyzing the complexity of the algorithm in terms of its input parameters. In Algorithm 3, the critical condition $B \cap S \neq \varnothing$ can likewise reduce runtime if B is tighter.

In Algorithm 4, the relevance of tightness hides within the Argmax computations, specifically each test for whether $a \succ_{\tau,\mathcal{T},C} b$. For a is much likelier to dominate b if the corresponding circle iterates $T_a(C)$ and $T_b(C)$ are smaller, and thereby eliminate the search branch over $T_b(F)$ due to invariance.

To conclude with an overall observation, an invariant bounding set approximates the fractal, in fact approaches it in the limit, with successive applications of the Hutchinson operator. So it is no great wonder, that this approximation results in more efficient numerical algorithms when the initial bound is a tighter set.

3.2 Bounding Circles

3.2.1 Introduction

A great variety of algorithms exist in the literature for finding bounding circles, polygons, or rectangles for IFS fractals, usually tackling the easier question in 2D first, as a basis for the 3D bounding problem. The existing algorithms for finding bounding circles are mostly approximative, with significant computational and methodological complexity. Hereby explicit formulas are introduced for bounding circles in the plane, and some generalizations to space, providing readily applicable bounding sets for IFS fractals.

The "general bounding circle" to be introduced resolves the bounding problem for any number of maps and dimensions. Meanwhile the introduced "circumcircles" for 2-map IFS, generalize the concept of the circumscribed circle of triangles in classical Euclidean geometry to IFS fractals, hinting at a novel polygonal view of IFS fractals.

This work is intended for mathematicians and computer scientists alike. The relevance of bounding sets for the visualization of fractals is well-established. Indeed these explicit bounding circle formulas present a numerical / algorithmic panacea for geometrical problems, according to the philosophy of Section 3.1.

Regarding computer science, Hart and DeFanti [38] provide a full description of the visualization of 3D IFS fractals. It emphasizes the importance and difficulties of the Fractal-Line Intersection Problem, hereby discussed in Sections 1.4.1, 1.5, 2.1, 3.1.2. The paper also describes a bounding sphere, and utilizes it for the rendering process.

One of the first pure efforts utilizing bounding circles, was determining the connectedness of 2-map IFS fractals via a numerical technique, which was first developed in a preprint and the subsequent PhD thesis by Hardin [37]. His bounding circle is a special case of the 2-map circumcircle introduced here. The technique was further discussed by Barnsley and Harrington [8], Vrscay [74], and most elaborately by Barnsley and Hardin [7]. The bounding circle by Vrscay is the most general, as it also involves shear IFS transforms, that method however does not optimize for a center, but always uses the origin. The method of Section 3.2.2 overcomes this limitation, resulting in optimal bounding circles.

The circle defined by Dubuc and Hamzaoui [26] comes even closer to our general bounding circle, having a variable center. However in this form, it is unclear how the optimal

center may be found in general, possibly using an optimization algorithm. By our alternative formulation however, it becomes clear that the minimization involved is equivalent to the computational geometric Smallest Circle Problem of finitely many points, for which specialized efficient algorithms exist.

Rice [64] introduces a method for n-map IFS, similar to our circumcircle method. In fact, the paper even conjectures the existence of the circumcircle, as an ideal tangential solution to the thereby presented numerical method, in the two-map case. Again this method gives no explicit formula, but assumes the use of an efficient optimization algorithm at each iterative step, leading to a bounding circle. The method presented by Canright [13] gives an algorithm for finding not a single bounding circle, but rather a finite set of circles whose union covers the fractal. An outer bounding circle to this set of circles can thus be calculated and will be a bounding circle of the fractal itself. Considering the figures, the method seems rather inefficient, and the size of the resulting bounding circle is generally quite large relative to the fractal. Both Edalat et al. [27] and Sharp et al. [66] assume an initial good center estimate which remains fixed throughout the algorithm, and makes no improvement upon it.

In [59] an algorithm is presented arriving at the absolute tightest bounding sphere of the fractal, via a series of subroutines. Clearly the iteration of the Hutchinson operator on any initial bounding circle converges to the fractal, so taking the bounding sphere of this union of spheres approaches the tightest bounding sphere - so in this sense the result of the algorithm is not surprising. The presented method is founded upon the theory of IFS moments and the simplex method from linear optimization, which has exponential complexity in the worst case. Thus the implementation of the method requires significant computational and methodological complexity.

This concludes our review of the literature. We now proceed to introducing the general bounding circle for n-map IFS (possibly with shear transforms in $\mathbb{R}^d$), and the circumcircles for 2- and 3-map IFS fractals (with similarity transforms in the plane). Though the former works in greater generality, the latter may prove to be tighter upon calculation, the virtues of which was detailed in Section 3.1.3.

In the following discussion, and as detailed in Section 1.3.1, we will variously deal with IFS maps of the increasingly more general forms:

$$z \mapsto T(z) = p + \varphi(z - p), \quad p, \varphi \in \mathbb{C}, \ |\varphi| < 1 \quad (z \in \mathbb{C})$$

$$z \mapsto T(z) = p + \lambda R(z - p), \quad p \in \mathbb{R}^d, R \in \mathbb{R}^{d \times d}, \lambda \in (0, 1), R^T R = I \quad (z \in \mathbb{R}^d, d \in \mathbb{N})$$

$$z \mapsto T(z) = p + M(z - p), \quad p \in \mathbb{R}^d, M \in \mathbb{R}^{d \times d}, \|M\| < 1 \quad (z \in \mathbb{R}^d, d \in \mathbb{N})$$

for some induced matrix norm $\|\cdot\|$. Such maps will form the usual IFS $\mathcal{T} = \{T_1, \ldots, T_n\}$ generating the attractor $F = \langle \mathcal{T} \rangle$ with index set $\mathcal{N} = \{1, \ldots, n\}$ (often $n = 2$).

We emphasize the polygonal nature of IFS fractals, which will become increasingly clear, by introducing the following terminology.

Definition 3.2.1 *We will say that an IFS fractal F is a* ***bifractal****,* ***trifractal****, or* ***polyfractal*** *if it is generated by $n = 2, 3$ or $n > 3$ planar similitudes, respectively. In the special case of $\vartheta_k \equiv 0 \pmod{2\pi},\ k \in \mathcal{N}$ we speak of* ***Sierpinski fractals****.*

3.2.2 The General Bounding Circle for Polyfractals

Let the radius function with respect to the IFS $\mathcal{T} = \{T_1, \ldots, T_n\}$ of planar similitudes $T_k(z) = p_k + \varphi_k(z - p_k),\ k \in \mathcal{N},\ z \in \mathbb{C}$ be denoted

$$\varrho(z) = \varrho_{\mathcal{T}}(z) := \max_k |p_k - z| \quad (z \in \mathbb{C}).$$

This is the radius of the smallest circle centered at z that contains all the fixed points $p_k \in \mathcal{P}$. It can be shown that ϱ is a continuous convex function, so it is a natural inquiry to look for its minimum - the center c_* which gives the lowest ϱ value. The minimizing circle $(c_*, \varrho(c_*))$ is called the minimum covering circle or minimal bounding circle (we also refer to this ordered pair as a "circle"). Its determination is the Smallest Circle Problem for a finite set of points in the plane, first investigated in modern times by Sylvester [70] in 1857. The minimum covering circle is known to be unique. Several algorithms exist for finding it, and the fastest run in linear time. We note the algorithms of Megiddo [62] and Welzl [78] specifically, both linear in runtime.

Theorem 3.2.1 *For any $c \in \mathbb{C}$, the circle $(c, r(c)) \in \mathbb{C} \times \mathbb{R}_+$ with*

$$r(c) := \frac{\mu_* \varrho(c)}{1 - \lambda_*}, \quad \lambda_* := \max_k |\varphi_k|, \quad \mu_* := \max_k |1 - \varphi_k|$$

is a bounding circle of F. With the center and radius

$$c_* = \operatorname{argmin}_{z \in \mathbb{C}}\ \varrho(z), \quad r_* := r(c_*)$$

*it is minimal, and we call it the **general bounding circle** of the IFS fractal F.*

Proof Considering the Containment Lemma 1.3.1, we see that $(c, r(c))$ must satisfy $T_k(B(c, r(c))) \subset B(c, r(c)),\ k \in \mathcal{N}$. Let k be fixed and arbitrary. Then we can see geometrically that this containment is equivalent to

$$|T_k(c) - c| + \lambda_k r(c) \le r(c) \ \Leftrightarrow\ |1 - \varphi_k| \cdot |c - p_k| \le (1 - \lambda_k) r(c).$$

Estimating the left-hand side by $\mu_* \varrho(c)$ from above, the right-hand side by $(1 - \lambda_*) r(c)$ from below, and the two estimates being equal, we have the desired inequality above. Therefore $H(B(c, r(c))) \subset B(c, r(c))$ so by the Containment Theorem we have that $F \subset B(c, r(c))$, which also holds for (c_*, r_*). □

The proof also works in higher dimensional spaces for a corresponding IFS with maps of the form $T_k : \mathbb{R}^d \to \mathbb{R}^d,\ T_k(z) = p_k + \lambda_k R_k(z - p_k),\ R_k^T R_k = I$ and $\mu_k := \|I - \lambda_k R_k\|$, where $\|\cdot\|$ is the matrix norm induced by the Euclidean norm, or whatever norm was used in the definition of ϱ (easy-to-compute compatible matrix norms with the vector norm are also sufficient). Thus in 3D we may talk about a general bounding sphere (c_*, r_*) of the above form, obtained from its corresponding minimal bounding sphere $(c_*, \varrho(c_*))$. Algorithms do exist for finding the minimal bounding sphere of a finite set of points as well [50].

It is important to note that the optimal (c_*, r_*) may not be an ideal bounding circle (Definition 3.1.2, relevant to Algorithm 4 etc.), since c may not fall within int Conv(F) (though this can often be verified), as it can easily be seen for the case of three maps with zero rotation angles. So instead we can work with the following convex combinations of the fixed points of the IFS, mostly providing reasonable estimates of c_*.

$$c_A := \frac{\sum_k p_k}{n}, \quad c_H := \frac{\sum_k \frac{1}{\varrho(p_k)} p_k}{\sum_k \frac{1}{\varrho(p_k)}}.$$

These are the arithmetic and harmonic convex combinations of the fixed points of the IFS. For these special centers, we may find by the convexity of ϱ that their value will be less than or equal to the arithmetic and harmonic mean of the ϱ values of the fixed points, thus proving these centers reasonable. Calculating the ϱ of both means, we may find whichever gives a lower value and use that center, rather than attempting the algorithmic calculation of the optimal c_*.

Philosophically speaking, we have reduced the problem of bounding an IFS fractal having an infinite number of points, to the bounding of a finite set of points, the fixed points of the IFS. Since we have pointed out specific efficient algorithms for finding c_*, as well as reasonable explicit centers c_A and c_H, the definition of these bounding circles can be considered an explicit one.

3.2.3 The Circumcircle for Trifractals

The bounding of polygons by circles is in general formulaically non-explicit, since the minimum covering circle of the vertices can only be determined algorithmically. When the polygon is a triangle however, such a circle - the circumcircle - may be determined explicitly. Since from a bounding perspective, Sierpinski polyfractals are essentially polygons of the fixed points of the IFS, their non-algorithmic explicit circular bounding seems to be a hopeless venture, for more than three maps. For the case of three or two maps however, such explicit circles may exist for any fractal. Since the Hutchinson of the circumcircle of a Sierpinski trifractal results in tangential iterates, it suggests a similar Apollonian definition for trifractals in general. This implies the following definition, illustrated by Figure 3.5.

Definition 3.2.2 *Let the* ***circumcircle of a trifractal*** $F = \langle T_1, T_2, T_3 \rangle$ *be the smallest circle* $C = (c, r) \in \mathbb{C} \times \mathbb{R}_+$ *satisfying the conditions*

$$|T_k(c) - c| + \lambda_k r = r, \quad k = 1, 2, 3.$$

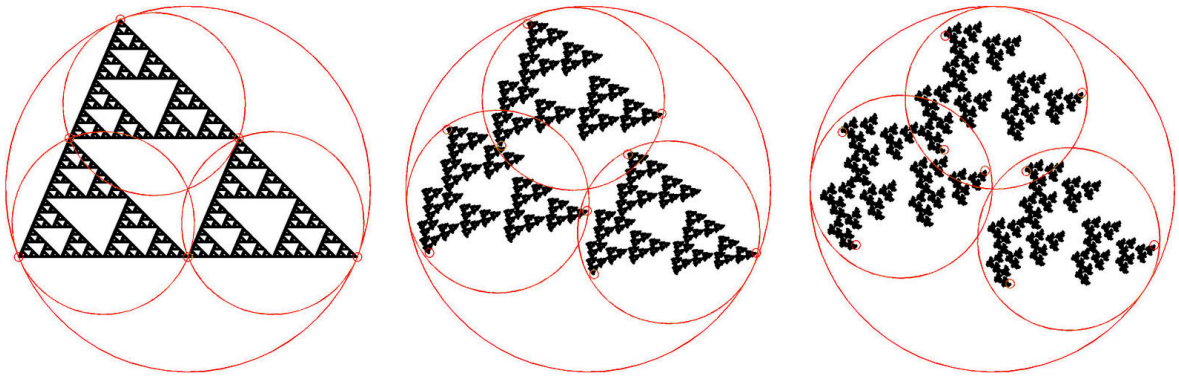

Figure 3.5: A Sierpinski trifractal under rotational perturbations.

Theorem 3.2.2 *Denote the dot and cross product of* $z_{1,2} \in \mathbb{C}$ *respectively by*

$$z_1 \bullet z_2 := \mathrm{Re}(z_1)\mathrm{Re}(z_2) + \mathrm{Im}(z_1)\mathrm{Im}(z_2), \quad z_1 \times z_2 := \mathrm{Re}(z_1)\mathrm{Im}(z_2) - \mathrm{Im}(z_1)\mathrm{Re}(z_2)$$

and let us introduce the following auxiliary variables

$$\alpha_k := \frac{1 - |\varphi_k|}{|1 - \varphi_k|}, \quad k = 1, 2, 3$$

$$A := (\alpha_3^2 - \alpha_2^2)p_1 + (\alpha_1^2 - \alpha_3^2)p_2 + (\alpha_2^2 - \alpha_1^2)p_3$$
$$B := (|p_2|^2 - |p_3|^2)p_1 + (|p_3|^2 - |p_1|^2)p_2 + (|p_1|^2 - |p_2|^2)p_3$$
$$C := 2(p_2 - p_1) \times (p_2 - p_3)$$
$$c_0 := \frac{B}{C\mathrm{i}}, \quad r_0 := |c_0 - p_1|, \quad c_1 := \frac{A}{C\mathrm{i}}$$
$$D := c_0 \bullet c_1 + \frac{1}{C}(\alpha_1^2\ p_2 \times p_3 + \alpha_2^2\ p_3 \times p_1 + \alpha_3^2\ p_1 \times p_2).$$

Then the circumcircle only if $C \neq 0$, meaning iff $p_{1,2,3}$ are non-collinear. If $A \neq 0$ and $D \leq -|c_1|r_0$ then the circumcircle has the parameters

$$c = c_0 + c_1 r^2, \quad r = \frac{1}{|c_1|}\sqrt{-D - \sqrt{D^2 - |c_1|^2 r_0^2}}.$$

If $A = 0$ then $c = c_0$ and $r = r_0/\alpha_1$. (Note: r_0 can be defined above via any p_k.)

Proof First we note that the circumcircle equations reduce to the conditions

$$|p_k - c|^2 - \alpha_k^2 r^2 = 0, \quad k = 1, 2, 3.$$

Denoting $p_{k1} := \mathrm{Re}(p_k)$, $p_{k2} := \mathrm{Im}(p_k)$, $x := \mathrm{Re}(c)$, $y := \mathrm{Im}(c)$ and expanding these conditions, then multiplying each by the factors $p_{31}-p_{21}$, $p_{11}-p_{31}$, $p_{21}-p_{11}$ respectively, and lastly summing the three equations, several terms drop out in the resulting equation, which we denote as $E_1 = 0$. We may do similarly with the factors $p_{32}-p_{22}$, $p_{12}-p_{32}$, $p_{22}-p_{12}$, resulting in an analogous equation $E_2 = 0$. Taking $E_1 + E_2\mathrm{i} = 0$ and collecting terms, we get that $Ar^2 + B - C\mathrm{i} \cdot c = 0$, which gives the formula for c iff $C \neq 0$. To find r, we expand the circumcircle condition say for $k = 1$, resulting in

$$0 = |c_1|^2 r^4 + 2\left(-\frac{\alpha_1^2}{2} + c_1 \bullet (c_0 - p_1)\right) r^2 + r_0^2 = |c_1|^2 r^4 + 2Dr^2 + r_0^2.$$

When $c_1 = 0$ (iff $A = 0$), we get the stated formula $r = r_0/\alpha_1$. When $c_1 \neq 0$ however, we may solve the above equation for r^2. Upon some calculation, we deduce that the coefficient of the r^2 term in the equation is $2D$. The quadratic formula gives the desired expression for r, by choosing the negative sign in $\pm$, since we have defined the circumcircle to be the smallest circle satisfying the conditions. □

We remark that if $\vartheta_k = 0$ for some $k \in \{1, 2, 3\}$, then $\alpha_k = 1$, so by the corresponding circumcircle condition, we get that $|p_k - c| = r$. This means that when $\vartheta_k = 0$, the fixed point p_k lies on the circumcircle. For Sierpinski trifractals, all three fixed points lie on the circumcircle, as expected.

3.2.4 The Circumcircle for Bifractals

Similarly to the case of three maps, we will define the two-map circumcircle in an Apollonian manner, to "optimally" satisfy the condition of the Containment Lemma. We derive it in quite a different manner however. Having any bounding circle to the fractal, we may get a potentially smaller one, by applying the Hutchinson operator to it, and then taking the outer tangential circle as in Figure 3.6 - this will be calculated using the map $M : \mathbb{C} \times \mathbb{R}_+ \to \mathbb{C} \times \mathbb{R}_+$ below. So the two-map circumcircle will then be defined as the fixed point - or fixed circle - of M, containing the fractal by its definition and the Containment Lemma.

Having two circles $(a, r_A), (b, r_B) \in \mathbb{C} \times \mathbb{R}_+$ their outer tangential circle (c, r_C) can be found according to the following figure, and the subsequent relations.

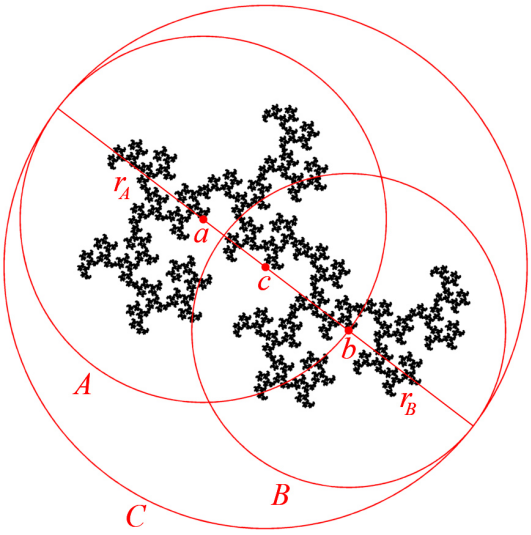

Figure 3.6: Derivation of the circumcircle for bifractals.

From the above figure, the following relations can be seen

$$c = \frac{1}{2}((a - r_A u_{AB}) + (b + r_B u_{AB})), \quad r_C = \frac{1}{2}(r_A + r_B + |b - a|), \quad u_{AB} := \frac{b - a}{|b - a|}$$

which suggest the following transformation. Given a circle $C = (c, r) \in \mathbb{C} \times \mathbb{R}_+$ in the plane, let $M = (m_1, m_2) : \mathbb{C} \times \mathbb{R} \to \mathbb{C} \times \mathbb{R}$ be defined for $T_1(c) \neq T_2(c)$ as

$$M(c, r) := \left(\frac{T_1(c) + T_2(c)}{2} + r\frac{\lambda_2 - \lambda_1}{2} \frac{T_2(c) - T_1(c)}{|T_2(c) - T_1(c)|}, \quad \frac{\lambda_1 + \lambda_2}{2} r + \frac{|T_2(c) - T_1(c)|}{2} \right).$$

Theorem 3.2.3 *Let the* ***circumcircle of a bifractal*** *be defined as the unique fixed point of M, which is given by the following $(c, r) \in \mathbb{C} \times \mathbb{R}_+$*

$$c = \frac{(1-\nu)(1-\varphi_1)p_1 + (1+\nu)(1-\varphi_2)p_2}{(1-\nu)(1-\varphi_1) + (1+\nu)(1-\varphi_2)}$$

$$r = \frac{|1-\varphi_1|\,|1-\varphi_2|}{(1-\lambda)|(1-\nu)(1-\varphi_1) + (1+\nu)(1-\varphi_2)|}\,|p_2 - p_1| = \frac{T_2(c) - T_1(c)}{2(1-\lambda)}$$

$$\lambda := \frac{\lambda_1 + \lambda_2}{2}, \quad \nu := \frac{\lambda_2 - \lambda_1}{2(1-\lambda)}.$$

Proof The fixed point equation $M(c, r) = (c, r)$ implies that $m_2(c, r) = r$ which implies that $r = \frac{1}{2}|T_2(c) - T_1(c)|/(1-\lambda)$. By plugging this into the equation $m_1(c, r) = c$ and some further manipulation, we get the above formula for c. To get the formula for r, according to the above equation it is sufficient to calculate $T_2(c) - T_1(c)$ in terms of $p_{1,2}$ and $\varphi_{1,2}$. Since we have calculated c, this is a matter of some further algebraic manipulation. The derivation shows that the fixed point of M not only exists, but that it is also unique. □

Note that c is the "complex combination" of p_1 and p_2. Also that from the two representations for r, we see that $r \neq 0$ and thus $T_1(c) \neq T_2(c)$.

3.2.5 Concluding Remarks

A brief but important note must be made here, also mentioned briefly in the Introduction. One need not be satisfied working with any given bounding circle $C = B(c, r)$ of F, since it can be easily improved. Having such a circle and taking some finite L-level iterate of it by the Hutchinson operator, ie. $\mathrm{H}^L(C)$, we can take the smallest enclosing circle (c', r') of the n^L centers $\mathrm{H}^L(\{c\})$, and then $(c', r' + \lambda_*^L r)$ will be a tighter bounding circle of F. For large enough L, we can get within any $\varepsilon > 0$ accuracy of the fractal. So we do not need any complex algorithms to arrive at the ε-tightest bounding circle - the minimum bounding circle and sphere algorithms resolve the problem. Although the improved bounding circle may not be ideal anymore (Definition 3.1.2), even if the original was.

Upon considering the various circles, one might contemplate whether there is any good reason to introduce these circumcircles for the case of two or three maps. There is however, in that they may be potentially tighter than the general bounding circle. According to our numerical experiments, in most cases the circumcircles are somewhat tighter (in about 2/3 of the cases), yet the general bounding circle still remains competent. In a few cases, it is even tighter than the circumcircle, so for applications, the programming of both types of circles is advised.

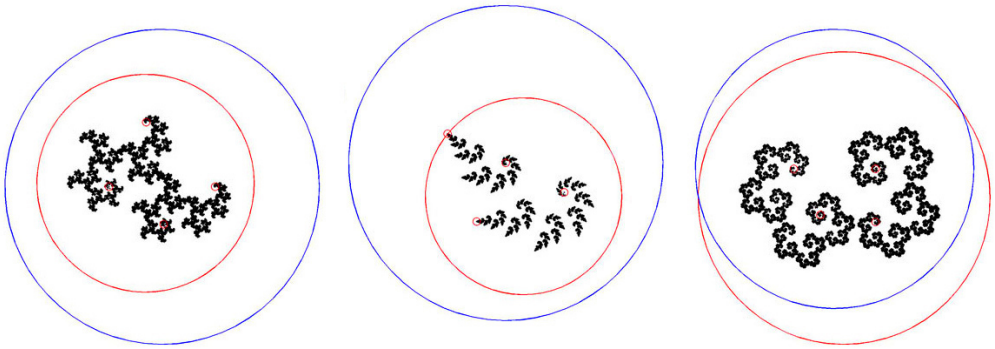

Figure 3.7: The circumcircle (red) vs. the general bounding circle (blue) for bifractals.

We note that cyclic polyfractals, where the fixed points lie on a circle, may be analogously rich in research potential, and may also possess an explicit bounding circle, expressible in terms of the circle along which the fixed points lie. The ultimate question of the explicit non-numerical tightest bounding circle of any IFS fractal lingers.

3.3 The Convex Hull

3.3.1 Introduction

This section presents the main results of the thesis on the geometry of IFS fractals, which we have reduced in Section 3.1 to the problem of bounding, most preferably by the convex hull.

We begin our discussion by excluding a broad class of IFS fractals, called "irrational fractals", for which the cardinality of extremal points is guaranteed to be infinite. Due to infinitesimal self-similarity at the vertices, the convex hull seems impossible to determine explicitly for this class. To save the day, we show the continuity of the IFS attractor in its angular parameters, implying that the irrational case can be approximated arbitrarily closely by "rational fractals", for which the cardinality of extrema can be finite.

We reduce the rational class further to "regular fractals", and derive the explicit convex hull via the Armadillo Method, with a finite number of extremal points as a consequence. The method exploits a single extremal point determined by linear optimization in a special target direction. Critical to the method is the application of Algorithm 4 to verify the defined condition of regularity. Such a special direction seemingly requiring trial-and-error, is derived heuristically for bifractals with opposite signed rotations. Examples are given to show the implementability of the method in practice.

Various numerical methods have been devised to find an approximation to the convex hull of IFS fractals, but our aim being the exact convex hull, only like-minded efforts will be reviewed. Deliu et al. [24] point out the relevance of finding the exact convex hull to resolving the inverse problem of planar IFS fractals - that is to determine the IFS parameters of a geometrical object $F \subset \mathbb{R}^d$, $d \in \mathbb{N}$. Their method works for "polyhulled disjoint (PHD)" attractors, where polyhulled refers to the fractal having a finite number of extremal points. The method - stated to be theoretical - is based on the following theorem and corollary.

Theorem 3.3.1 (Berger [9]) *For the convex hull C_F and extrema E_F of an IFS fractal $F = \langle \mathcal{T} \rangle$ we have $E_F \subset \mathrm{H}_{\mathcal{T}}(E_F)$ and $\mathrm{H}_{\mathcal{T}}(C_F) \subset C_F$.*

Corollary 3.3.1 (Deliu, Geronimo, Shonkwiler [24]) *For a PHD F there exists an IFS $\mathcal{T} = \{T_1, \ldots, T_n\}$ and an extremal point $e_0 \in \mathrm{Ext}(F)$ such that $F = \langle \mathcal{T} \rangle$ and any other extremal point is its finite iterate*

$$\forall e \in \mathrm{Ext}(F)\ \exists a \in \mathcal{A}_{fin} :\ e = T_a(e_0).$$

Their a priori assumption that the geometrical object (for which they wish to determine the IFS parameters) has a finite number of extrema, seems to be an innocent and trivial one. As we will see it certainly is not, and cannot be determined by mere inspection of some plot. By the aforementioned continuity of the attractor in angular parameters (Theorem 3.3.8), one can easily plot an irrational fractal having an infinite number of extrema, and an approximating rational fractal having a finite number, while the plots would look identical to the naked eye or even an analyzing algorithm! In fact, the number of extrema if finite, seems to be the end result of any effort to determine the convex hull.

Nevertheless, the polyhulled condition to their resolution of the planar inverse problem certainly underlines the fundamental relevance of determining the cardinality of extrema, and possibly the convex hull. Wang et al. [69, 45, 77] also discuss these questions regarding self-affine tiles, by introducing methods which are potentially generalizable to the broader class of IFS fractals.

We further note the work of Mandelbrot and Frame [56] who in their effort to characterize "self-contacting binary trees" (bifractals), determine a periodic address leading to a particular extremal point, and reason that it can be written explicitly. Their reasoning is equivalent to our explicit formula for a periodic point stated in Corollary 1.3.1 to the Slope Lemma 1.3.2. Their method highlights the relevance of finding the exact convex hull, for resolving the question of connectedness of IFS fractals.

The author is not aware of any other article where an extremal point has been determined explicitly. A number of such examples will be given in Section 3.3.5 as a result of the presented method in Section 3.3.3. We now proceed to discussing the cardinality of extrema of planar similarity IFS fractals.

3.3.2 The Number of Extrema

The objective of this section is to show that the cardinality of extrema is infinite for any "irrational", while potentially finite for "rational" polyfractals $F = \langle T_1, \ldots, T_n \rangle$.

Definition 3.3.1 *We say that a point s in a compact set S is extremal if it is a vertex of the convex hull* $\mathrm{Conv}(S)$ *meaning* $\nexists s_{1,2} \in S, \lambda \in (0,1) : s = \lambda s_1 + (1-\lambda)s_2$ *and call it an* ***extremal point*** *or extremum. Denote the set of extremal points as* $\mathrm{Ext}(S)$.
We say that an ***address is extremal*** *in an IFS fractal (with respect to some primary fixed point), if the corresponding fractal point is extremal.*

Theorem 3.3.2 *For any extremal point $e \in \mathrm{Ext}(F)$, base $p \in \mathcal{P}$, and any truncation $a < \mathrm{adr}_p(e)$, the* ***inverse iterate*** $T_a^{-1}(e)$ *is also extremal.*

Proof Suppose indirectly that $T_a^{-1}(e) \in F$ is not extremal, meaning there are two points $f_{1,2} \in F \setminus \{e\}$ and some $\lambda \in (0,1)$ for which $T_a^{-1}(e) = (1-\lambda)f_1 + \lambda f_2$. Since T_a is an affine map, applying it to both sides we have $e = (1-\lambda)T_a(f_1) + \lambda T_a(f_2)$ where $T_a(f_{1,2}) \in F$ contradicting that e is extremal. □

Corollary 3.3.2 *The cycle of a periodic extremal address is also extremal. Meaning for any $p_x \in \mathrm{Ext}(F)$, $x \in \mathcal{A}_{fin}$ we have* $\mathrm{Cyc}(x) = \{p_{ba} : \ x = ab\} \subset \mathrm{Ext}(F)$.

Proof This follows trivially from the observation that $T_a^{-1}(p_x) = p_{ba}$. □

Corollary 3.3.3 *Inverse iteration of a non-eventual extremal point $e \in \mathrm{Ext}(F) \setminus \mathrm{Eve}(F)$ generates an infinite number of distinct extrema.*

Proof If x denotes the address of the point $e \in \mathrm{Ext}(F)$, then $|x| = \infty$ necessarily with respect to any base, since e is non-eventual and $\mathcal{P} \subset \mathrm{Per}(F)$. Suppose indirectly that the inverse iterates of e are non-distinct, meaning that for some truncations $a < b < x : \ T_a^{-1}(f) = T_b^{-1}(f)$. Then $\exists c \in \mathcal{A}_{fin} : b = ac$ and $T_b^{-1} = T_c^{-1}T_a^{-1}$ so $T_a^{-1}(e) = T_b^{-1}(e) = T_c^{-1}T_a^{-1}(e)$ implying that $e = T_a T_c T_a^{-1}(e)$ contradicting by Theorem 1.3.3 that e is non-eventual. □

Definition 3.3.2 *Let the* ***value*** *of a finite address $a \in \mathcal{A}_{fin}$ be defined as $\nu(a) := \vartheta_a \bmod (-\pi, \pi]$. We say that an* ***address is focal*** *if its value is zero, and* ***strictly focal*** *if it is focal and possesses each element of the index set $\mathcal{N}$ as a coordinate. We say that a* ***fractal point is focal*** *if its address is a focal periodic one, in other words it is the fixed point of a focal address. Denote the set of all focal points of F as* $\mathrm{Foc}(F)$.

Theorem 3.3.3

$$\mathrm{Ext}(F) \cap \mathrm{Per}(F) = \mathrm{Ext}(F) \cap \mathrm{Foc}(F).$$

Proof By definition $\mathrm{Foc}(F) \subset \mathrm{Per}(F)$ so the $\supset$ direction of containment follows. Now suppose that an extremal point e is periodic, meaning there is an $x \in \mathcal{A}_{fin}$ for which $e = p_x$. Then by Corollary 1.3.2 $T_x(z) = p_x + \varphi_x(z - p_x),\ z \in \mathbb{C}$. Suppose indirectly that $\nu(x) \neq 0$ or in other words $\varphi_x \in \mathbb{C} \setminus \mathbb{R}$. Then the trajectory $t \mapsto T_x^t(z_0)$ traces out a logarithmic spiral for any $z_0 \in \mathbb{C},\ t \in \mathbb{R}$. In the case $|\nu(x)| < \pi$ taking any fractal point $f \in F \setminus \{p_x\}$ the iterates $T_x^k(f) \in F,\ k = 0, 1, 2$ trace out a triangle which contains p_x contradicting that it is extremal. When $\nu(x) = \pi$ the segment $[f, T_x(f)]$ contains p_x in its interior, again contradicting its extremality. Thus we must have $\nu(x) = 0$ implying by definition that $e = p_x \in \mathrm{Foc}(F)$. $\square$

Definition 3.3.3 *We say that a polyfractal is* ***irrational*** *if it has no focal points* $\mathrm{Foc}(F) = \varnothing$*, and* ***rational*** *if it does.*

Theorem 3.3.4 *If all normalized factors* $\frac{\varphi_k}{|\varphi_k|} = \mathrm{e}^{\vartheta_k \mathrm{i}},\ k \in \mathcal{N}$ *are roots of unity, meaning* $\frac{\vartheta_k}{2\pi} \in \mathbb{Q}$*, then the fractal is rational. We will refer to such a case as a* ***fractal of unity****.*

Proof If each $\frac{\vartheta_k}{2\pi} \in \mathbb{Q},\ k \in \mathcal{N}$ then clearly there is a non-trivial linear combination $k_1\vartheta_1 + \ldots + k_n\vartheta \equiv 0 \pmod{(-\pi, \pi]}$ with $k_j \in \mathbb{N}$. So for any address $x \in \mathcal{A},\ |x| < \infty$ for which $\vartheta_x = k_1\vartheta_1 + \ldots + k_n\vartheta_n$ we have $\nu(x) = 0$ meaning $p_x \in \mathrm{Foc}(F)$ which implies that $\mathrm{Foc}(F) \neq 0$. $\square$

Theorem 3.3.5 *If a fixed point of the IFS* $p_k \in \mathcal{P}$ *is extremal then* $\nu(k) = 0$*, meaning* $\mathcal{P} \cap \mathrm{Ext}(F) \subset \mathrm{Foc}(F)$*. If* $\mathcal{P} \subset \mathrm{Ext}(F)$ *then* F *is Sierpinski, meaning* $\nu(k) = 0,\ \forall k \in \mathcal{N}$*.*

Proof For the first statement, suppose indirectly that some $p_k \in \mathcal{P} \cap \mathrm{Ext}(F)$ but $\nu(k) \neq 0$ which is iff $\varphi_k \in \mathbb{C} \setminus \mathbb{R}$. Then for any $f \in F \setminus \{p_k\}$ the trajectory $l \mapsto T_k^l(f), l \in \mathbb{N} \cup \{0\}$ envelops p_k in its convex hull (see the proof of Theorem 3.3.3), so p_k cannot be extremal, which is a contradiction. The second statement clearly follows. $\square$

Theorem 3.3.6 *All extrema of an irrational polyfractal are non-eventual.*

Proof Let us suppose indirectly that some extremal point $e \in \mathrm{Ext}(F)$ is eventual, meaning $\exists a \in \mathcal{A}_{fin}, p \in \mathrm{Per}(F) :\ e = T_a(p)$. Then by Theorem 3.3.2 the inverse iterate $p = T_a^{-1}(e) \in \mathrm{Ext}(F)$ so $p \in \mathrm{Ext}(F) \cap \mathrm{Per}(F) \neq \varnothing$.
By the irrationality of F however $\mathrm{Foc}(F) = \varnothing$ so by Theorem 3.3.3 we get the empty intersection $\mathrm{Ext}(F) \cap \mathrm{Per}(F) = \varnothing$ which is a contradiction. $\square$

Theorem 3.3.7 (Cardinality of Extrema)
An irrational polyfractal has at least a countably infinite number of extremal points.

Proof Theorem 3.3.6 and Corollary 3.3.3 imply that inverse iterating the address of any extremal point will generate a countably infinite number of distinct extrema, so we must have $|\mathrm{Ext}(F)| \geq \aleph_0$. $\square$

We may add to the above theorem upon some contemplation, that by the lack of extremal focality in an irrational fractal, the extrema tend to infinitesimally cluster around the vertices of the convex hull. Thus the corners are "rounded off self-similarly" in an infinite number of extrema, so finding the exact convex hull of an irrational fractal seems hopelessly difficult. We may however turn our efforts to finding the potentially finite convex hull of rational fractals, and fortunately by the theorem below, they approximate the irrational case.

Theorem 3.3.8 (Continuity in Angular Parameters)
Keeping the rotation angles variable as a vector $\vartheta := (\vartheta_1, \ldots, \vartheta_n)$ while the other parameters of the IFS constant, and denoting the resulting attractor as $F[\vartheta]$, the map $\vartheta \mapsto F[\vartheta]$ is continuous in the following domain and range metrics respectively

$$\delta_\infty(\vartheta, \vartheta') := \max_{k \in \mathcal{N}} |\vartheta_k - \vartheta'_k| \quad \textit{and} \quad d_\infty(F, F') := \sup_{a \in \mathcal{A}} |T_a(p) - T'_a(p)|.$$

Proof It is clear that both δ_∞ and d_∞ are metrics. Let $F[\vartheta]$ be a generate of the IFS $T_k[\vartheta](z) = p_k + \lambda_k \mathrm{e}^{\vartheta_k \mathrm{i}}(z - p_k),\ k \in \mathcal{N}$ leaving only the rotation angles variable in the IFS parameters. Then we refer to some composition of maps variable in ϑ as $T_a[\vartheta], a \in \mathcal{A}$. Let the p seed be any fixed point $p_k \in \mathcal{P}$. By the compactness of $F[\vartheta]$ for a fixed ϑ we reasonably restrict the approximating domain in a bounded manner to $D_\vartheta := \{\vartheta' \in (-\pi, \pi]^n : \mathrm{diam}(F[\vartheta']) < D[\vartheta]\}$ where $D[\vartheta] > \mathrm{diam}(F[\vartheta])$ is fixed and arbitrary. We need to show the following statement for continuity:

$$\forall \vartheta \in (-\pi, \pi]^n\ \forall \varepsilon > 0\ \exists \delta > 0\ \forall \vartheta' \in D_\vartheta\ (\delta_\infty(\vartheta, \vartheta') < \delta) :\ d_\infty(F[\vartheta], F[\vartheta']) < \varepsilon.$$

In our quest, we first observe that for any finite address $a \in \mathcal{A}, |a| \leq L$ and seed $p \in \mathcal{P}$ the map $\vartheta \mapsto T_a[\vartheta](p)$ is continuous, meaning

$$\forall L \in \mathbb{N}\ \forall a \in \mathcal{A}\ (|a| \leq L)\ \forall \vartheta \in (-\pi, \pi]^n\ \forall \varepsilon > 0\ \exists \delta_a > 0$$

$$\forall \vartheta' \in D_\vartheta\ (\delta_\infty(\vartheta, \vartheta') < \delta) :\ |T_a[\vartheta](p) - T_a[\vartheta'](p)| < \varepsilon.$$

Then with the notations $d_\infty^L(F,F') := \max_{|a|\le L} |T_a(p) - T'_a(p)|$ and $\delta := \min_{|a|\le L} \delta_a$ we get the following reinterpretation of the above logical statement (since $\forall$ terms are logically commutative) which means continuity in d_∞^L.

$$\forall L \in \mathbb{N}\ \forall \vartheta \in (-\pi,\pi]^n\ \forall \varepsilon > 0\ \exists \delta > 0\ \forall \vartheta' \in D_\vartheta\ (\delta_\infty(\vartheta,\vartheta') < \delta):\ d_\infty^L(F[\vartheta],F[\vartheta']) < \varepsilon.$$

We now sidetrack briefly, and derive an inequality between d_∞ and d_∞^L. First we make the observation using the Slope Lemma that for any $a,b \in \mathcal{A}_{fin}, |a| = L$ with the notation $\lambda_* := \max_{k\in\mathcal{N}} \lambda_k$ we can rewrite and estimate the quantity $|T_{ab}[\vartheta](p) - T_{ab}[\vartheta'](p)|$ for $\vartheta \in (-\pi,\pi]^n,\ \vartheta' \in D_\vartheta$ as follows

$$|T_{ab}[\vartheta](p) - T_{ab}[\vartheta'](p)| =$$

$$= |(T_{ab}[\vartheta](p) - T_a[\vartheta](p)) + (T_a[\vartheta](p) - T_a[\vartheta'](p)) + (T_a[\vartheta'](p) - T_{ab}[\vartheta'](p))| \le$$

$$\le \lambda_a |T_b[\vartheta](p) - p| + |T_a[\vartheta](p) - T_a[\vartheta'](p)| + \lambda_a |p - T_b[\vartheta'](p)| \le$$

$$\le |T_a[\vartheta](p) - T_a[\vartheta'](p)| + 2\lambda_*^L D[\vartheta]\ \Rightarrow$$

$$\sup_{|a|>L} |T_a[\vartheta](p) - T_a[\vartheta'](p)| \le d_\infty^L(F[\vartheta],F[\vartheta']) + 2\lambda_*^L D[\vartheta].$$

We now show the aforementioned inequality between d_∞ and d_∞^L.

$$d_\infty(F[\vartheta],F[\vartheta']) = \max\left(\max_{|a|\le L}\ |T_a[\vartheta](p) - T_a[\vartheta'](p)|,\ \sup_{|a|>L}\ |T_a[\vartheta](p) - T_a[\vartheta'](p)|\right) \le$$

$$\le \max(d_\infty^L(F[\vartheta],F[\vartheta']),\ d_\infty^L(F[\vartheta],F[\vartheta']) + 2\lambda_*^L D[\vartheta]) \le d_\infty^L(F[\vartheta],F[\vartheta']) + 2\lambda_*^L D[\vartheta].$$

Finally, we proceed to showing the desired continuity in angular parameters. Let the locus of desired continuity $\vartheta \in (-\pi,\pi]^n$ and the accuracy $\varepsilon > 0$ be fixed and arbitrary. We choose some $L \in \mathbb{N}$ so that $\lambda_*^L D[\vartheta] < \frac{\varepsilon}{4}$. Then by the continuity in d_∞^L above, we have for these $L, \vartheta, \varepsilon$ fixed numbers that

$$\exists \delta > 0\ \forall \vartheta' \in D_\vartheta\ (\delta_\infty(\vartheta,\vartheta') < \delta):\ d_\infty^L(F[\vartheta],F[\vartheta']) < \varepsilon$$

and with this same δ and any such ϑ' we have by the above inequalities that

$$d_\infty(F[\vartheta],F[\vartheta']) \le d_\infty^L(F[\vartheta],F[\vartheta']) + 2\lambda_*^L D[\vartheta] < \frac{\varepsilon}{2} + \frac{\varepsilon}{2} = \varepsilon$$

implying the desired property of continuity. $\square$

3.3.3 The Convex Hull of Regular IFS Fractals

We now turn to the main result of the thesis: determining the convex hull of polyfractals, as the exact resolution of the Thesis Problem. We emphasize "exactness" throughout, so as to be clear that the resulting extrema are the actual explicit extremal points, and not merely approximate or theoretical as often is the case in the literature. The presented method can be carried out in practice, as shown in the examples of Section 3.3.5.

As we have seen in the previous section, the case of irrational fractals seems hopelessly difficult, so we restrict our attention to the rational class which by continuity in parameters can approximate the irrational case. Thus for the remainder of our discussion $\mathrm{Foc}(F)$ will be assumed to be nonempty, for some polyfractal $F = \langle T_1, \ldots, T_n \rangle$.

To briefly outline our technique for determining the convex hull, we shall discuss certain ideal linear target directions - called "regular directions" - for finding one focal extremal point, which will be exploited through its "cycle" to find a set of neighboring extrema. These extrema when iterated by each IFS map alone, will map out the entire convex hull by the "Armadillo Method". As a corollary, we get that the fractal has a finite number of extrema. This is only when the existence of such a regular direction is known - in the next section we introduce a general heuristic candidate for bifractals, called the "principal direction". We begin by defining some basic terminology.

Definition 3.3.4 *We will say that two distinct extrema are* ***neighbors*** *if the polyfractal is a subset of a closed half-space determined by the line connecting them. The* ***right/left neighbor*** *of an extremal point is the neighbor which comes counter/clockwise around the vertices of the convex hull. We denote the left neighbor of* $e \in \mathrm{Ext}(F)$ *as* e'*, and call the angle* $\mathrm{Arg}(e'-e) \in (-\pi, \pi]$ *the* ***state*** *of* e*, denoted as* $\sigma(e)$*. We call the connecting line* $\overline{e'e}$ *the* ***stateline*** *of* e*. A subset of extrema is* ***consecutive*** *if each element has a neighbor in the subset, and we call such a subset a* ***plate****. A focal address* $x \in \mathcal{A}, |x| < \infty, \nu(x) = 0$ *is* ***consecutive*** *if* $p_x \in \mathrm{Ext}(F)$ *and* $\mathrm{Cyc}(x) \subset \mathrm{Ext}(F)$ *is consecutive around* $\mathrm{Conv}(F)$*; furthermore we say that* p_x *is a* ***consecutive focal point****.*

Theorem 3.3.9 (Exclusion Principle of Extrema) *State is strictly monotonic clockwise around the extrema, and no two extrema may have the same state.*

Proof State is clearly strictly monotonic with say clockwise traversion of the extremal points, otherwise three of them would lie on the same line, contradicting that the one in between is extremal. Strict monotonicity directly implies the injectivity of state, which reworded gives the second part of the statement. □

Definition 3.3.5 *We say that $\tau \in \mathbb{C}$ is a **target direction** if our aim is to maximize the linear **target function** $z \mapsto \langle \tau, z \rangle$ over a polyfractal $F = \langle T_1, \ldots, T_n \rangle$. Since IFS fractals are compact, a target function attains its optimum in an extremal point, which we shall refer to as a **maximizer** of τ (also as: a maximizing extremal point). We call the address of such a maximizer (with respect to some primary fixed point) a **maximizing address** of τ.*

Theorem 3.3.10 *If the maximizing address(es) of a target direction $\tau \in \mathbb{C}$ begin with a common focal address $x \in \mathcal{A}_{fin}$ then the maximizer of τ over F is unique and it is $p_x \in \mathrm{Ext}(F)$.*

Proof Let a maximizer be denoted as $e \in \mathrm{Ext}(F)$, and we show that necessarily $e = p_x$. Since the address of e begins with x we have $e \in T_x(F) \subset F$ so $\exists f_1 \in F : e = T_x(f_1)$. Since $T_x(f_1)$ is a maximizer of τ over $T_x(F)$, this f_1 must also be a maximizer of τ over F, since $T_x(F)$ is a non-rotated reduced copy of F by a factor of $\varphi_x = \lambda_x \in (0, 1)$ due to $\nu(x) = 0$. So by the condition of the theorem, we must have that $\exists f_2 \in F : f_1 = T_x(f_2)$. Continuing this argument inductively, we see that $e = T_x^k(f_k),\ k \in \mathbb{N}$ and taking the limit as $k \to \infty$ we have that $e = p_x$. $\square$

Definition 3.3.6 *A target direction is **regular** if its maximizing extremal point is unique, strictly focal, and consecutive. A polyfractal is regular if it has a regular target direction.*

Since focality is a requirement, only rational polyfractals can be regular. As we shall see, having a candidate direction, it is easy to verify whether it is regular. So the challenge is to deduce a candidate which is likely to be regular, potentially via a general heuristic argument, as we will for bifractals in the next section.

The utility of regularity began to unfold with the above theorem, and will be revealed fully by the end of this section. By the above theorem, it sufficient to verify for regularity that the maximizing address(es) of a candidate direction begin with a common focal address, which we can verify using Algorithm 4. That this address is strictly focal, is easy to verify, we just need to check if each $k \in \mathcal{N}$ occurs in it.

The consecutiveness of the maximizing p_x can also be verified using Algorithm 4, since what we need is for the lines connecting neighbors in $\mathrm{Cyc}(x)$ to be statelines. To see if $e_{1,2} \in \mathrm{Cyc}(x) \subset \mathrm{Ext}(F)$ are neighbors, we can take an outward normal $\tau_0 \in \mathbb{C}$ to the line connecting them, and run Algorithm 4 to see what $|x|$-long truncations come up as maximizers. If only those of e_1 and e_2 do, then they must be neighbors by the following theorem.

Theorem 3.3.11 *If a target direction $\tau_0 \in \mathbb{C}$ has only two maximizing focal truncations $x_{1,2} \in \mathcal{A}_{fin}$ of some length $L \in \mathbb{N}$, for which $p_{x_1}, p_{x_2} \in \mathrm{Ext}(F)$, then they are neighbors on the convex hull.*

Proof Suppose indirectly that they are not neighbors, meaning either p_{x_1} or p_{x_2} (or both) is not a maximizer of τ_0 over F (if they both were, then they would have to be neighbors by definition). Denote some other maximizer as $e \in \mathrm{Ext}(F) \setminus \{p_{x_1}, p_{x_2}\}$. Then $e \in T_{x_1}(F) \cup T_{x_2}(F)$ since $x_1 \neq x_2$ are the only two maximizing truncations, with respect to τ_0. Since $x_{1,2}$ are focal, this property transfers to $T_{x_1}(F)$ and $T_{x_2}(F)$, so necessarily

$$e \in (T_{x_1}T_{x_1}(F) \cup T_{x_1}T_{x_2}(F)) \cup (T_{x_2}T_{x_1}(F) \cup T_{x_2}T_{x_2}(F)).$$

Continuing by induction, we see that

$$e \in \mathrm{H}^L_{\mathcal{T}_0}(F)\ \forall L \in \mathbb{N} \ \text{ with the IFS } \ \mathcal{T}_0 := \{T_{x_1}, T_{x_2}\}.$$

Taking the limit as $L \to \infty$, we get that $e \in \langle T_{x_1}, T_{x_2}\rangle$ which is a 1-dimensional Cantor set (IFS fractal) along the line $\overline{p_{x_1}p_{x_2}}$. So necessarily both p_{x_1} and p_{x_2} are maximizers of τ_0, which contradicts what we supposed. □

Therefore what we need to know a priori, is the order in which the elements of $\mathrm{Cyc}(x)$ are arranged among the vertices of the convex hull, so that we know which pairs to verify to be neighboring extrema. This question is answered by the following theorem: the value of the truncations of x imply the ordering.

Theorem 3.3.12 *For a focal extremal point $e = p_x \in \mathrm{Ext}(F) \cap \mathrm{Foc}(F),\ x = ab$ we have*

$$\nu(b) = \sigma(T_b(e)) - \sigma(e) \bmod (-\pi, \pi].$$

This means that e and $T_b(e)$ differ in state by $\nu(b)$, so the value $\nu(a) = -\nu(b)$ of the truncations $a < x$ imply the order of $\mathrm{Cyc}(x)$ among the vertices of the convex hull.

Proof Let s denote the stateline of e. Since T_b rotates by an angle of $\nu(b)$ and the fractal lies on one side of s, then $T_b(F)$ must also lie on one side of $T_b(s)$. We argue that $T_b(s)$ is the stateline of $T_b(e)$. For let us assume indirectly that there is a fractal point $f \in F$ on the other side of $T_b(s)$. Then mapping f and $T_b(s)$ back by T_a and thus rotating by an angle of $\nu(a) = -\nu(b)$ we have that $T_aT_b(e) = e,\ T_aT_b(s) = s$ while $T_a(f)$ lies on the corresponding "other" side of s, contradicting that s is the stateline of e. □

We finally show the main result, which exploits the maximizing extremal point of a regular target direction, and generates a plate which is then mapped simply by the iterates of each IFS map to give the entire convex hull - the iterated plates potentially overlapping, just like in the armor of an armadillo. The surprising corollary will be that if a regular target direction exists, the polyfractal has a finite number of extrema - clearly only possible in the rational case by Theorem 3.3.7.

Theorem 3.3.13 (Armadillo Method)
Let $p_x \in \mathrm{Ext}(F) \cap \mathrm{Foc}(F)$ be the maximizer of a regular target direction. Then the iterates of the plate $\mathrm{Cyc}(x)$ by each $T_k \in \mathcal{T}$ generate all the extrema of F, specifically

$$\mathrm{Conv} \bigcup_{k=1}^{n} \bigcup_{l=0}^{\left\lceil \frac{\pi}{|\vartheta_k|} \right\rceil} T_k^l \left(\mathrm{Cyc}(x)\right) = \mathrm{Conv}(F).$$

Therefore a regular polyfractal has a finite number of extrema.

Proof By regularity we have that $\mathrm{Cyc}(x) \subset \mathrm{Ext}(F)$ are consecutive extrema. By the strict focality of x we have that each $k \in \mathcal{N} = \{1, \ldots, n\}$ occurs in x so

$$\forall k \in \mathcal{N} \ \exists e_{1,2} \in \mathrm{Cyc}(x) : \ e_1 = T_k(e_2)$$

thus the angle with vertex at p_k and spanned by $\mathrm{Cyc}(x)$ is at least $|\vartheta_k|$ for each $k \in \mathcal{N}$. So the iterated plate $T_k^l(Cyc(x)), l \in \mathbb{N}$ produces more (potentially overlapping) plates of extrema. Since each T_k traces a logarithmic spiral trajectory, we only need to iterate up to a $\lceil \pi/|\vartheta_k| \rceil$ number of times for each $k \in \mathcal{N}$. This gives the convex hull identity in the theorem.
The identity also implies that F has a finite number of extrema, since on the left of the identity we have a finite union of finite sets. □

As we discussed, regularity can be verified for a candidate direction via Algorithm 4, so the challenge is always to find such a direction. For certain bifractals, a general heuristic candidate is introduced in the next section.

3.3.4 The Principal Direction of C-IFS Fractals

In this section, we restrict our attention to rational bifractals in our quest to find a reasonable candidate target direction - called the "principal direction" - the regularity of which can then be verified via the methods discussed in the previous section. Nevertheless, we provide a detailed heuristic reasoning for the likelihood of its regularity, even though a de facto proof has eluded us (and may not be possible in general). In the next section we give specific examples for the application of the principal direction, and further discuss the computational likelihood of regularity.

For the sake of simplicity, it is often preferable to transform a bifractal to "normal form", i.e. to normalize the primary and secondary fixed points $p_{1,2} \in \mathcal{P}$ of the IFS to 0 and 1. This can be accomplished by the affine similarity transform $N(z) := (z - p_1)/(p_2 - p_1)$. It is entirely up to our preference which maps or fixed points we select to be primary (seed) and secondary, though by our notation $p_1 = 0$ will always be primary in the bifractal $F = \langle T_1, T_2 \rangle$.

Theorem 3.3.14 (Normal Form) *For the above N map, we have for $k = 1, 2$ that*

$$T'_k(z) := N \circ T_k \circ N^{-1}(z) = N(p_k) + \varphi_k(z - N(p_k)), \text{ where } N(p_1) = 0, N(p_2) = 1$$

and $N(F) = \langle T'_1, T'_2 \rangle$ which we call the normal form of F. Furthermore for any $x \in \mathcal{A}_{fin}$ using $T'_x = NT_xN^{-1}$ we can express the periodic point $p_x = T_x(p_x)$ as

$$p_x = \frac{T_x(0)}{1 - \varphi_x} = p_1 + \frac{T'_x(0)}{1 - \varphi_x}(p_2 - p_1).$$

Proof The first sentence follows from the Affine Lemma 1.3.3. To show the second property, we first observe that $T'_x = NT_xN^{-1}$ is trivial by the cancellation of N terms in the compositions of $T'_k, k \in \mathcal{N}$. So we have

$$T'_x(0) = NT_xN^{-1}(0) = NT_x(p_1) = N(p_x + \varphi_x(p_1 - p_x)) = \frac{(1 - \varphi_x)(p_x - p_1)}{p_2 - p_1}$$

$$p_1 + \frac{T'_x(0)}{1 - \varphi_x}(p_2 - p_1) = p_1 + \frac{(1 - \varphi_x)(p_x - p_1)}{(p_2 - p_1)(1 - \varphi_x)}(p_2 - p_1) = p_x. \ \square$$

Essentially, the above theorem tells us that we can scale down the IFS fractal to normal form, examine its geometrical properties (such as its convex hull), and then transform back the results, since N is an affine similarity transform and

$$F = N^{-1}\langle N \circ T_1 \circ N^{-1}, N \circ T_2 \circ N^{-1} \rangle.$$

Fundamentally, we also recognize that the factors $\varphi_{1,2}$ entirely characterize the geometry of a bifractal, since they remain unchanged under normalization. We will thus be discussing normalized bifractals only, and drop the apostrophes, so the maps become

$$T_1(z) = \varphi_1 z \quad \text{and} \quad T_2(z) = 1 + \varphi_2(z-1).$$

Theorem 3.3.15 *All finite compositions of $T_{1,2}$ ending in T_2 with seed $p_1 = 0$ take the following form when like terms are collected*

$$T_1^{n_0} T_2 T_1^{n_1} T_2 \dots T_1^{n_L} T_2(0) = (1-\varphi_2) \sum_{j=0}^{L} \varphi_1^{s_j} \varphi_2^j \quad \text{where} \quad L \in \mathbb{N},\ n_j \geq 0,\ s_j := \sum_{k=0}^{j} n_k.$$

Proof It is clear that all such address compositions can be brought to the above form on the left by collecting terms, so in order to prove the form on the right, we proceed to showing the following more general property:

$$T_1^{n_0} T_2 T_1^{n_1} T_2 \dots T_1^{n_L} T_2(z) = (1-\varphi_2) \left(\sum_{j=0}^{L} \varphi_1^{s_j} \varphi_2^j \right) + \varphi_1^{n_L} \varphi_2^{L+1} z$$

from which the earlier one follows with $z = 0$. We show the property by induction. For $L = 0$ we have

$$T_1^{n_0} T_2(z) = \varphi_1^{n_0}(1 + \varphi_2(z-1)) = \varphi_1^{n_0} + \varphi_1^{n_0}\varphi_2 z - \varphi_1^{n_0}\varphi_2 = (1-\varphi_2)\varphi_1^{n_0}\varphi_2^0 + \varphi_1^{n_0}\varphi_2 z.$$

Now suppose that it holds up to $L = l$ and we show it for $L = l+1$. With $z = T_1^{n_{l+1}} T_2(z_0)$ for any $z_0 \in \mathbb{C}$ we have by the associativity of composition that

$$T_1^{n_0} T_2 T_1^{n_1} T_2 \dots T_1^{n_l} T_2 \left(T_1^{n_{l+1}} T_2(z_0) \right) =$$

$$= (1-\varphi_2) \left(\sum_{j=0}^{l} \varphi_1^{s_j} \varphi_2^j \right) + \varphi_1^{n_l} \varphi_2^{l+1} \left(\varphi_1^{n_{l+1}} (1 + \varphi_2(z_0 - 1)) \right) =$$

$$= (1-\varphi_2) \left(\sum_{j=0}^{l+1} \varphi_1^{s_j} \varphi_2^j \right) + \varphi_1^{n_{l+1}} \varphi_2^{(l+1)+1} z$$

which is the expected form. With the seed $z = 0$ we have the desired formula. □

We further restrict our discussion from bifractals to C-IFS fractals.

Definition 3.3.7 *We will say that a bifractal is* ***C-type*** *(after the Lévy C curve), if its rotation angles $\vartheta_{1,2} \in (-\pi, \pi]$ have opposite sign and are neither zero nor π. We may assume that $\vartheta_1 < 0,\ \vartheta_2 > 0,\ |\vartheta_1| \le \vartheta_2$ without restriction of geometrical generality. Otherwise a bifractal is* ***S-type****. We will also refer to such fractals as* ***C-IFS*** *and* ***S-IFS fractals*** *respectively.*

Heuristic 3.3.1 *Let $F = \langle T_1, T_2 \rangle$ be a normalized C-IFS fractal of unity with*

$$\vartheta_1 = -\frac{2\pi P}{M},\ \vartheta_2 = \frac{2\pi Q}{M} \quad \text{where} \quad P, Q, M \in \mathbb{N},\ 0 < P \le Q < \frac{M}{2}.$$

Then the target direction $\tau_* := \mathrm{i}(1-\varphi_2)\mathrm{Log}\ \varphi_1$ called the ***principal direction****, is likely to be regular, and its maximizer is likely to be the periodic point p_x where*

$$x \in \mathcal{A}_{fin}: \quad |x| = \frac{P+Q}{\gcd(P,Q)}$$

$$T_x = T_2 T_1^{n_1} \dots T_2 T_1^{n_J},\ n_j = s_j - s_{j-1},\ j = 1, \dots, J := \frac{P}{\gcd(P,Q)},\ n_0 = s_0 = 0$$

$$s_j := \operatorname{argmax}\left(\lambda_1^s \cos(\vartheta_1 s + \vartheta_2 j + \alpha) :\ s = \left\lfloor \frac{Qj}{P} \right\rfloor, \left\lceil \frac{Qj}{P} \right\rceil \right) \quad \alpha := \arctan\left(\frac{\ln \lambda_1}{\vartheta_1} \right).$$

Let the maximizer with respect to the principal direction be called the ***principal extremal point****, denoted as e_*.*

Reasoning First of all, we calculate the Euclidean inner product of the principal direction τ_* with a general normalized fractal point given by Theorem 3.3.15, and connect it to τ_j. Our calculation is aided by the identity $\forall u, v \in \mathbb{C} : \langle u, v \rangle = \mathrm{Re}(u\bar{v})$. Denoting $t_j(s) := \lambda_1^s \cos(\vartheta_1 s + \vartheta_2 j + \alpha)$ we have

$$\left\langle \mathrm{i}(1-\varphi_2)\mathrm{Log}\ \varphi_1,\ (1-\varphi_2)\sum_{j=0}^{L} \varphi_1^{s_j}\varphi_2^j \right\rangle = |1-\varphi_2|^2 \sum_{j=0}^{L} \left\langle \mathrm{iLog}\ \varphi_1, \varphi_1^{s_j}\varphi_2^j \right\rangle =$$

$$= |1-\varphi_2|^2 |\mathrm{Log}\ \varphi_1| \sum_{j=0}^{L} \lambda_1^{s_j}\lambda_2^j \cos \angle\left(\mathrm{iLog}\ \varphi_1, \varphi_1^{s_j}\varphi_2^j\right) = |1-\varphi_2|^2 |\mathrm{Log}\ \varphi_1| \sum_{j=0}^{L} \lambda_2^j t_j(s_j)$$

$$\text{since} \quad \angle\left(\mathrm{iLog}\ \varphi_1, \varphi_1^{s_j}\varphi_2^j\right) \equiv \mathrm{Arg}(\varphi_1^{s_j}\varphi_2^j) - \mathrm{Arg}(-\vartheta_1 + \mathrm{i}\ln\lambda_1) \equiv$$

$$\equiv (\vartheta_1 s_j + \vartheta_2 j) - \arctan\left(-\frac{\ln\lambda_1}{\vartheta_1}\right) \equiv \vartheta_1 s + \vartheta_2 j + \alpha \pmod{2\pi}.$$

So we deduced that in order to maximize $z \mapsto \langle \tau_*, z \rangle$ over $F = \langle T_1, T_2 \rangle$ we need to maximize the sum $\sum_{j=0}^{L} \lambda_2^j t_j(s_j)$ over all $L \in \mathbb{N}$ and $0 \leq s_j \leq s_{j+1}$ $(j = 0, 1, 2, \ldots)$.
We temporarily drop the latter optimization constraint, and just consider each $s \mapsto t_j(s)$ function individually, and see where its local extrema are. Taking the derivative

$$t_j'(s) = (\ln \lambda_1)\lambda_1^s \cos(\vartheta_1 s + \vartheta_2 j + \alpha) - \vartheta_1 \lambda_1^s \sin(\vartheta_1 s + \vartheta_2 j + \alpha) =$$

$$= (\ln \lambda_1)\lambda_1^s \left[\cos(\vartheta_1 s + \vartheta_2 j)\cos(\alpha) - \sin(\vartheta_1 s + \vartheta_2 j)\sin(\alpha)\right] -$$

$$-\vartheta_1 \lambda_1^s \left[\sin(\vartheta_1 s + \vartheta_2 j)\cos(\alpha) + \cos(\vartheta_1 s + \vartheta_2 j)\sin(\alpha)\right] =$$

$$= \lambda_1^s \left(\cos(\vartheta_1 s + \vartheta_2 j)\left[(\ln \lambda_1)\cos\alpha - \vartheta_1 \sin\alpha\right] - \sin(\vartheta_1 s + \vartheta_2 j)\left[(\ln \lambda_1)\sin\alpha + \vartheta_1 \cos\alpha\right]\right)$$

$$= -\lambda_1^s \sin(\vartheta_1 s + \vartheta_2 j)\left[(\ln \lambda_1)\sin\alpha + \vartheta_1 \cos\alpha\right] =$$

$$= |\vartheta_1|(\cos\alpha)(1 + (\tan\alpha)^2)\sin(\vartheta_1 s + \vartheta_2 j)$$

since

$$(\ln \lambda_1)\cos\alpha - \vartheta_1 \sin\alpha = (\cos\alpha)\vartheta_1(\tan\alpha - \tan\alpha) = 0$$

$$(\ln \lambda_1)\sin\alpha + \vartheta_1 \cos\alpha = \vartheta_1(\cos\alpha)((\tan\alpha)^2 + 1) \neq 0$$

where $\cos\alpha > 0$ by $\alpha = \arctan\left(\frac{\ln \lambda_1}{\vartheta_1}\right) \in \left(0, \frac{\pi}{2}\right)$ due to $\frac{\ln \lambda_1}{\vartheta_1} > 0$. So remarkably

$$\operatorname{sgn}\ t_j'(s) = \operatorname{sgn}\ \sin(\vartheta_1 s + \vartheta_2 j) = -\operatorname{sgn}\ \sin(|\vartheta_1| s - \vartheta_2 j)$$

which ultimately followed from our special choice of τ_*. Since the $\vartheta_1 < 0$ factor flips the oscillation of sin, the local maxima occur at

$$\vartheta_1 s + \vartheta_2 j = 2\pi k,\ k \in \mathbb{Z}$$

$$s \in \left\{ -\frac{\vartheta_2 j}{\vartheta_1} + \frac{2\pi}{\vartheta_1} k :\ k \in \mathbb{Z} \right\} = \left\{ \frac{Qj}{P} + \frac{M}{P} k :\ k \in \mathbb{Z} \right\}.$$

Denote by s_j the heuristically most reasonable sequence $j = 0, 1, 2, \ldots$ for maximizing $f \mapsto \langle \tau_*, f \rangle, f \in F$. For $j = 0$ the likely solution is $s_0 = 0$ with $k = 0$, since for $k < 0$ the number $\frac{Qj}{P} + \frac{M}{P} k$ is negative, and for $k \geq 1$ the maximal values of t_j decrease, since $s \mapsto t_0(s)$ oscillates between the decreasing exponential curves $s \mapsto \pm\lambda_1^s$. Therefore we conclude heuristically that $s_0 = 0$.
We further reason that $s_j \in \left\{ \left\lfloor \frac{Qj}{P} \right\rfloor, \left\lceil \frac{Qj}{P} \right\rceil \right\}$ for each $j \in \mathbb{N}$. Since $\frac{Qj}{P}$ occur with a spacing of $\frac{Q}{P} < \frac{M}{2P}$ while the local maxima of t_j occur with a spacing of $\frac{M}{P}$ then assuming heuristically the somewhat stricter constraint $s_j < s_{j+1},\ j \in \mathbb{N}$ we necessarily have that s_j occurs in an integer near $\frac{Qj}{P}$.

We may thus conclude the heuristic statement that the maximizer with respect to τ_* is likely to have the collected exponents $n_j = s_j - s_{j-1},\ j \in \mathbb{N}$ where

$$s_j = \operatorname{argmax}\left(t_j(s):\ s = \left\lfloor \frac{Qj}{P} \right\rfloor, \left\lceil \frac{Qj}{P} \right\rceil\right).$$

We show that this address is periodic according to the map

$$T_x = T_2 T_1^{n_1} \dots T_2 T_1^{n_J},\ j = 1, \dots, J = \frac{P}{\gcd(P,Q)}$$

or equivalently that n_j is periodic by J. If we can show that $s_{j+J} = s_j + s_J$ then it would follow that

$$n_{j+J} = s_{j+J} - s_{j+J-1} = (s_j + s_J) - (s_{j-1} + s_J) = s_j - s_{j-1} = n_j.$$

First of all, $s_J = \frac{QJ}{P}$ necessarily, so $\vartheta_1 s_J + \vartheta_2 J = 0$ implying

$$t_{j+J}(s + s_J) = \lambda_1^{s+s_J} \cos(\vartheta_1(s + s_J) + \vartheta_2(j + J) + \alpha) = \lambda_1^{s_J} t_j(s).$$

Since the optimum of t_j with respect to the global target τ_* was deduced to be $s_j \in \left\{\left\lfloor \frac{Qj}{P} \right\rfloor, \left\lceil \frac{Qj}{P} \right\rceil\right\}$ and due to

$$s_{j+J} \in \left\{\left\lfloor \frac{Q(j+J)}{P} \right\rfloor, \left\lceil \frac{Q(j+J)}{P} \right\rceil\right\} = s_J + \left\{\left\lfloor \frac{Qj}{P} \right\rfloor, \left\lceil \frac{Qj}{P} \right\rceil\right\}$$

we necessarily have $s_{j+J} = s_j + s_J$ implying the periodicity of n_j by J.
Thus the maximizer of τ_* is heuristically likely to be the fixed point of x, which is strictly focal since $\nu(x) = \vartheta_1 s_J + \vartheta_2 J = 0$ and T_x contains both T_1 and T_2.
Using Algorithm 4 and Theorem 3.3.11 we can verify if this p_x is indeed the maximizer of τ_*, in which case then necessarily $\mathrm{Cyc}(x) \subset \mathrm{Ext}(F)$. With this algorithm, we can also verify the consecutiveness of the cycle, which has mostly been the case in our computational experiments, meaning τ_* is usually a regular target direction. □

Method 3.3.1 (Exact) *The exact method for finding the convex hull of rational C-IFS fractals of unity, based on the heuristic prediction that the principal direction is likely to be regular, is as follows.*

1. *Normalize the IFS maps to* $T_1(z) = \varphi_1 z,\ T_2(z) = 1 + \varphi_2(z - 1)$.
2. *Calculate the principal direction* $\tau_* = \mathrm{i}(1 - \varphi_2)\mathrm{Log}\ \varphi_1$.

3. *Run Algorithm 4 with* $L = \frac{P+Q}{\gcd(P,Q)}$ *and a larger* M*, and see if it gives a unique focal maximizing truncation* $x \in \mathcal{A}$ *of this length. If it does, then we can conclude by Theorem 3.3.10 that the maximizer is* p_x *and we may proceed - this is then the principal extremal point, calculated by Corollary 1.3.1. (Otherwise, we must try a different candidate direction.)*

4. *Next we deduce the order of* $\mathrm{Cyc}(x) \subset \mathrm{Ext}(F)$ *on the convex hull according to Theorem 3.3.12 and check if they are consecutive. Connecting each extremal point with its likely neighbor, we check using Algorithm 4 in the normal direction to the connecting line, whether the maximizing truncation of length* L *above, is any other than the connected periodic addresses in the cycle. If not, then by Theorem 3.3.11 necessarily they are neighbors. (If the cycle turns out not to be consecutive, then we must try a different candidate direction.)*

5. *We iterate the cycle* $\mathrm{Cyc}(x)$ *by each IFS map according to the Armadillo Method (Theorem 3.3.13) to find the rest of the extrema.*

6. *Lastly, we map the determined extrema back by the inverse of the normalizing map* $N^{-1}(z) = p_1 + z(p_2 - p_1)$ *to get the extrema of the original fractal.*

If all steps can be carried out, then this method results in the exact convex hull of a rational C-IFS fractal of unity.

Method 3.3.2 (Heuristic) *The predictive method based on Heuristic 3.3.1 for finding the convex hull of C-IFS fractals, is as follows.*

1. *Normalize the IFS maps to* $T_1(z) = \varphi_1 z,\ T_2(z) = 1 + \varphi_2(z-1)$.

2. *Calculate the principal direction* $\tau_* = \mathrm{i}(1-\varphi_2)\mathrm{Log}\ \varphi_1$ *and* $J = \frac{P}{\gcd(P,Q)}$.

3. *Calculate* $s_j = \mathrm{argmax}\left(\lambda_1^s \cos(\vartheta_1 s + \vartheta_2 j + \alpha) :\ s = \left\lfloor \frac{Qj}{P} \right\rfloor, \left\lceil \frac{Qj}{P} \right\rceil\right),\ 1 \le j \le J$.

4. *Calculate* $n_j = s_j - s_{j-1}$ *and* x *such that* $T_x = T_2 T_1^{n_1} \dots T_2 T_1^{n_J}$ *and the resulting* p_x *by Corollary 1.3.1.*

5. *We iterate the cycle* $\mathrm{Cyc}(x)$ *by each IFS map, according to the heuristic application of the Armadillo Method, to find the rest of the extrema.*

6. *Lastly we map the determined extrema back by the inverse of the normalizing map to get the extrema of the original fractal.*

This method results in the vertices of a polygon, which is heuristically predicted to be the convex hull of the C-IFS fractal.

3.3.5 Examples

Example 3.3.1 (Lévy C Curve [15, 29, 52, 2], Figure 3.8)
Find the extrema of the C-IFS fractal of unity in normal form with IFS factors

$$\varphi_1 = \frac{1}{\sqrt{2}} \exp\left(-\frac{\pi}{4}\mathrm{i}\right), \quad \varphi_2 = \frac{1}{\sqrt{2}} \exp\left(\frac{\pi}{4}\mathrm{i}\right).$$

Solution Applying Method 3.3.1, we optimize in the principal direction

$$\tau_* = \mathrm{i}(1-\varphi_2)\mathrm{Log}\ \varphi_1 \approx 0.2194 - 0.5660\mathrm{i}$$

and using Algorithm 4 we arrive at the unique focal maximizing truncation $x = (2,1)$ resulting in the principal extremal point and its cycle

$$e_* = p_x = \frac{T_x(0)}{1-\varphi_x} = \frac{1-\varphi_2}{1-\varphi_1\varphi_2} = 1 - \mathrm{i}$$

$$\mathrm{Cyc}(x) = \{e_*, T_1(e_*)\} = \left\{\frac{1-\varphi_2}{1-\varphi_1\varphi_2},\ \frac{\varphi_1(1-\varphi_2)}{1-\varphi_1\varphi_2}\right\} = \{1-\mathrm{i},\ -\mathrm{i}\}.$$

Next we deduce by Theorem 3.3.12 and Algorithm 4 that the cycle is consecutive (meaning $e_*, T_1(e_*)$ are neighbors). Lastly, we iterate the cycle according to the Armadillo Method (Theorem 3.3.13) to get the rest of the extrema

$$\mathrm{Ext}(F) = \{e_*,\ T_1(e_*),\ T_1^2(e_*),\ T_1^3(e_*),\ T_1^4(e_*),\ T_2(e_*),\ T_2^2(e_*),\ T_2^3(e_*)\}.\ \square$$

Example 3.3.2 (Twindragon / Davis-Knuth Dragon [23], Figure 3.9)
Find the extrema of the C-IFS fractal of unity in normal form with IFS factors

$$\varphi_1 = \frac{1}{\sqrt{2}} \exp\left(-\frac{\pi}{4}\mathrm{i}\right), \quad \varphi_2 = \frac{1}{\sqrt{2}} \exp\left(\frac{3\pi}{4}\mathrm{i}\right).$$

Solution Applying Method 3.3.1, we optimize in the principal direction

$$\tau_* = \mathrm{i}(1-\varphi_2)\mathrm{Log}\ \varphi_1 \approx 1.0048 - 0.9126\mathrm{i}$$

and using Algorithm 4 we arrive at the unique focal maximizing truncation $x = (2,1,1,1)$ or $T_x = T_2T_1^3$ resulting in the principal extremal point and its cycle

$$e_* = p_x = \frac{T_x(0)}{1-\varphi_x} = \frac{1-\varphi_2}{1-\varphi_1^3\varphi_2} = 2 - \frac{2}{3}\mathrm{i}$$

$$C_x := \mathrm{Cyc}(x) = \{e_*,\ T_1(e_*),\ T_1^2(e_*),\ T_1^3(e_*)\} =$$
$$= \left\{ \frac{1-\varphi_2}{1-\varphi_1^3\varphi_2},\ \frac{\varphi_1(1-\varphi_2)}{1-\varphi_1^3\varphi_2},\ \frac{\varphi_1^2(1-\varphi_2)}{1-\varphi_1^3\varphi_2},\ \frac{\varphi_1^3(1-\varphi_2)}{1-\varphi_1^3\varphi_2} \right\} =$$
$$= \left\{ 2 - \frac{2}{3}\mathrm{i},\ \frac{2}{3} - \frac{4}{3}\mathrm{i},\ -\frac{1}{3} - \mathrm{i},\ -\frac{2}{3} - \frac{1}{3}\mathrm{i} \right\}.$$

Next we deduce by Theorem 3.3.12 and Algorithm 4 that the cycle is consecutive. Lastly, we iterate the cycle according to the Armadillo Method (Theorem 3.3.13) to get the rest of the extrema $\mathrm{Ext}(F) \subset C_x \cup T_1(C_x) \cup T_2(C_x)$. □

Example 3.3.3 (Sink singularities of Section 2.2.13 and Figure 3.10)
Find the extrema of the C-IFS fractal of unity in normal form with IFS factors

$$\varphi_1 = 0.65 \exp\left(-\frac{2\pi}{6}\mathrm{i}\right), \quad \varphi_2 = 0.65 \exp\left(\frac{3\pi}{6}\mathrm{i}\right).$$

Solution Applying Method 3.3.1, we optimize in the principal direction

$$\tau_* = \mathrm{i}(1-\varphi_2)\mathrm{Log}\ \varphi_1 \approx 0.7672 - 1.1115\mathrm{i}$$

and using Algorithm 4 we arrive at the unique focal maximizing truncation $x = (2,1,1,2,1)$ or $T_x = T_2T_1^2T_2T_1$ resulting in the principal extremal point and its cycle

$$e_* = p_x = \frac{T_x(0)}{1-\varphi_x} = \frac{(1-\varphi_2)(1+\varphi_1^2\varphi_2)}{1-\varphi_1^3\varphi_2^2} \approx 1.2993 - 1.0655\mathrm{i}$$
$$C_x := \mathrm{Cyc}(x) = \{e_*,\ T_1(e_*),\ T_2T_1(e_*),\ T_1T_2T_1(e_*),\ T_1^2T_2T_1(e_*)\}.$$

Next we deduce by Theorem 3.3.12 and Algorithm 4 that the cycle is consecutive. Lastly, we iterate the cycle according to the Armadillo Method (Theorem 3.3.13) to get the rest of the extrema

$$\mathrm{Ext}(F) \subset C_x \cup T_1(C_x) \cup T_1^2(C_x) \cup T_2(C_x) \cup T_2^2(C_x).\ \square$$

In the figures that follow, the principal extremal point e_* is marked by a blue dot, where the blue line (perpendicular to the principal target direction τ_*) touches the convex hull. The fixed points $p_{1,2}$ are plotted with red $\odot$ and the iterates $T_1(p_2), T_2(p_1)$ with magenta. The cycle vertices are circled in red. Figures 3.11, 3.14, and 3.15 clearly show the utility of the introduced method, as none of these convex hulls could have been determined via say mere plotting.

The IFS factors and the principal extrema for the rest of the figures:

- Figure 3.11: $\varphi_1 = 0.6177\exp\left(-\frac{99\pi}{180}\mathrm{i}\right)$, $0.8594\exp\left(\frac{163\pi}{180}\mathrm{i}\right)$
  $T_x = T_2(T_a^4T_b)^2(T_a^5T_b)^4T_aT_2^{-1}$, $e_* = p_x \approx 2.7130 - 0.5959\mathrm{i}$
  with $T_a = T_1^2T_2T_1T_2T_1^2T_2$, $T_b = T_1T_2T_1^2T_2$ and
  $|x| = 1 + 2(4|a| + |b|) + 4(5|a| + |b|) + |a| - 1 = 29|a| + 6|b| = 262$.
- Figure 3.12: $\varphi_1 = 0.6\exp\left(-\frac{8\pi}{12}\mathrm{i}\right)$, $\varphi_2 = 0.8\exp\left(\frac{9\pi}{12}\mathrm{i}\right)$
  $|x| = 17$, $T_x = (T_2T_1)^4T_1(T_2T_1)^4$, $e_* = p_x \approx 2.9439 - 0.5767\mathrm{i}$.
- Figure 3.13: $\varphi_1 = 0.5479\exp\left(-\frac{5\pi}{45}\mathrm{i}\right)$, $\varphi_2 = 0.9427\exp\left(\frac{12\pi}{45}\mathrm{i}\right)$
  $|x| = 17$, $T_x = (T_2T_1^2T_2T_1^3)^2T_2T_1^2$, $e_* = p_x \approx 0.5203 - 0.9244\mathrm{i}$.
- Figure 3.14: $\varphi_1 = 0.9\exp\left(-\frac{6\pi}{45}\mathrm{i}\right)$, $\varphi_2 = 0.5\exp\left(\frac{35\pi}{45}\mathrm{i}\right)$
  $|x| = 41$, $T_x = (T_2T_1^6)^3T_2T_1^5(T_2T_1^6)^2$, $e_* = p_x \approx 1.8720 - 0.4808\mathrm{i}$.
- Figure 3.15: $\varphi_1 = 0.9421\exp\left(-\frac{2\pi}{180}\mathrm{i}\right)$, $\varphi_2 = 0.9561\exp\left(\frac{17\pi}{180}\mathrm{i}\right)$
  $|x| = 19$, $T_x = T_2T_1^9T_2T_1^8$, $e_* = p_x \approx 0.1958 - 0.6532\mathrm{i}$.

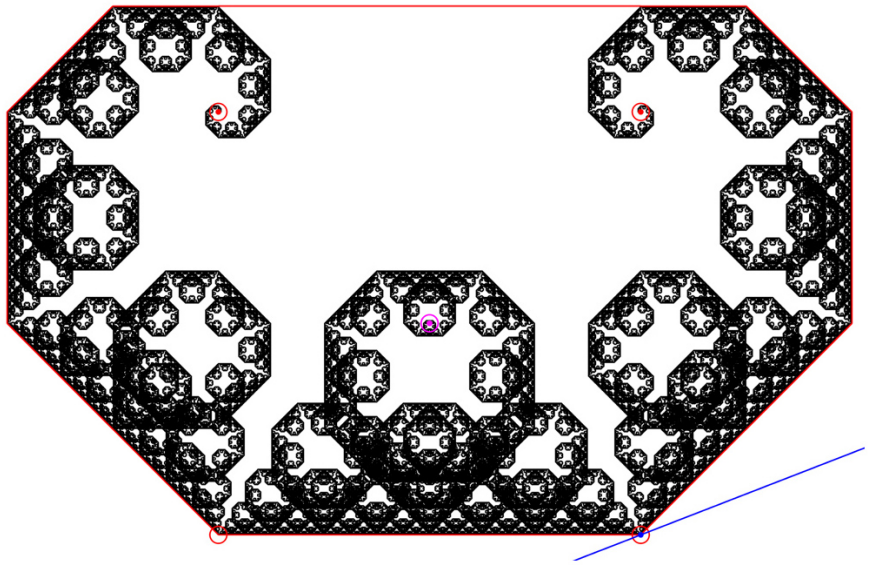

Figure 3.8: Lévy C Curve, Example 3.3.1.

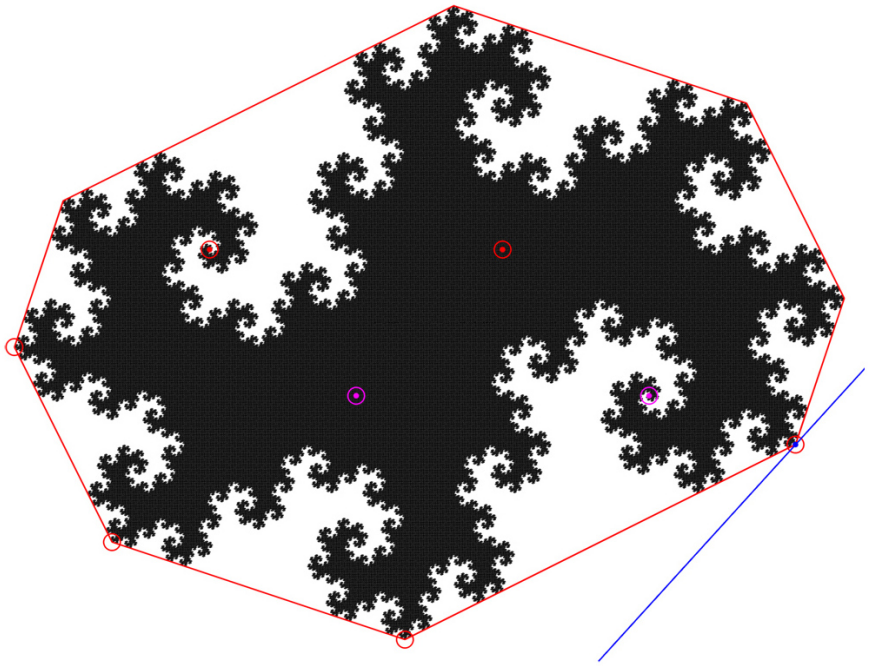

Figure 3.9: Twindragon, Example 3.3.2.

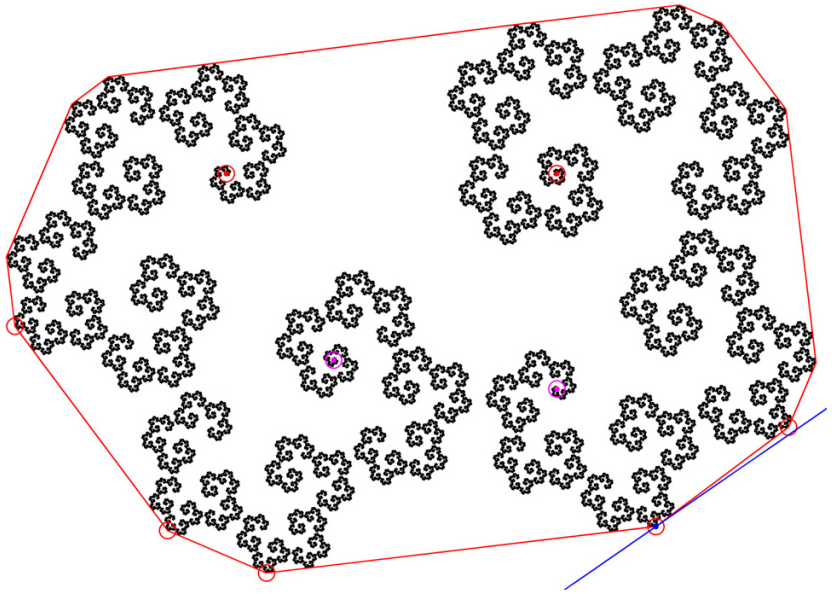

Figure 3.10: Sink singularities of Section 2.2.13; Example 3.3.3.

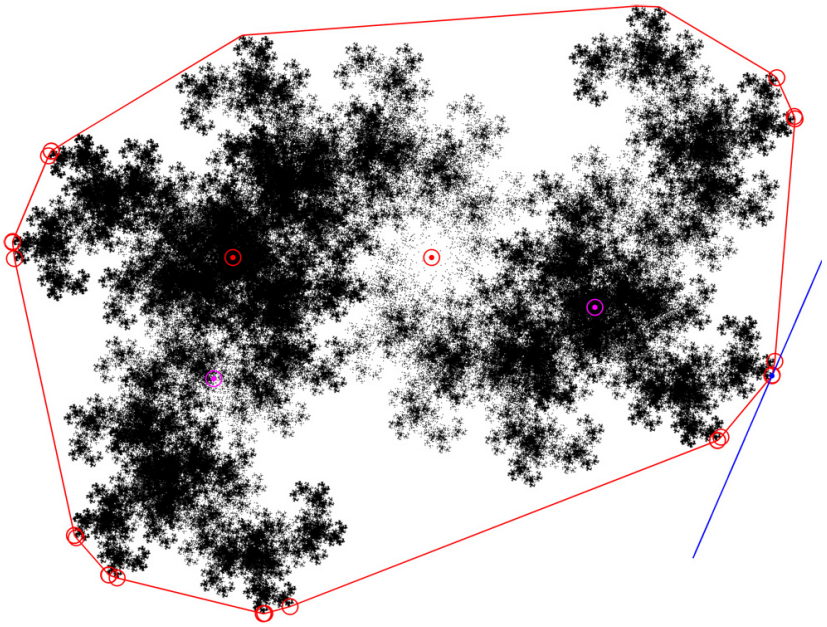

Figure 3.11: Illustration of the subtlety of convex hull determination: $|\mathrm{Ext}(F)| \geq 262$.

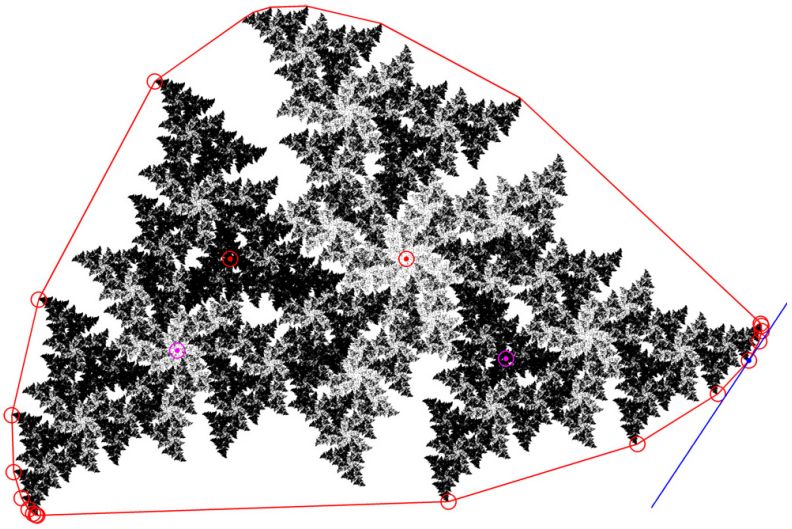

Figure 3.12: A random C-IFS fractal.

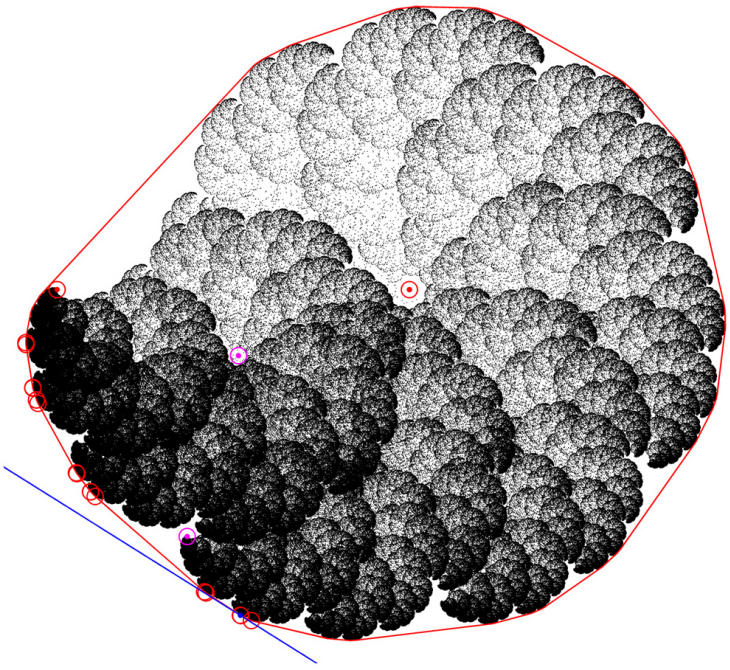

Figure 3.13: A random C-IFS fractal.

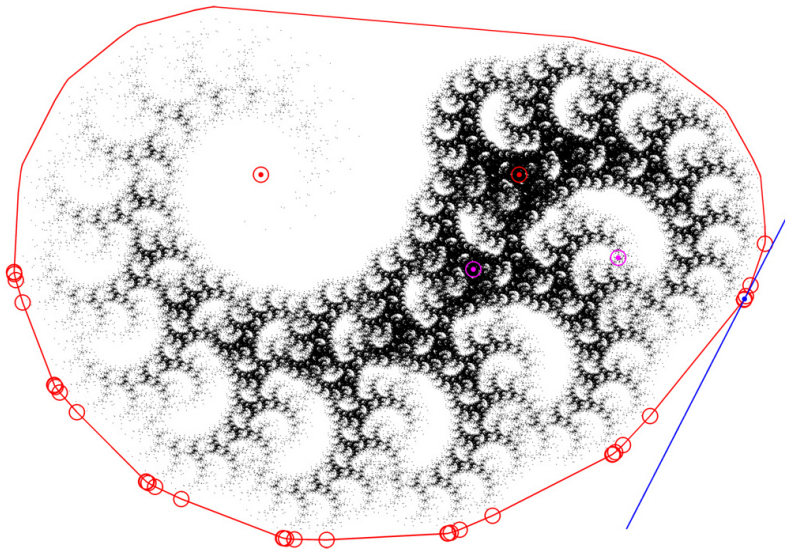

Figure 3.14: Illustration of the method's predictive nature; iteration level $L = 20$.

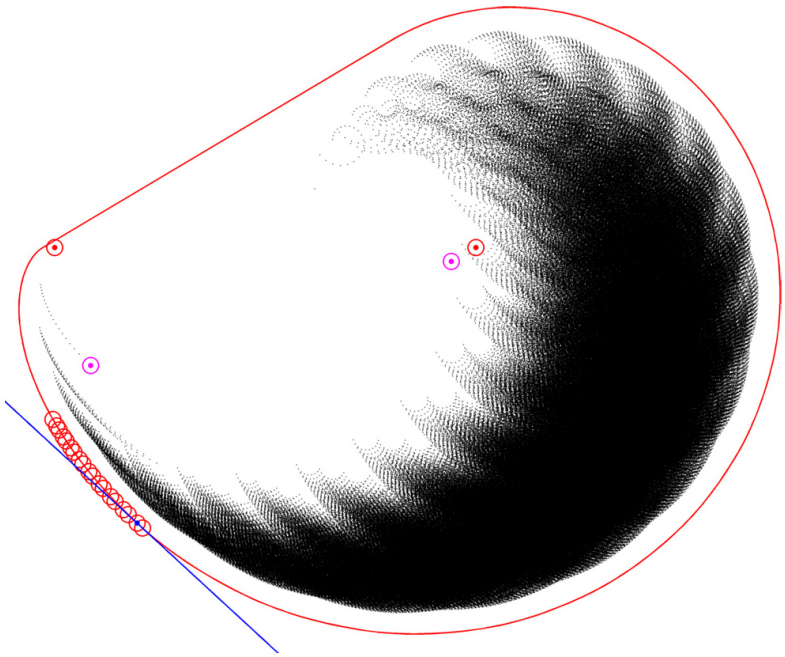

Figure 3.15: Illustration of the method's predictive nature; iteration level $L = 20$.

3.3.6 Concluding Remarks

We have introduced a method to determine the exact (not approximate) convex hull of certain rational IFS fractals. If a special kind of target direction - called "regular" - can be found, then the corresponding maximizing periodic extremal point may be exploited via its cycle to generate the rest of the convex hull. Furthermore, a heuristic method has been introduced for C-IFS fractals for a reasonable regular target direction candidate. Sections 3.3.2-3.3.3 are applicable to planar polyfractals of any number of maps, and Section 3.3.4 to bifractals in particular.

One may still be left to wonder how the convex hull of an irrational fractal could be found. As we have stressed after Theorem 3.3.7, due to the infinitesimal clustering of its vertices, the convex hull may well be impossible to determine explicitly in such a case, particularly since they are infinite in number. So by Theorem 3.3.8 one may resort to finding the extrema of increasingly better rational fractal approximations to the original. With respect to Method 3.3.2, this means that for such an irrational fractal, the n_j exponents in Heuristic 3.3.1 will never become focal periodic (since irrationality implies the lack of focality by definition), and the exponents are generated ad infinitum.

The entire Section 3.3 was designed with potential generalization to 3D IFS fractals in mind, so that the convex hull of L-system trees, or curiosities like the Romanesco Broccoli, may once be found. Remaining in the plane, the heuristic reasoning of Section 3.3.4 for C-IFS fractals, may well be generalized to polyfractals in general, possibly in space.

Lastly, let us recall the utility of the convex hull as reasoned throughout the thesis, particularly in Sections 1.5, 2.1.3, and 3.1.

Conclusion

The thesis approached the geometry of IFS fractals from a new angle, reasoning that it reduces both numerically and theoretically to finding invariant bounding sets to the fractal, such as ideal bounding circles and the convex hull. This is due to self-similar iterative containment.

Various applications, both real-life and theoretical, have been outlined in detail. A resolution of the Fractal-Line Intersection Problem has been presented, relevant to fractal antenna design; as well as the model of Fractal Potential Flows, relevant to both intermittent turbulence and Fractal Analysis.

Lastly, with sufficient motivation from applications, the main results of the thesis on the convex hull of IFS fractals have been presented. Novel definitions have been introduced, such as the rationality of IFS fractals, and fundamental results have been shown, such as the infinite cardinality of the extrema of irrational fractals. Several examples have been detailed to show the practicality of the introduced methods.

Though not detailed in the thesis, testing of these methods required their implementation in many lines of MatLab code (to be released as a program package on the author's website). At times, these efforts spanned months per program. The visualization of the figures in Section 2.2.13 for instance, required the development of a sequential rendering program due to computing limitations.

References

[1] N. Alves, W. Crespo-Miranda, F. Fernandes, F. Santana, R. G. Hohlfeld, and N. Cohen. Fractal element antenna genetic optimization using a PC cluster. 2002.

[2] S. Bailey, T. Kim, and R. S. Strichartz. Inside the Lévy Dragon. *The American mathematical monthly*, 109(8):689–703, 2002.

[3] J. W. Baish and R. K. Jain. Fractals and cancer. *Cancer research*, 60(14):3683–3688, 2000.

[4] M. F. Barnsley. *Fractals Everywhere*. Academic Press, Boston, second edition, 1993.

[5] M. F. Barnsley and S. Demko. Iterated function systems and the global construction of fractals. *Proceedings of the Royal Society*, A399, 1985.

[6] M. F. Barnsley, V. Ervin, D. Hardin, and J. Lancaster. Solution of an inverse problem for fractals and other sets. In *Proceedings of the National Academy of Sciences of the United States of America*, volume 83, pages 1975–1977. National Academy of Sciences, 1986.

[7] M. F. Barnsley and D. P. Hardin. A Mandelbrot set whose boundary is piecewise smooth. *Transactions of the American Mathematical Society*, 315(2):641–659, 1989.

[8] M. F. Barnsley and A. N. Harrington. A Mandelbrot set for pairs of linear maps. *Physica D: Nonlinear Phenomena*, 15(3):421–432, 1985.

[9] M. A. Berger. Random affine iterated function systems: mixing and encoding. In *Diffusion Processes and Related Problems in Analysis*, volume 2, pages 315–346. Springer, 1992.

[10] A. S. Besicovitch. On the fundamental geometric properties of linearly measurable plane sets of points III. *Math. Annalen*, 116:349–357, 1939.

[11] J. Brandt, C. Cabrelli, and U. Molter. An algorithm for the computation of the Hutchinson distance. *Information processing letters*, 40(2):113–117, 1991.

[12] C. Cabrelli, U. Molter, and E. Vrscay. Moment matching for the approximation of measures using iterated function systems. 1992.

[13] D. Canright. Estimating the spatial extent of the attractors of iterated function systems. *Computers and Graphics*, 18(2):231–238, 1994.

[14] P. Centore and E. R. Vrscay. Continuity of attractors and invariant measures for iterated function systems. *Canad. Math. Bull*, 37(3):315–329, 1994.

[15] E. Cesaro. Fonctions continues sans dérivée. *Archiv der Math. und Phys.*, 10:57–63, 1906.

[16] X. Chen. *Simulation and Design of Printed Fractal Antennas*. PhD thesis, University of Waterloo, 2002.

[17] N. Cohen. Fractal antennas part I. *Communications Quarterly*, 9:7–22, 1995.

[18] N. Cohen. Fractal antenna ground counterpoise, ground planes, and loading elements, Oct. 31 2000. US Patent 6,140,975.

[19] N. Cohen. Microstrip patch antenna with fractal structure, Oct. 3 2000. US Patent 6,127,977.

[20] N. Cohen. Tuning fractal antennas and fractal resonators, Aug. 15 2000. US Patent 6,104,349.

[21] N. Cohen. Fractals' new era in military antenna design. *Journal of RF design*, 2005.

[22] R. O. Davies. On accessibility of plane sets and differentiation of functions of two real variables. *Proc. Camb. Phil. Soc.*, 48:215–232, 1952.

[23] C. Davis and D. E. Knuth. Number representations and dragon curves, I, II. *Journal of Recreational Mathematics*, 3:161–181, 1970.

[24] A. Deliu, J. Geronimo, and R. Shonkwiler. On the inverse fractal problem for two-dimensional attractors. *Philosophical Transactions of the Royal Society of London*, 355(1726):1017–1062, 1997.

[25] V. Drakopoulos and N. P. Nikolaou. Efficient computation of the Hutchinson metric between digitized images. *Image Processing, IEEE Transactions on*, 13(12):1581–1588, 2004.

[26] S. Dubuc and R. Hamzaoui. On the diameter of the attractor of an IFS. Technical report, C.R. MATH. REP. SCI. CANADA, 1994.

[27] A. Edalat, D. W. Sharp, and R. L. While. Bounding the attractor of an IFS. Technical report, Imperial College, 1996.

[28] R. Eglash. *African Fractals: Modern Computing and Indigenous Design*. Rutgers, New Jersey, second edition, 2002.

[29] G. Faber. Über stetige funktionen. *Mathematische Annalen*, 69(3):372–443, 1910.

[30] K. J. Falconer. Sets with prescribed projections and Nikodym sets. *Proc. Lond. Math. Soc.*, 53:48–64, 1986.

[31] K. J. Falconer. *Fractal Geometry*. Wiley, Chichester, second edition, 2003.

[32] K. J. Falconer and J. D. Howroyd. Packing dimensions of projections and dimension profiles. *Math. Proc. Cambridge Philos. Soc.*, 121:269–286, 1997.

[33] H. Federer. The (φ, k) rectifiable subsets of n-space. *Transactions of the American Mathematical Society*, 62:114–192, 1947.

[34] B. Forte and E. R. Vrscay. Solving the inverse problem for measures using iterated function systems: a new approach. *Advances in applied probability*, pages 800–820, 1995.

[35] L. E. Frenzel. Welcome to antennas 101. *Electronic Design*, 56(16):51, 2008.

[36] J. Gianvittorio. *Fractal antennas: design, characterization, and applications*. PhD thesis, University of California, Los Angeles, 2000.

[37] D. P. Hardin. *Hyperbolic iterated function systems and applications*. PhD thesis, Georgia Institute of Technology, 1985.

[38] J. C. Hart and T. A. DeFanti. Efficient antialiased rendering of 3-D linear fractals. volume 25 of *Computer Graphics*, pages 91–100, Las Vegas, 1991. SIGGRAPH.

[39] R. G. Hohlfeld and N. Cohen. Self-similarity and the geometric requirements for frequency independence in antennae. *Fractals*, 7:79–84, 1999.

[40] J. D. Howroyd. Box and packing dimensions of projections and dimension profiles. *Math. Proc. Cambridge Philos. Soc.*, 130:135–160, 2001.

[41] J. E. Hutchinson. Fractals and self similarity. *Indiana University Mathematics Journal*, 30:713–747, 1981.

[42] G. M. Julia. Memoire sur l'iteration des fonctions rationelles. *Journal de Mathematiques Pures et Appliquees*, 83(4):47–245, 1918.

[43] L. Kantorovich and G. Rubinstein. On the space of completely additive functions. *Ser. Mat. Mekh. i Astron.*, 13(7):52–59, 1958.

[44] R. Kaufman. On the Hausdorff dimension of projections. *Mathematika*, 15:153–155, 1968.

[45] R. Kenyon, J. Li, R. S. Strichartz, and Y. Wang. Geometry of self affine tiles II. *Indiana University mathematics journal*, 48(1):25–42, 1999.

[46] J. Kigami. A harmonic calculus on the Sierpinski spaces. *Japan Journal of Applied Mathematics*, 6(2):259–290, 1989.

[47] J. Kigami. Harmonic calculus on pcf self-similar sets. *Transactions of the American Mathematical Society*, 335(2):721–755, 1993.

[48] J. Kigami. *Analysis on fractals*, volume 143. Cambridge University Press, 2001.

[49] H. Kunze, D. L. Torre, F. Mendivil, and E. Vrscay. *Fractal-based methods in analysis*. Springer, 2012.

[50] T. Larsson. Fast and tight fitting bounding spheres. In *Proceedings of The Annual SIGRAD Conference*, pages 27–30, November 2008.

[51] G. W. Leibniz. The principles of philosophy known as monadology. *Jonathan Bennett Edition*, 2004. Originally published in 1714.

[52] P. Lévy. Plane or space curves and surfaces consisting of parts similar to the whole. *Classics on Fractals*, 1993. Reprint of 1938 article.

[53] A. Lindenmayer and P. Prusinkiewicz. *The Algorithmic Beauty of Plants*. Springer-Verlag, second edition, 1996.

[54] N. Lu. *Fractal imaging*. Morgan Kaufmann Publishers Inc., 1997.

[55] B. B. Mandelbrot. *The Fractal Geometry of Nature*. Freeman, San Francisco, 1982.

[56] B. B. Mandelbrot and M. Frame. The canopy and shortest path in a self-contacting fractal tree. *The Mathematical Intelligencer*, 21(2):18–27, 1999.

[57] G. Mantica and A. Sloan. Chaotic optimization and the construction of fractals: solution of an inverse problem. *Complex Systems*, 3:37–62, 1989.

[58] J. M. Marstrand. Some fundamental geometrical properties of plane sets of fractional dimensions. *Proc. Lond. Math. Soc.*, 4:257–302, 1954.

[59] T. Martyn. Tight bounding ball for affine IFS attractor. *Computers and Graphics*, 27(4):535–552, 2003.

[60] P. Mattila. Hausdorff dimension, orthogonal projections and intersections with planes. *Ann. Acad. Sci. Fennicae*, A 1:227–244, 1975.

[61] P. Mattila. *Geometry of Sets and Measures in Euclidean Spaces*. Cambridge University Press, Cambridge, 1995.

[62] N. Megiddo. Linear-time algorithms for linear programming in $\mathbb{R}^3$ and related problems. *SIAM Journal on Computing*, 12:759–776, 1983.

[63] F. Mendivil and T. D. Taylor. Thin sets with fat shadows: Projections of cantor sets. *The American Mathematical Monthly*, 115:451–456, 2008.

[64] J. Rice. Spatial bounding of self-affine iterated function system attractor sets. pages 107–115. Graphics Interface, 1996.

[65] A. J. Seely and P. Macklem. Fractal variability: an emergent property of complex dissipative systems. *Chaos: An Interdisciplinary Journal of Nonlinear Science*, 22(1):013108–013108, 2012.

[66] D. W. Sharp and R. L. While. A tighter bound on the area occupied by a fractal image. Technical report, Imperial College, 1999.

[67] R. Singh. Multiband fractal antenna design and characterisation using antenna miniaturization techniques. 2012. Masters thesis.

[68] R. S. Strichartz. Analysis on fractals. *Notices AMS*, 46(10):1199–1208, 1999.

[69] R. S. Strichartz and Y. Wang. Geometry of self-affine tiles I. *Indiana University mathematics journal*, 48(1):1–24, 1999.

[70] J. J. Sylvester. A question in the geometry of situation. *Quarterly Journal of Mathematics*, 1:79, 1857.

[71] J. Vass. Explicit bounding circles for IFS fractals. Submitted, arXiv/1301.1378, 2012.

[72] J. Vass. On intersecting IFS fractals with lines. Submitted, arXiv/1301.1379, 2012.

[73] J. Vass. Fractal potential flows as an exact model for fully developed turbulence. Reviewed and to be submitted, arXiv/1301.1380, 2013.

[74] E. R. Vrscay. Mandelbrot sets for pairs of affine transformations in the plane. *J. Phys. A: Math. Gen.*, 19:1985–2001, 1986.

[75] E. R. Vrscay. Iterated function systems: theory, applications and the inverse problem. *Fractal Geometry and Analysis*, pages 405–468, 1991.

[76] E. R. Vrscay and C. J. Roehrig. Iterated function systems and the inverse problem of fractal construction using moments. In *Computers and Mathematics*, pages 250–259. Springer, 1989.

[77] Y. Wang. Self-affine tiles. In K.-S. Lau, editor, *Advances in Wavelets*, pages 261–285. 1999.

[78] E. Welzl. Smallest enclosing disks (balls and ellipsoids). *New Results and New Trends in Computer Science, Lecture Notes in Computer Science*, 555:359–337, 1991.

[79] D. H. Werner and S. Ganguly. An overview of fractal antenna engineering research. *Antennas and Propagation Magazine*, 45(1):38–57, 2003.

[80] D. H. Werner, R. L. Haupt, and P. L. Werner. Fractal antenna engineering: The theory and design of fractal antenna arrays. *Antennas and Propagation Magazine, IEEE*, 41(5):37–58, 1999.

[81] G. B. West, J. H. Brown, and B. J. Enquist. A general model for the origin of allometric scaling laws in biology. *Science*, 276(5309):122–126, 1997.

[82] B. Zeide. Fractal analysis of foliage distribution in loblolly pine crowns. *Canadian Journal of Forest Resources*, 28:106–114, 1998.